CHAPTER- IV

LABORATORY TEST RESULTS AND DISCUSSION

4.1 INTRODUCTION

This chapter discusses the results of various laboratory experiments conducted on the MSW fines and reinforced MSW fines with the considered fibers from the waste. A detailed geotechnical and physico-chemical characterization of the MSW fines (finer fraction of MSW below 4.75 mm) conducted in the laboratory has been discussed here. The tests are separated into two sets according to the loading conditions, i.e., static, and dynamic laboratory test results. The tests were conducted for the unreinforced and reinforced MSW fines under both loading conditions according to the methodology already discussed in the previous chapter. The dynamic parameters of the considered materials were analyzed by strain-controlled cyclic triaxial and bender element tests.

4.2 STATIC LABORATORY TEST RESULTS

This section of the chapter consists of the basic characterization (geotechnical, physical, and chemical) of the considered MSW fines and laboratory tests to analyze the compaction, shear strength, and consolidation characteristics of the unreinforced and reinforced MSW fines.

4.2.1 Morphology, Mineralogy, and Chemical Characteristics

The various tests that were conducted on the MSW fine sample to analyze the chemical, morphological, and mineralogical characteristics were pH, organic content, percentage of total dissolved solids, elemental analysis, and surface morphology.

4.2.1.1 pH

Previous research has shown that the leachate produced by the MSW has a higher likelihood of being alkaline in nature (Naveen et al., 2014b; Somani and colleagues, 2018). This is due to the organic decomposition of the matter in MSW and the production of carbon dioxide and ammonia. However, the current MSW sample is unusually acidic, with a pH of 6.4, which may be due to the presence of low organic matter waste with high inert content.

4.2.1.2 Organic Content

The organic content of the soil influences its compressibility, maximum dry density, consistency limits, and shear strength. The tolerance limit of organic content for earth fill or subgrade varies by country, ranging from 1% in Australia (specified by the Department of Transport and Main Roads) to 7% in the United States (specified by the Department of Transportation), with 5.9% for this study. Before field application, the performance of the MSW under compression and decomposition must be investigated, and if the settlement or deformations exceed the allowable limits, additional attention may be required.

4.2.1.3 Total Dissolved Solids

The total dissolved solids in the present MSW sample was found to be 0.81%.

4.2.1.4 Chloride and Total Dissolved Sulphate Content

The chloride and total dissolved sulphate content were found to be 0.018% and 0.092% respectively. The percentage of TDS, chloride, and sulphate content is very low and almost in the range of soils for different landfill sites in India (Delhi, Hyderabad, etc.) (Somani et al., 2018).

4.2.1.5 Colour Unit Test

The colour of leachates produced was light yellow (Figure 4.1) and the colour unit of the sample comes in the range of 450 Pt-Co by platinum-cobalt visual comparison method. The colour of the leachates obtained from the waste is a matter of concern because, if the MSW fines are to be used as backfilling or embankment fill material, it may cause contamination of the local water bodies.

Figure 4.1 Colour of leachates noticed from MSW fines

4.2.1.6 Elemental/ Compound Analysis

The Energy Dispersive X-Ray (EDX) and X-Ray Diffraction (XRD) methods were used to examine the elements and compounds present in the finer portion of MSW. The elements detected by EDX analysis were C, O, Ti, K, Ca, Fe, Mg, Al, and Si which include

heavy metals (Ti and Fe) (Figure 4.2(a)). The most common heavy metals detected in other landfills in India as well as in other countries were Hg, As, Ni, Cd, Pb, Cu, Cr, Zn, Co, Fe, and Mn (Zhang et al., 2008; Kaartinen et al., 2013; Jani et al., 2016; Somani et al., 2018).

The abundance of different compounds was estimated from the height of the corresponding peaks from XRD analysis (Figure 4.2(b)). The graph shows that quartz or silica peaks are predominant in the present MSW sample. The presence of compounds in the MSW fines are listed in Table 4.1. The elements and compounds detected by the EDX and XRD test were validated by the XRF (X-ray fluorescence spectroscopy) which is a non-destructive test to determine the elemental composition of the material (Figure 4.2(c)). The considered waste consists maximum of silica (Si) compound, approximately 49%, and negligible concentration of barium (Ba), copper (Cu), and zinc (Zn) compounds. The heavy metal concentration of titanium (Ti) and iron (Fe) is about 1% and 5% respectively.

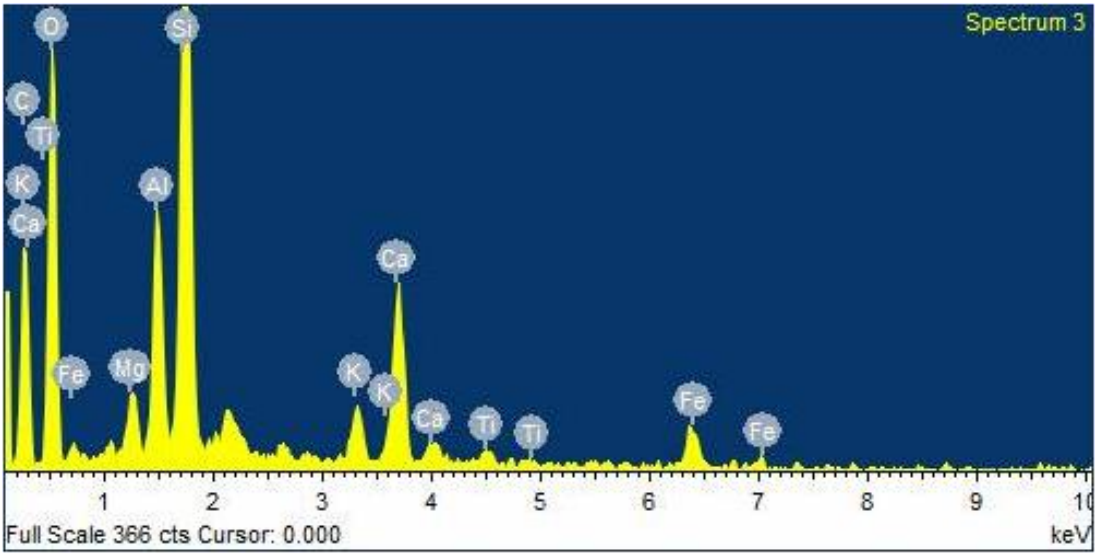

(a)

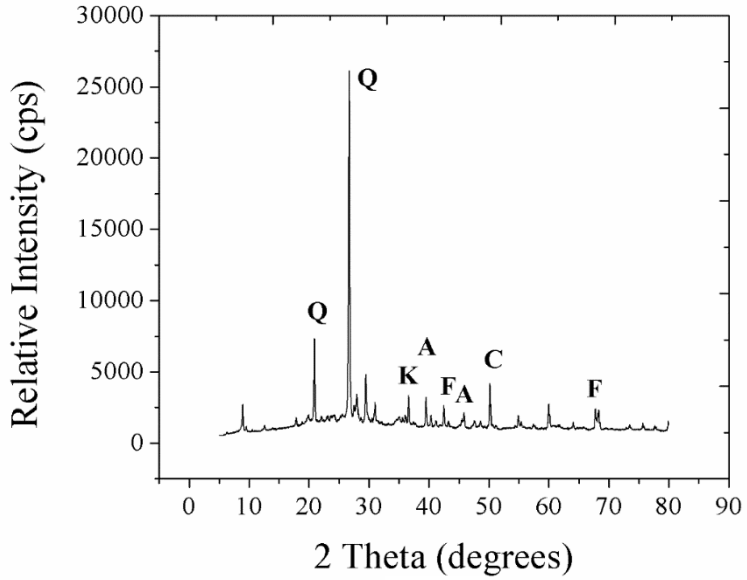

(b)

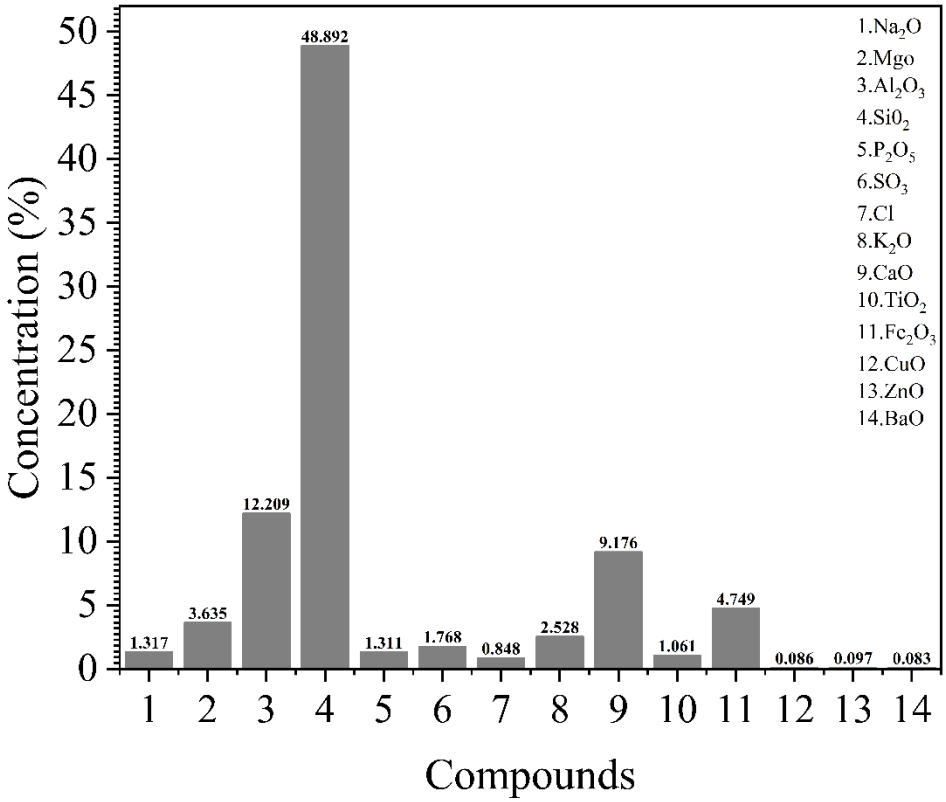

(c)

Figure 4.2(a) EDX spectral image (**b)** X-ray diffraction pattern **(c)** Percentage of compounds by XRF (X-ray fluorescence spectroscopy) for MSW fines

Table 4.1 List of compounds present in MSW fines.

Compound Name	Symbol
Quartz (SiO_2)	Q
Aluminum Oxide (Al_2O_3)	A
Potassium Oxide (K_2O)	K
Hematite (Fe_2O_3)	F
Calcium Oxide (CaO)	C

4.2.1.7 Scanning Electron Microscope (SEM) Test

The images of SEM results are shown in Figure 4.3 at different magnifications; at 1.00 kX magnification, it can be seen that the shape of particles are irregular and non-uniform, i.e. particles are of different shapes (some elongated particles can also be seen) and size with sharp edges. At a higher magnification of 5 or 10 kX single grain can be seen with rough surface and few voids. A similar type of result was also noticed for MSW incinerated ash (Zekkos et al., 2013b).

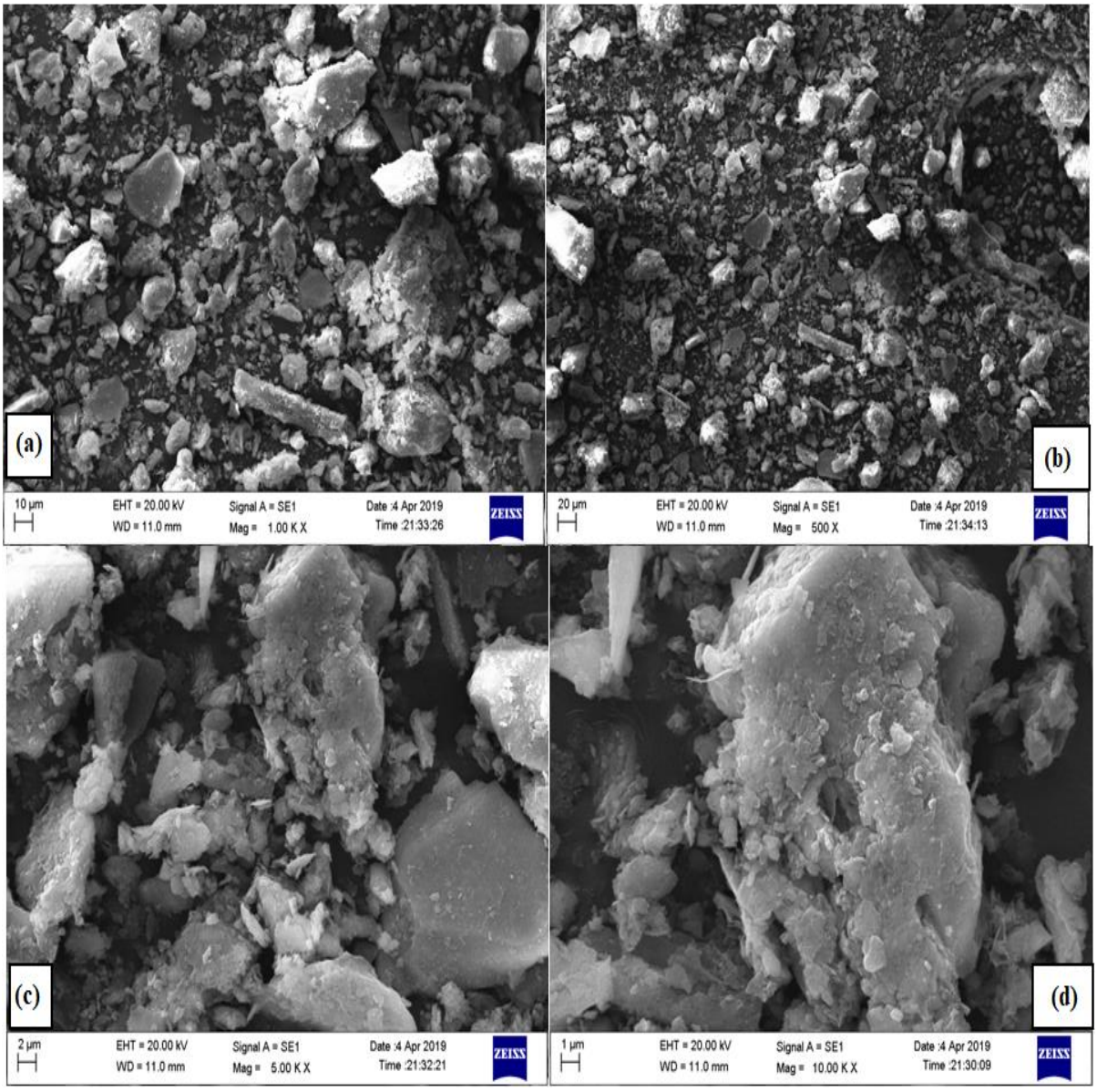

Figure 4.3 Scanning electron micrographs of MSW fraction below 75 microns at magnification of **(a)** 1.00 kX; **(b)** 500X; **(c)** 5.00 kX; and **(d)** 10.00 kX

Table 4.2 Summarized chemical characteristics of MSW landfills in India.

Chemical Characteristics	Present Study (Varanasi)	Delhi Landfill	Hyderabad Landfill	Kadapa Landfill	Jalandhar Landfill	References
pH	6.4	7.4 (5 year old) 7.6 (10 year old) 7.6 (15 year old)				Naveen et al., 2014; Somani et al., 2018
Organic Content (%)	5.9	6.5-6.7	11-12	6.8-7.4	6.8(±0.26)	Somani et al., 2018
Total Dissolved Solids (%)	0.81	1.4-1.5	1.8-1.85	0.5-0.55	2.0189	Somani et al., 2018 Sethi et al., 2012
Chloride Content (%)	0.018	0.7-0.75	0.5-0.55	0.36-0.38		Somani et al., 2018 Sethi et al., 2012
Sulphate Content (%)	0.092	0.4-0.45	0.8-0.85	0.09-0.1		Somani et al., 2018

The chemical analysis on the aged and fine portion of MSW from site-1 concludes that a few parameters like TDS and colour of leachates is objectionable and need attention, whereas TDS, chloride, and sulphate contents are comparatively on the lower side. Table 4.2 shows some chemical parameters from different landfill sites in India. Few heavy metals are detected in the present study material (Fe and Ti). This material may need some treatment before its application in the field like washing (to normalize the colour), blending with local soils or lime (to maintain pH and organic content) or it may require some biological or thermal treatment (to decompose or burn the organic content). The other alternative can be to barricading with some liner before its implementation.

4.2.2 Geotechnical Characterization of MSW Fines

The geotechnical characterization of the MSW fines were conducted by Indian standard codes already mentioned in the previous chapter 3. The geotechnical properties consist of the classification of MSW fines through soil classification systems considering the particle size distribution, specific gravity, and Atterberg limits. The other tests performed were the standard Proctor test, one-dimensional oedometer test, permeability test, California bearing ratio (CBR) test, static triaxial and unconfined compression (UCS) test to determine the compaction, consolidation, hydraulic conductivity, CBR value, and shear strength characteristics of the MSW fines respectively.

4.2.2.1 Grain Size Analysis

The particle size distribution was done using dry as well as wet analysis methods. The MSW fine is classified as poorly graded silty sand (SM) as per the Indian standard (IS) and Unified soil classification system (USCS). The larger particles, i.e., above 10 mm were categorized as plastic, fabric, and other wastes and were removed. The finer particles, i.e., less than 2 micron were almost negligible. The coefficient of curvature (C_c) and coefficient of uniformity (C_u) were found to be 0.88 and 25.76 respectively. The particle size distribution graph for the field-collected sample from site-1 (Ramana open dump) and considered MSW fines sample is shown in Figure 4.4. The visual representation of the particles below 4.75 mm can be seen in Figure 4.5.

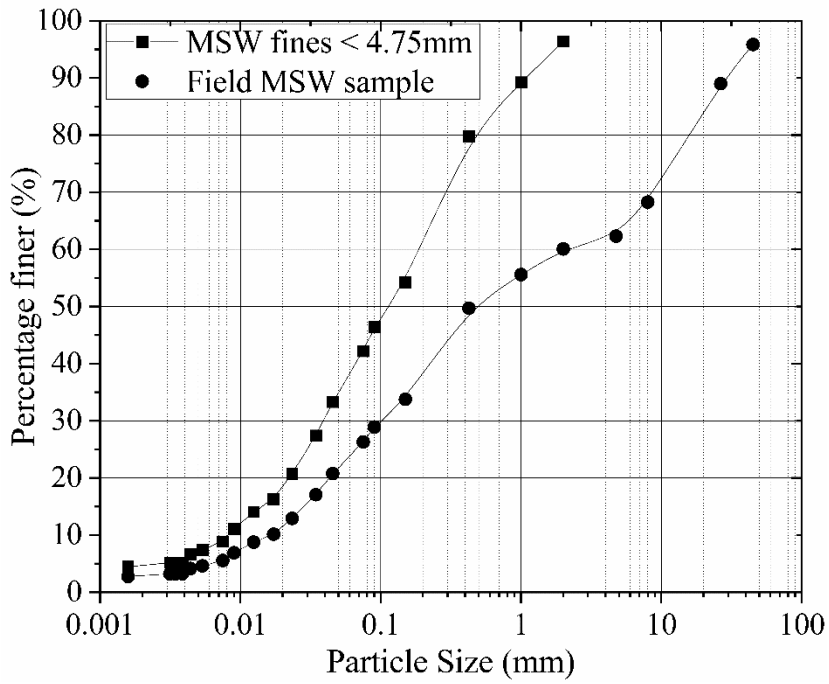

Figure 4.4 Grain size distribution curve of MSW sample (site 1) collected from field and finer portion used as MSW fines (below 4.75 mm)

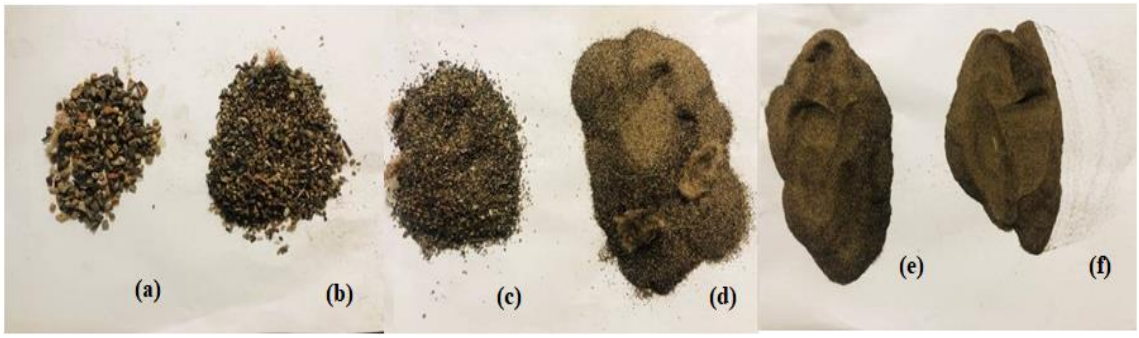

Figure 4.5 Typical images of particles of MSW retained on (a) 2 mm; (b) 1 mm; (c) 425 micron; (d) 150 micron; (e) 90 micron; and (f) 75 micron IS sieve

From the particle distribution graphs, it can be observed that more than 60% of the waste is under 4.75 mm and can be considered as MSW fines. The literature also validates this point that in most landfills 60-70% of the waste can be considered as fines or soil-like, which are used as cover soil in the landfills (Hogland et al., 1997; Kurian et al., 2003; Somani et al., 2018).

4.2.2.2 Specific Gravity

A density bottle was used for measuring the specific gravity of MSW fines. The specific gravity of MSW fines was found to be 2.32 (i.e., less than the specific gravity of silty sand soils (2.6 to 2.7)). The specific gravity considered is the average of 6 to 7 trials of the last mixed batch (the final product). The reduction in specific gravity may be because of the presence of fibers and lighter particles in the waste sample.

The studies on MSW show low specific gravity values i.e., 1.93 (Havangi et al., 2017), 1.90 to 2.55 (Ramiah et al., 2017), and 2.35 (Ramaiah and Ramana, 2014). The average value obtained from the pycnometer and density bottle was reported as 1.26 (Babu and Lakshminathan, 2014). The mean specific gravity of 2.4 was noticed for a fine fraction MSW (< No. 200 mesh) (Gabr and Valero, 1995).

4.2.2.3 Atterberg Limit

The liquid limit determined from the fall cone penetrometer was 33.34%, corresponding to 20 mm height of the cone. The fines were reported as non-plastic as plastic limit cannot be performed. Many studies indicated MSW as non-plastic or in the low plastic category (Zekkos et al., 2013b; Ramaiah and Ramana, 2014; Havangi et al., 2017; Ramaiah et al., 2017).

4.2.1.4 Compaction Characteristics

The lightweight Proctor compaction test evaluates the optimum moisture content (OMC) and maximum dry density (MDD) of the MSW fines as 18.40% and 1.51 g/cc, respectively (Figure 4.6). It is very difficult to maintain the desired density in the field; hence, the variation of other geotechnical parameters with different relative compaction (i.e., R_C: 95%–99%) was studied.

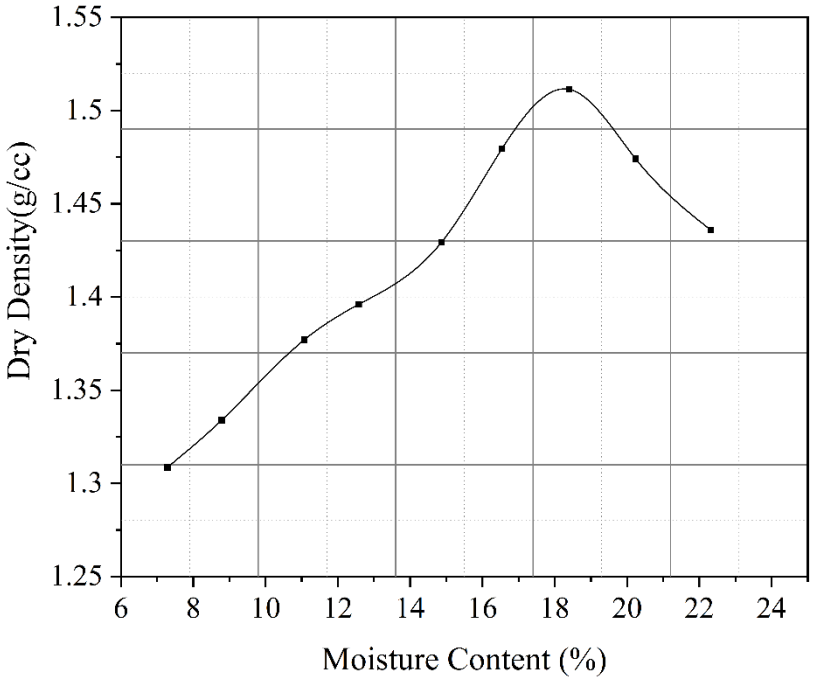

Figure 4.6 Compaction curve for the MSW fines sample

4.2.2.5 Compressibility Characteristics

The consolidation characteristics of the MSW fines were calculated at five considered R_C. From the consolidation results, it can be noticed that the compression index decreases as R_C increases (Figure 4.7(a)) whereas, for the coefficient of consolidation it shows no trend (Figure 4.7(b)). This is very common that when the material is densified its compressibility decreases. As compared with the waste from the Delhi landfill sites, the compression index of the present MSW fines is on the slightly higher side, that is, the present MSW fines are comparatively more compressible (Havangi et al., 2017; Ramaiah et al., 2017). The average value of the coefficient of consolidation of all five R_C's categorized MSW in the range of sandy silty clay (ML-CL) (Van Tul et al., 1985). The initial void ratio decreases from 0.62 to 0.55 with the increase in R_C from 95% to 99%. The variation of the void ratio with applied stress at 97% R_C of MSW fines in Figure 4.7(c)

shows abnormal trend, the only reason could be the heterogeneity in the MSW fines and the much lower weight variations between different relative compaction of the MSW fine sample.

4.2.2.6 Permeability Characteristics

A falling head permeability test was conducted for the MSW fine samples at five different R_C's. The permeability of the MSW fines varies from 3.45×10^{-7} to 1.17×10^{-7} m/s for different R_C (95% to 99%) (Figure 4.7 (d)). The general trend in Figure 4.7(d) shows that as density or R_C increases, waste permeability decreases, which is supported by Figure 4.7(c), which also shows that the void ratio decreases with R_C. The permeability of silty sand soil ranges between 10^{-5} and 10^{-7} cm/s. This concluded that the MSW fines are in the range of low to medium permeable soil-like material.

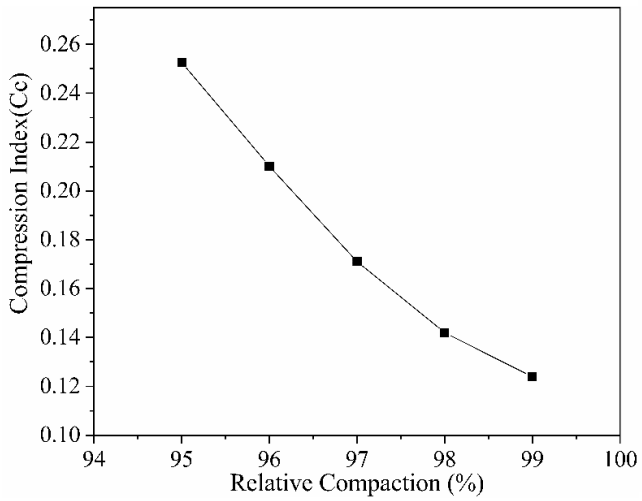

(a)

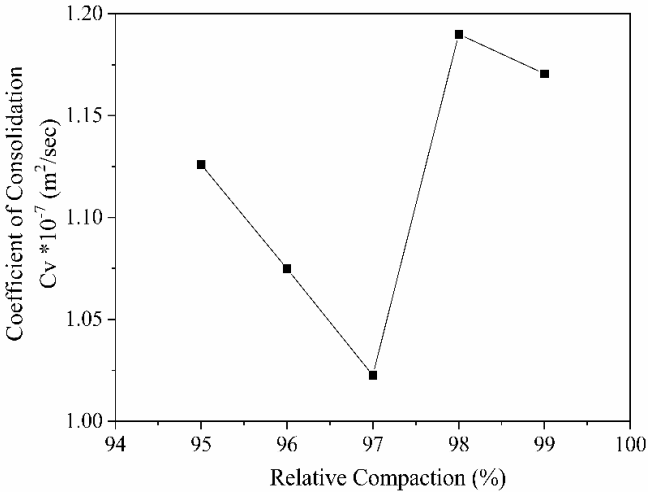

(b)

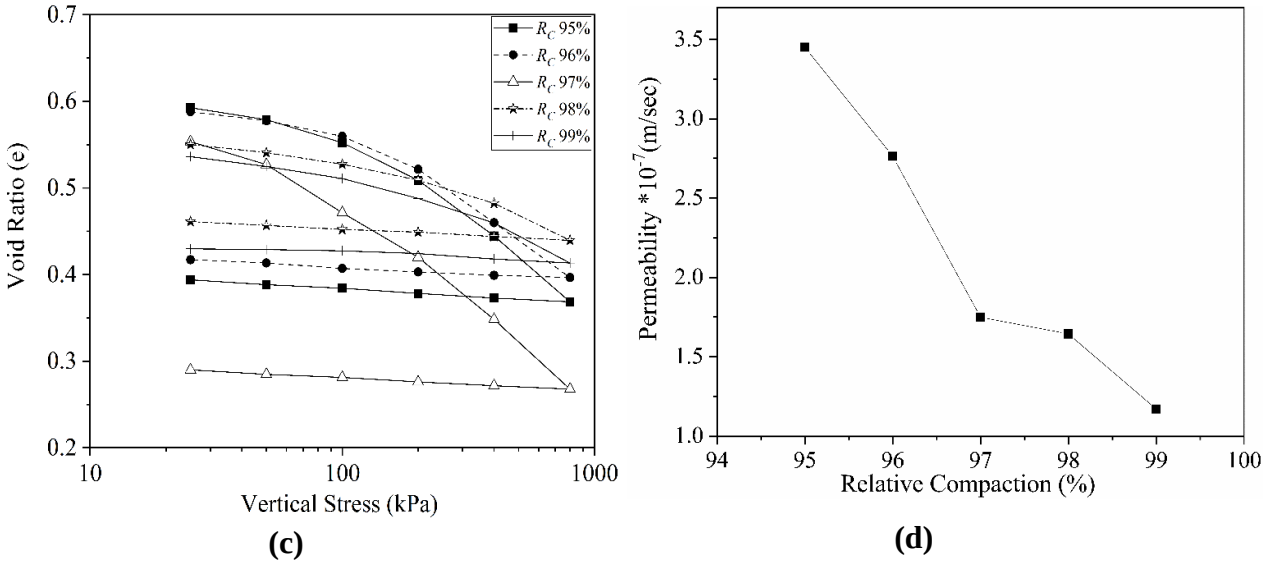

(c) **(d)**

Figure 4.7(a) Variation of compression index (C_c); **(b)** coefficient of consolidation (C_v) with increase in percentage of R_C; **(c)** variation of void ratio with applied stress at different R_C; and **(d)** variation of permeability with increase in percentage of R_C of MSW fine samples

4.2.2.7 CBR Test

The CBR test is a widely used penetration test for different engineering materials. It is also used as an indirect method to determine the strength of the soil. The CBR values for both unsoaked and soaked MSW fine samples were determined for 95 to 99% R_C. Usually, the CBR value is taken at 2.5 mm deformation but even after repeated trials, the maximum values were obtained at 5 mm deformation. Hence, CBR values were considered corresponding to 5 mm deformation. The soaked CBR tests were performed after 96 hours of soaking the sample in water. Figure 4.8 (a) shows a typical variation of load versus deformation curve for the soaked and unsoaked CBR test at 95% R_C. The range of unsoaked CBR value varies from 14.21% to 19.74%, whereas for soaked CBR it goes from 10.6% to 12.6% for varying R_C. There is an exceptional decrease in CBR value in the soaked case for 99% R_C, even after a few trials, the general trends of CBR values for both soaked and

unsoaked was increased with R_C (Figure 4.8(b)). As per the IRC (Indian Road Congress) specifications, the minimum CBR value required for subgrades and earthen shoulders (R_C not less than 98%) is 10% and for embankment (R_C not less than 97%) it is 5%. The present MSW fine meet the minimum requirements to use as fill material.

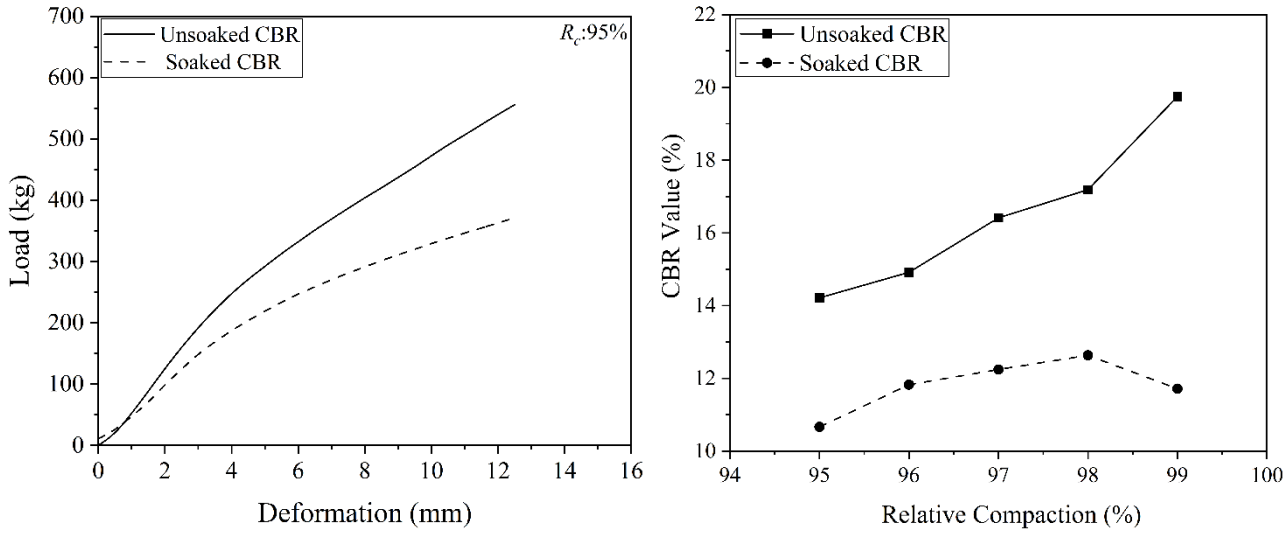

Figure 4.8(a) Load versus deformation graph for unsoaked and soaked CBR test at 95% R_C of MSW sample; and **(b)** variation of CBR values with increase in percentage of R_C of MSW samples at 5 mm deformation

4.2.2.8 UCS Test

The unconfined compressive strength (q_u) values obtained for MSW fines shows an increase in strength from 83.30 kPa to 99.94 kPa with R_C increment from 95 to 99%. The variations in the strength and cohesion obtained from the UCS test can be seen in Table 4.3.

Table 4.3 Variation of unconfined compressive strength (q_u) and cohesion (c) with increase in Maximum Dry Density (%).

Percentage of Maximum Dry Density (%)	Unconfined Compressive Strength (q_u) (kPa)	Cohesion (c) (kPa)
95	83.31	41.65
96	85.08	42.54
97	90.96	45.48
98	97.35	48.67
99	99.95	49.97

4.2.2.9 Static Triaxial Tests

The unconsolidated undrained triaxial test on the MSW fines sample (Height:76 mm; Diameter: 38 mm) shows improvement in the shear strength parameters with R_C variation (Figure 4.9). A typical variation of cohesion (c) and internal friction (ϕ) angle with R_C is listed in Table 4.4.

The geotechnical parameters of the present MSW fines have been compared with others' work in Table 4.5. The above geotechnical parameters summarize the present study waste (MSW fines) as non-plastic silty sand with medium compressibility and low to medium permeability soil-like material. From the literature as well as from the present study it was noticed that 60-70% of the waste can be categorized under fines. The preliminary geotechnical investigations on MSW fines of the Varanasi open dump area made this material suitable for backfill as well as embankment fill material. However, before applying MSW fines in the field, it may require some treatment such as; mixing with local soil, installing any artificial drainage system, or a layer of more permeable soil to increase the permeability and reduce the compressibility and future settlements. The

material also fulfills the minimum criteria required for the shear strength and bearing capacity of the soil, which can further be enhanced by stabilizing or reinforcing the waste.

Table 4.4 Variation of cohesion and angle of internal friction with increase in R_C of MSW fines.

Relative Compaction (R_C %)	c (kPa)	ϕ (°)
95	39.09	26.69
96	31.37	30.75
97	33.53	30.75
98	39.42	30.28
99	42.19	30.75

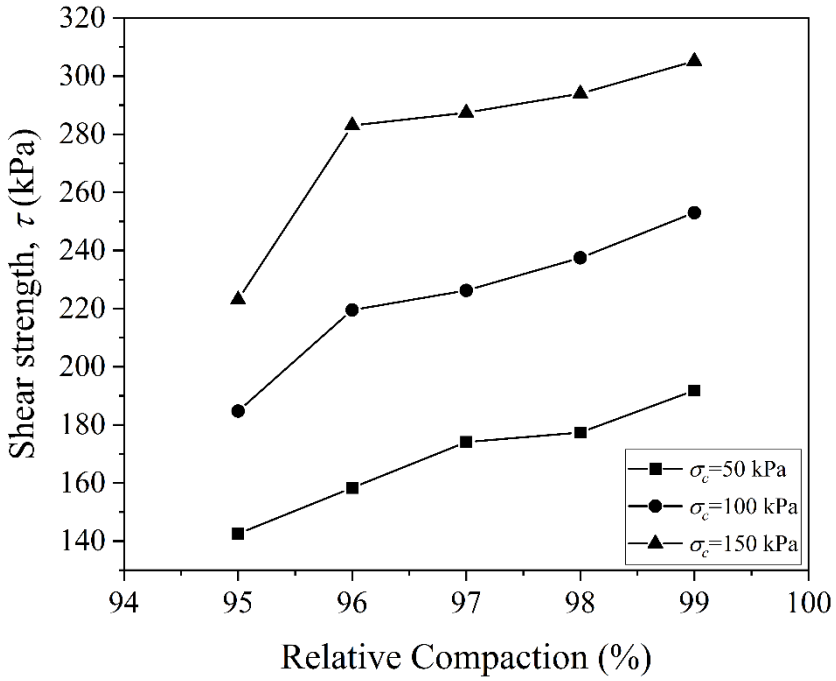

Figure 4.9 Variation of shear strength with increase in percentage of R_C of MSW samples at different confining pressure (σ_c)

Table 4.5 Summarized geotechnical characteristics of MSW fines.

Geotechnical Characteristics	Present Study	Past Studies	References
Grain Size	60% finer (Silty Sand)	Categories as silty sand or well or poorly graded sand with silt or gravel	Havangi et al., 2017; Athanasopoulos et al., 2008; Zekkos et al., 2013b
Specific Gravity	2.32	1.93 1.9 to 2.55 2.35 1.26 (avg. value of pycnometer and density bottle) 2.4 (for fine fraction <No.200 mesh)	Havangi et al., 2017 ; Ramaiah et al., 2017 Abreu and Vilar, 2017; Babu and Lakshmikanthan, 2015; Gabr and Valero, 1995
Plasticity	Non-Plastic	Nonplastic or low plastic category	Havangi et al., 2017; Ramaiah et al., 2017; Abreu and Vilar, 2017; Zekkos et al., 2013b
Compaction Parameters	MDD=1.51g/cc OMC=18.40%	<u>Delhi landfill sites</u> MDD=1.6g/cc OMC=14% MDD=16.7 kN/m^3(5 yrs. waste) MDD=16 kN/m^3(10 yrs. waste) MDD=15.5 kN/m^3(15 yrs. waste) MDD=11 to 14kN/m^3 <u>Tirso landfill, Portugal</u> 11 to 14 kN/m^3 <u>Michigan monofill</u> OMC=18.9 to 28.4% MDD=11.65 to 16.4 kN/m^3	Havangi et al., 2017; Somani et al., 2018; Ramaiah et al., 2017 Ramaiah and Ramana, 2014; Zekkos et al., 2013b
Consolidation Parameters	C_c=0.253 to 0.124; e=0.62 to 0.55 (For RC 95 to 99%)	<u>Qizhishan landfill (China)</u> C_c'=0.1 to 0.3 <u>Delhi landfill</u> C_c=0.141,0.160 and 0.190 (for 5,10 and 15 yrs. old waste) C_c=0.11 to 0.17 C_v=2.43×10^{-6},4.14×10^{-6} and	Chen et al., 2009; Havangi et al., 2017; Ramaiah et al., 2017; Gabr and Valero, 1995

		$5.56*10^{-6}$(for 5,10 and 15 yrs. old waste) Pennsylvania landfill C_c=0.4 to 0.9 Secondary consolidation range (0.03 to 0.009) higher organic content	
Shear Strength Parameters	c=32 to 42 kPa; ϕ=27º to31º (For RC 95 to 99%)	Delhi landfill c=20kN/m^2; ϕ =35º (5 yrs. old waste) c=25kN/m^2; ϕ =28º (10 yrs. old waste) c=10kN/m^2; ϕ =38º (15 yrs. old waste) MSWI c=52.4kPa and ϕ =44.5º (Triaxial test) c=20.1kPa and ϕ =42º (Direct Shear test)	Havangi et al., 2017; Zekkos et al., 2013b
Permeability	3.45×10^{-7} to1. × 10^{-7} m/sec (For RC 95 to 99%)	$k=1.55\times10^{-9}$ to1.21×10^{-8} m/sec $k=2.09\times10^{-8}$ m/sec (particle size<5mm) $k=1.0\times10^{-7}$to 6.0×10^{-3} cm/sec (China landfill)	Havangi et al., 2017; Gavelytė at al., 2015
CBR (%)	14.21 to 19.74(Unsoaked) 10.6 to 12.6(Soaked), (For RC 95 to 99%)	CBR=5 to 30% (silty sand soil) CBR=16.4% (MSWI)	Zhang et al., 2016; Rehman et al., 2017

4.2.3 Fiber-Reinforced MSW Fines

This section includes the effect of waste fibers (segregated from the waste collected from site 2) on the strength parameters of fiber-reinforced MSW fines. The compaction, consolidation, and shear strength characteristics of the MSW fines reinforced with fibers at different fiber content (FC) (0.5, 1, 2, 4, 8, and 10%) are discussed below.

4.2.3.1 Compaction Characteristics of Fiber-Reinforced MSW Fines

In the case of fiber-reinforced waste, the specific gravity of the sample reduces with the increment of the fiber content (through linear interpolation G reduces from 2.31 to 2.17 for 0.5 to 10% fiber content). The fibers are lighter in weight, which justifies the decrement in specific gravity. The compaction characteristics with fiber reinforcement are shown in Figure 4.10. The MDD decreases with the increase in fiber content and the curves shift towards the right with the increment of fiber content, i.e., because of the absorption of water by fibers.

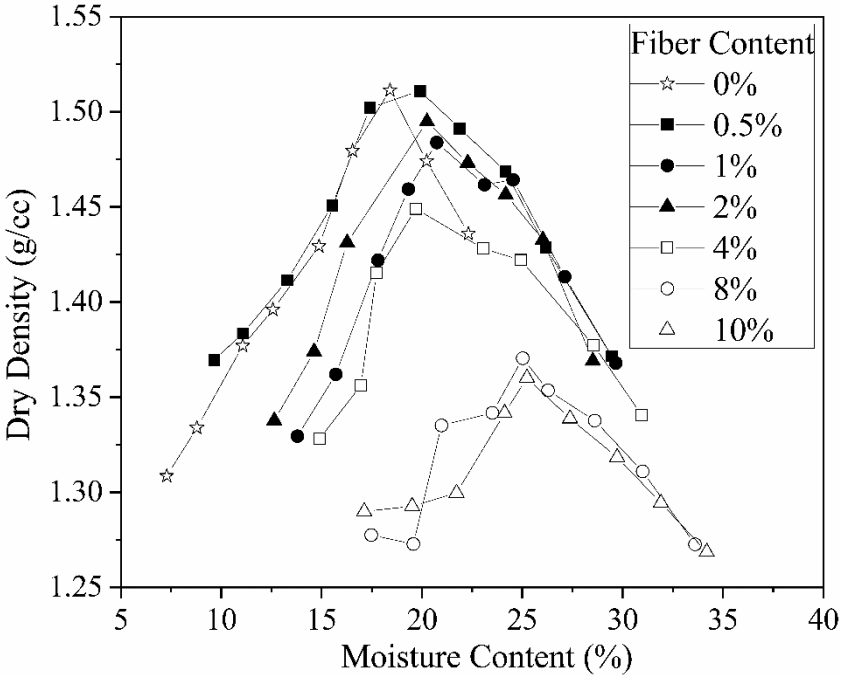

Figure 4.10 Compaction curves for MSW fines and MSW fines mixed with different fiber content

4.2.3.2 Compressibility Characteristics of Fiber-Reinforced MSW Fines

Standard oedometer tests were carried out to explore the influence of fiber content on the consolidation behaviour of MSW fines.

4.2.3.2.1 Compressibility Parameters

The settlement of the composite sample was measured at each pressure increment. The final settlement after the loading and unloading cycles can be observed in Table 4.6. For the unreinforced MSW fines, the maximum settlement after the loading and unloading cycles was observed to be 3 mm and 2.64 mm, respectively. The settlement was reduced when fibers are mixed with MSW fines up to FC of 2% then increases for 4 and 8% and finally, the minimum settlement can be seen for 10% fiber reinforcement. The uneven distribution of fibers in the sample can cause randomness in the settlement trends. The change in the thickness or settlement at a different level of pressure can be correlated with the void ratio. The variation of void ratio (e) versus vertical stress (σ_v) (Figure 4.11(a)) also demonstrates that the settlement of the sample is due to the change in void ratio. The change in void ratio from initial zero vertical stress (σ_v) to final σ_v of 800 kPa can be seen in Figure 4.11(b), which has good alignment with the settlement response (shown in Table 4.6), i.e., the higher the change in the void ratio, the higher is the settlement. Fiber-reinforced sands also show a greater void ratio compared to unreinforced sand because of the high resistance of fiber-reinforced composite against compaction (Gray and Refeai, 1986; Nataraj and McManis, 1997; Ibraim and Fourmont, 2007; Choo et al., 2017). At low vertical stress of 7 kPa, which results in an increased compression index (C_c) with the increment in FC. This is because the fibers can easily be compressed, bent, or stretched (depending on the type of fibers) with an increase in applied stress (Choo et al., 2017). The earlier studies also show that the C_c for fiber-reinforced sands at very high applied stress (>3 MPa) is not affected by the addition of fibers (Consoli et al., 2005; Dos Santos et al., 2010; Pino and Baudet, 2010). The fibre reinforced MSW, on the other hand, exhibits little complex behaviour for the C_c, as discussed below. Figure 4.12(a) demonstrates the linear fluctuations in the

compression index (C_c) with the change in stress ranges at different fiber content. The C_c represents the slope of the e versus log σ_v curve (Figure 11(a)) in Equation 4.1.

$$C_c = -\frac{\Delta e}{\Delta \log(\sigma)} \tag{4.1}$$

The composite sample becomes more compressible as the C_c value rises, confirming Figure 4.12(a), which shows that the compressibility increases with the increase in vertical stress. The effect of fibers on the compressibility of the composite sample can be observed in Figure 4.12(b), where fiber inclusion fluctuates the C_c values. At a low-stress range, i.e., below 200 kPa, a drop in C_c can be seen at FC of 1%, then steadily increases up to 8%, and then decreases for FC of 10%. Whereas at a high-stress range, i.e., 200–400 kPa, it is very predominant for 10% FC by hitting the lowest C_c value. The stress range of 400–800 kPa shows almost constant C_c after 2% FC. The C_c data show that fiber content reduces the settlement at higher vertical stresses (> 200 kPa). Table 4.7 projects the percentage change in C_c values between the unreinforced (FC = 0%) and reinforced MSW fines. The positive change depicts the decrease in C_c for a particular FC compared to the unreinforced sample. For all the FC, a drastic improvement or settlement can be noticed for the stress range of 200–400 kPa, and 10% reinforcement. This point can be treated as an anomaly because of unusual behaviour. The fibers used in this study are significantly different from those used in previous studies. The fibers studied in previous studies were classified as synthetic or natural fibers. However, the fibers used in the present study are part of the waste itself and does not fall into any of the previously listed categories because they were discarded and are quite diverse in terms of material composition (most of the part include fabric threads, plastic fibers, etc.), aspect ratio and makes a very heterogeneous mix composition. Hence, it is very difficult to compare the results of present reinforced MSW fines with the past studies. But, if we divide the FC into two ranges, i.e., from 0 to 2% and 2 to 8%, in the first

range the final settlement decreases up to 2% FC and can be regarded as optimum in this case (at 800 kPa). When the FC exceeds 2%, the fiber inclusion increases the final settlement up to 8%. Here, the fibers were mixed up to 10%, but it was very difficult to mix and compact the sample at a high percentage of fiber, and this point can be treated as an anomaly because of unusual behaviour.

Table 4.6 Settlement analysis with fiber content.

FC (%)	Final settlement after loading (mm)	Final settlement after unloading (mm)	Regain in height (mm)
0	3.00	2.64	0.36
0.5	2.84	2.70	0.14
1	2.59	2.26	0.33
2	2.54	2.08	0.46
4	2.90	2.50	0.40
8	2.95	2.50	0.45
10	2.35	1.98	0.37

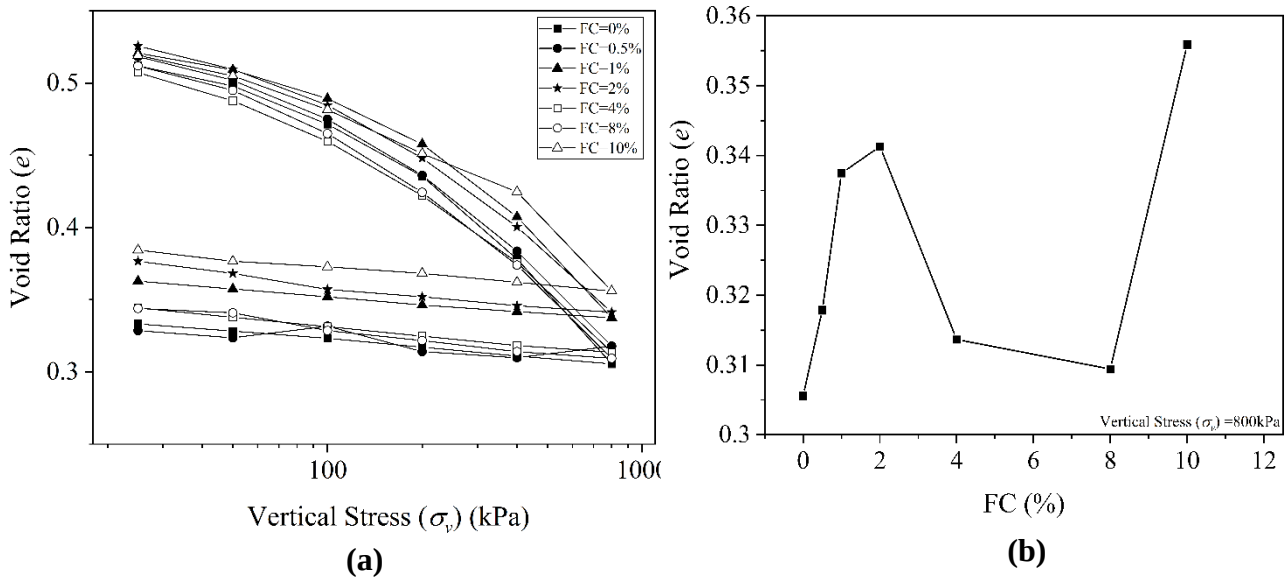

Figure 4.11(a) Variation of void ratio (e) Vs log of vertical stress (σ_v) **(b)** Change in void ratio (e) with fiber content (FC)

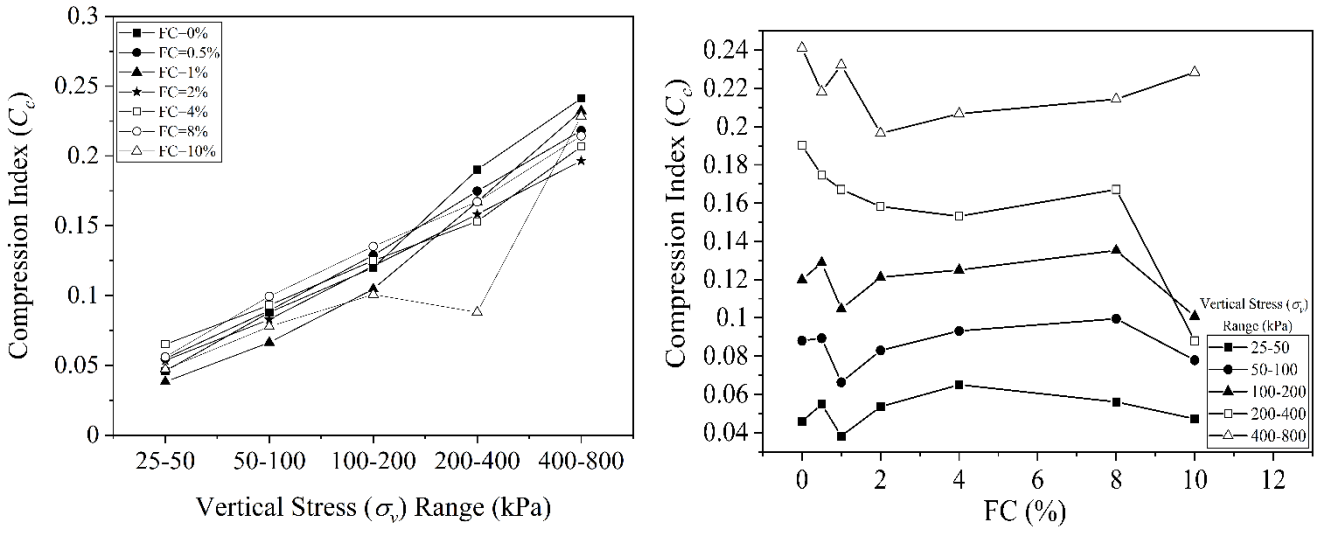

Figure 4.12(a) Compression index (C_c) variation with stress range for all FC **(b)** Compression index (C_c) variation with fiber content (FC)

Table 4.7 Percentage change in compression index (C_c) between reinforced and unreinforced MSW fines.

σ_v (kPa) / FC (%)	25-50	50-100	100-200	200-400	400-800
0.5	-19.44	-1.45	-7.45	8.05	9.52
1	16.67	24.64	12.76	12.08	3.70
2	-16.65	5.79	-1.07	16.77	18.52
4	-41.64	-5.80	-4.26	19.46	14.28
8	-22.20	-13.05	-12.76	12.08	11.11
10	-2.764	11.59	15.96	53.69	5.29
*All values are in %					

4.2.3.2.2 Determination of Coefficient of Consolidation

The physical significance of the coefficient of consolidation (C_v) parameter is the rate at which any soil undergoes consolidation when subjected to an increase in external pressure. The permeability of the soil, compressibility, layer thickness, and boundary conditions are the factors that influence the C_v of any soil. The logarithm of time technique, square root of time method, and computational method are the three approaches that fit to measure the C_v parameter of reinforced MSW fines. The first two methods are the most useful and extensively used in routine laboratory tests (Feng and Lee, 2001). Figure 4.13 illustrates the consolidation curves for both the methods at σ_v of 800 kPa for varying FC, and Figure 4.14 depicts the effect of FC on C_v values with σ_v increments. The C_v value calculated using the logarithm of time method (Figure 4.14(a)) demonstrates that at unreinforced or low reinforcement of 0.5% cases, the fluctuation in the C_v values is more pronounced and increases at higher stresses. Although at higher FC (0.5%), the trends are almost constant after σ_v of 300 kPa. Similarly, for the computational technique (Figure 4.14 (c)), the overall trends for all FC the σ_v gradually increase beyond 300 kPa, except for 8%, where the trend decreases. The square root of time method of calculating C_v produces significantly different results than the other two methods. In this method (Figure 4.14 (b)), the peaks of reinforced MSW fines shift to the left, indicating low stress in comparison to the unreinforced sample. The same thing can be seen in Table 4.8, where the maximum C_v values obtained by all three methods are compared, and the maximum values computed by the square root of time method are on the lower side of σ_v. The C_v prediction values for the logarithm of time method are lower than those for the other two methods. The primary compression affects the C_v more than the secondary compression in the square root of time method, resulting in higher C_v values than the logarithm of time method (Sridharan and Prakash,1995; Cortellazzo, 2002).

The considered MSW fines (reinforced or unreinforced) have high initial settlements, as shown by the consolidation curves for both methods (Figure 4.13(a) and (b)), so the emphasis should be on a method that emphasizes the primary consolidation part more, namely the square root of time method. When the values of C_v obtained from the three methods are compared, the square root of time method and the computational method show comparable ranges, whereas the logarithm of time method shows a lower value because it considers both primary and secondary compression as a part of the consolidation curve. The C_v obtained by all three methods confirms that the increased fiber content in MSW fines slows the consolidation process (as shown in Figure 4.14 and Table 4.8). The heterogeneity of the fibers and random distribution could be the cause of low permeability and indirectly the reduced C_v. Figure 4.14 also shows that at a higher FC of 8%, the C_v values are consistently low, especially at higher stresses.

Table.4.8 Maximum values for coefficient of consolidation (C_v).

FC (%)	σ_v (kPa)	Logarithm-of-time method	σ_v (kPa)	Square-root-of-time method	σ_v (kPa)	Computational method
0	800	1.64E-04	400	1.57E-03	25	2.46E-03
0.5	800	1.82E-04	50	8.83E-04	800	2.23E-03
1	400	2.19E-06	400	2.62E-05	800	3.11E-05
2	400	2.19E-06	200	1.47E-05	200	3.46E-05
4	400	1.82E-06	100	2.62E-05	200	3.03E-05
8	400	1.71E-06	100	7.79E-06	200	2.89E-05
10	800	1.56E-06	800	1.47E-05	800	2.85E-05
* C_v values are in cm^2/sec						

There are past studies that validate that the permeability of fiber-reinforced soil samples decreases as compared to the unreinforced ones and hence reduces the seepage velocity and increases the piping resistance in non-plastic and non-cohesive soils (Furumoto et al., 2002; Sivakumar Babu and Vasudevan, 2008; Das and Viswanadham, 2010; Das et al., 2009; Estabragh et al., 2014). The trends shown in Figure 4.14 for the variation of C_v with vertical stress (σ_v) for all FC by different methods were found to be extremely random. The random variation of C_v with applied stress has also been reported by many researchers in past studies for coal ashes, soils, and MSW (Sridharan et al., 1987, Naveen et al., 2018, Ram et al., 2022). The reason may be the heterogeneity of both MSW fines and fibers and the random distribution of the fibers.

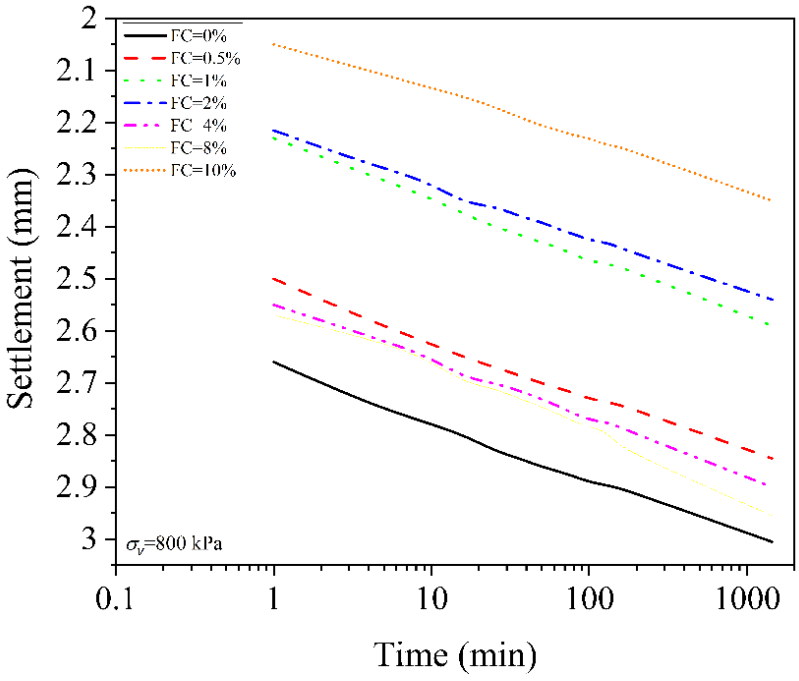

(a)

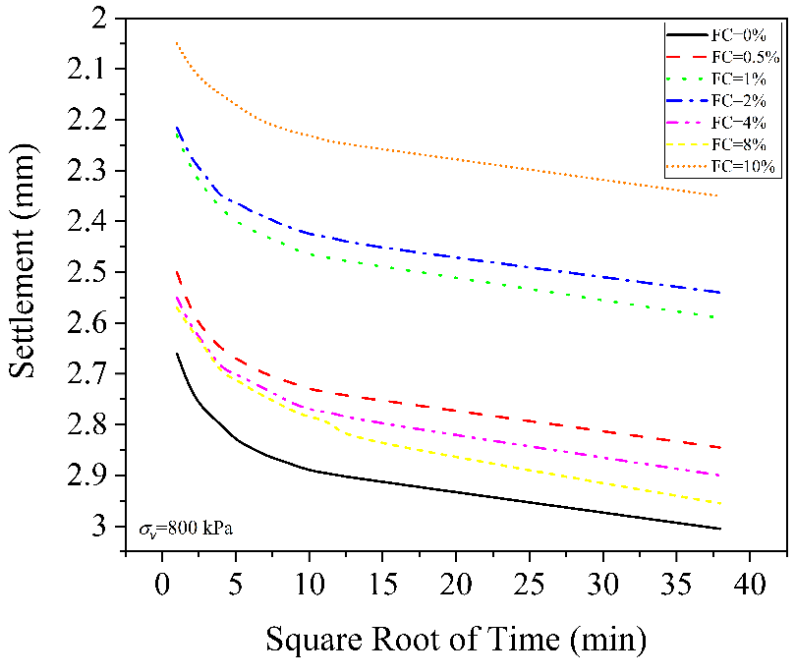

(b)

Figure 4.13(a) Determination of C_v through a logarithm of time method **(b)** square root of time method at σ_v (800 kPa)

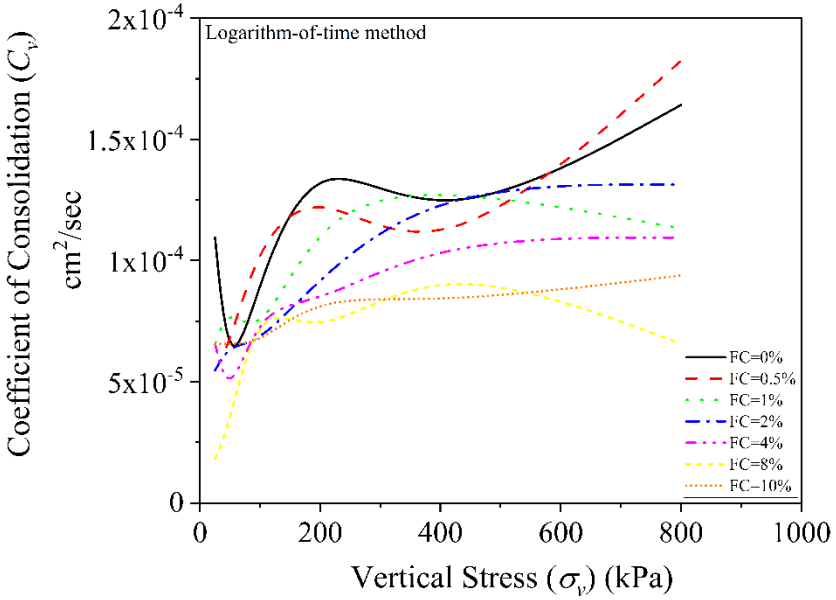

(a)

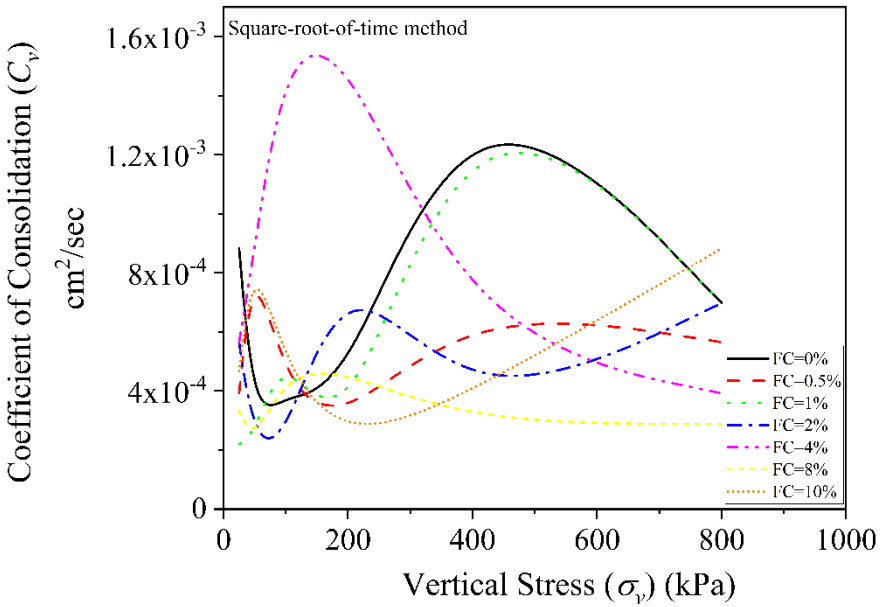

(b)

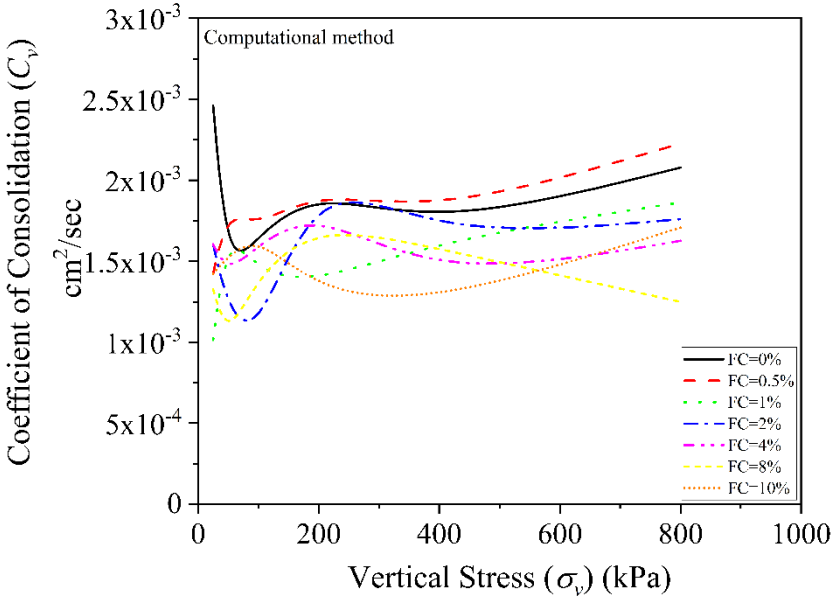

(c)

Figure 4.14 Coefficient of consolidation (C_v) variation with vertical stress (σ_v) for all FC by **(a)** logarithm of time method **(b)** square root of time method and **(c)** computational method

4.2.3.3 Shear Strength Behaviour of Fiber-Reinforced MSW Fines

4.2.3.3.1 Unconsolidated Undrained Triaxial Test on MSW Fine Samples (Diameter: 38mm; Height:76mm)

The strength characteristics of the reinforced MSW fines were determined using unconsolidated undrained triaxial tests. Two sets of UU (unconsolidated undrained) tests were conducted: (1) with the dry density constant (i.e., 1.15 g/cc, MDD of MSW fines) and (2) with varying density (as shown in Figure 4.10). Table 4.9 shows the strength parameter variation chart for both sets. By considering the friction angle (φ) variation, it is clear from both the sets that either φ value almost remains constant or reduces after an 8% addition of fibers. The average shear strength plot (Figure 4.15) validates this, showing a 140% increase in strength for 8% fiber content when compared to unreinforced MSW fines. The same plot (Figure 4.15) shows shear strength variations at different σ_c and confirms that the confining pressure increases the strength of the samples. The stress-strain variation of the fiber-induced MSW fines can be observed in Figure 4.16.

Table 4.9 Variation of strength parameters with fiber content.

	Fixed Density (1.51 g/cc)		Varying Density (from Figure 4.10)	
Fiber %	ϕ (°)	c (kPa)	ϕ (°)	c (kPa)
0	30.61	57.11	30.61	57.11
0.5	29.48	80.17	32.84	55.40
1	29.42	80.26	28.50	56.96
2	33.93	70.47	33.79	58.71
4	32.29	94.55	31.68	70.61
8	39.22	104.42	35.32	66.14
10	39.29	85.513	32.49	50.90

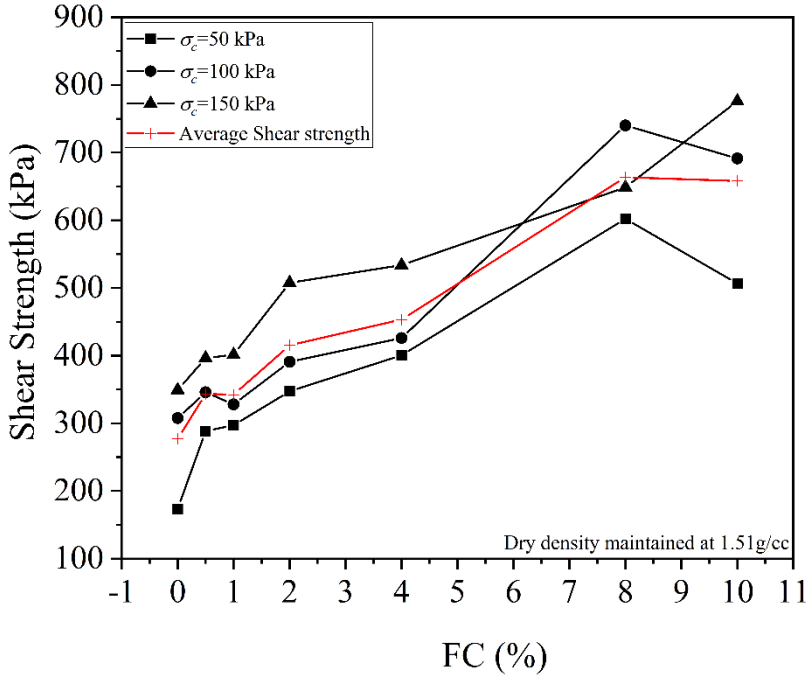

Figure 4.15 Shear strength variations with FC at different confining pressure

The strength ratio (SR) is the ratio of reinforced material deviator stress (static loading case), σ_d to the unreinforced material that also predicts the strength improvement after reinforcement. The plots of SR for different σ_c with varying fiber content (Figure 4.17) show SR values greater than one for every reinforced sample, indicating that the inclusion of fibers improved the strength of MSW fines. Regardless of the percentage of fiber content, the strength improvement was greater for low confining pressure (50 kPa) than for the higher confining pressure (100 and 150 kPa).

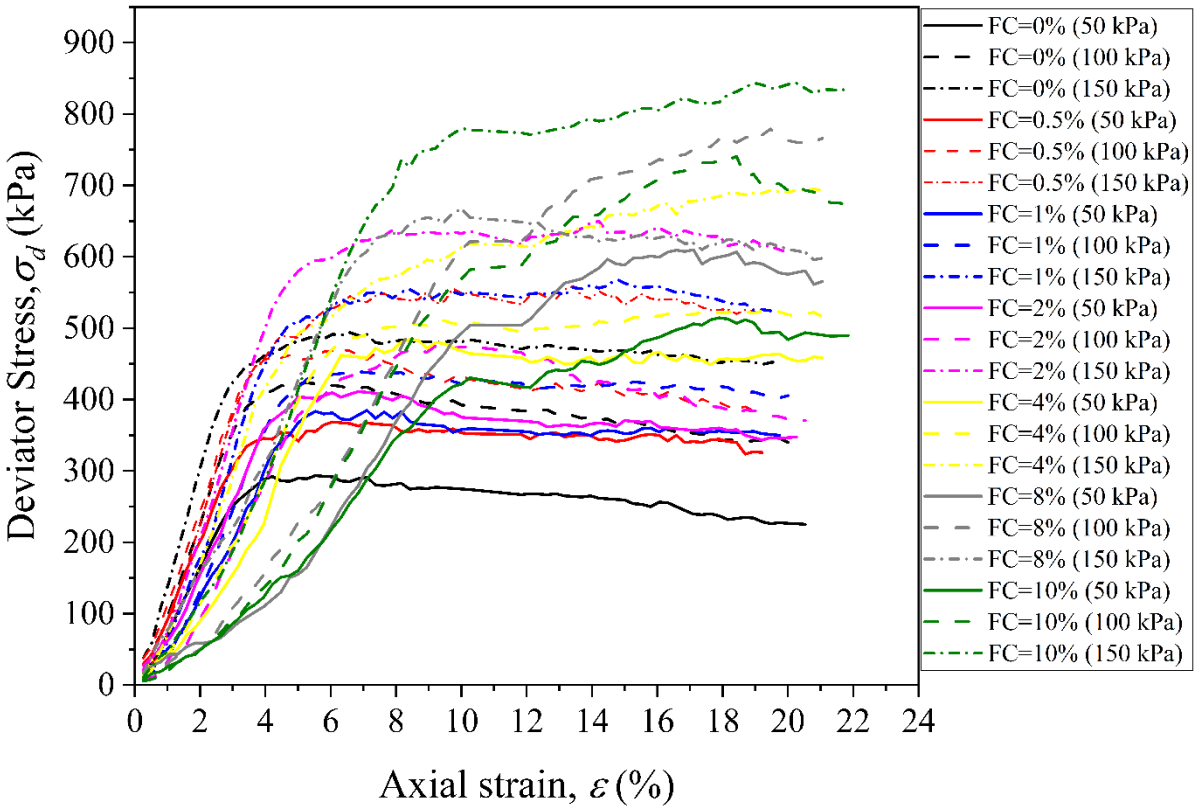

Figure 4.16 Stress-strain variation of fiber-induced MSW fines

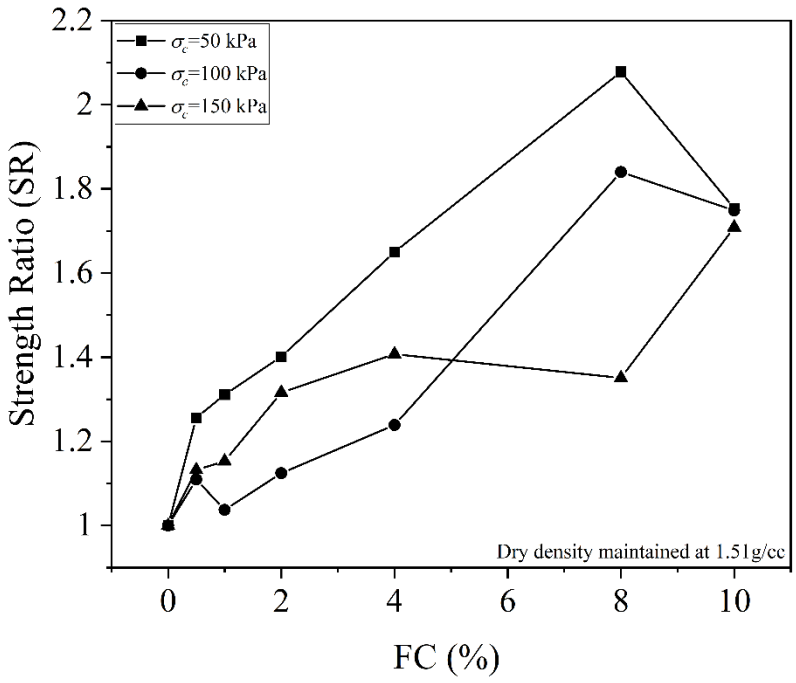

Figure 4.17 Strength Ratio variations with FC at different confining pressure

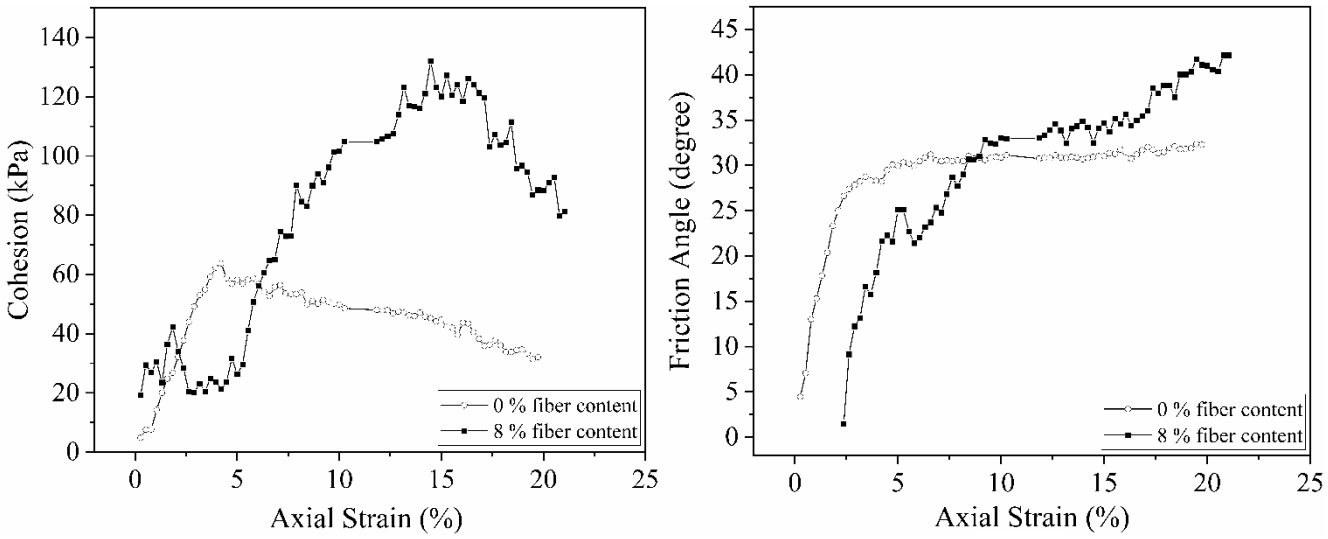

(a) **(b)**

Figure 4.18(a) Mobility of cohesion (c); and **(b)** friction angle (ϕ) with axial strain for MSW fines (0% fiber content) and optimum fiber content (8% fiber content)

The mobility behaviour of c and ϕ can be seen in Figure 4.18(a and b). The graph depicts the increase in mobilized cohesion and friction angle at higher axial strains (10%) for reinforced MSW fines with an optimum fiber content of 8%. This also concludes that at higher axial stains fiber reinforcement is very effective.

4.2.3.3.2 Triaxial Test on MSW Fine Samples (Diameter: 50mm; Height:100mm)

The MSW fines and reinforced MSW fines with the optimum fiber content (8% fiber content) recommended from the previous section were tested under UU (unconsolidated undrained), CU (consolidated undrained), and CD (consolidated drained) conditions for the triaxial test with a sample size of 50mm diameter and 100mm height. The shear strength parameters shown in Table 4.10, under all three conditions confirmed the improvement due to fiber reinforcement in MSW fines. Under CU triaxial test, due to the saturation and undrained conditions which unable to reduce the pressure developed in

the pores and causes the reduction of internal friction as compared to the UU and CD testing conditions. The substitution of fibers can be a great advantage under undrained conditions.

Table 4.10 Shear strength parameters for unreinforced and reinforced MSW fines with fibers under different triaxial conditions.

		UU			CU			CD		
MSW fines	σ_c or σ'_c (kPa)	σ_d (kPa)	c (kPa)	ϕ	σ_d (kPa)	c (kPa)	ϕ	σ_d (kPa)	c (kPa)	ϕ
	50	290.51	43.92	32.84	133.52	36.70	14.59	250.29	32.06	34.64
	100	370.67			151.05			381.97		
	150	519.12			198.42			508.31		
MSW fines +8% fibers	50	510.74	76.78	40.30	282.09	71.85	24.53	539.45	79.18	39.56
	100	690.12			393.49			630.76		
	150	1159.40			412.63			869.45		
UU= Unconsolidated undrained; CU= Consolidated undrained; CD=Consolidated drained; σ_c= Confining pressure; σ'_c = Effective confining pressure; σ_d= Deviator stress; ϕ= Angle of friction; c= cohesion										

Figure 4.19 shows the stress-strain behaviour of the unreinforced and reinforced MSW fines with fibers under three different confining pressures (50, 100, and 150 kPa) up to the axial strain of 15%. It can be observed that the behaviour of the unreinforced MSW fines under any condition (UU, CU, and CD) shifted from ductile to elastic material when reinforced with 8% fiber. The considered material after reinforcement can be suggested as embankment or subgrade fill material. Due to its elastic properties, it can regain deformations. The elastic behaviour of the material also shows that the material can store energy or can work as a damping material and can be useful for damping manual or earthquake-induced vibrations.

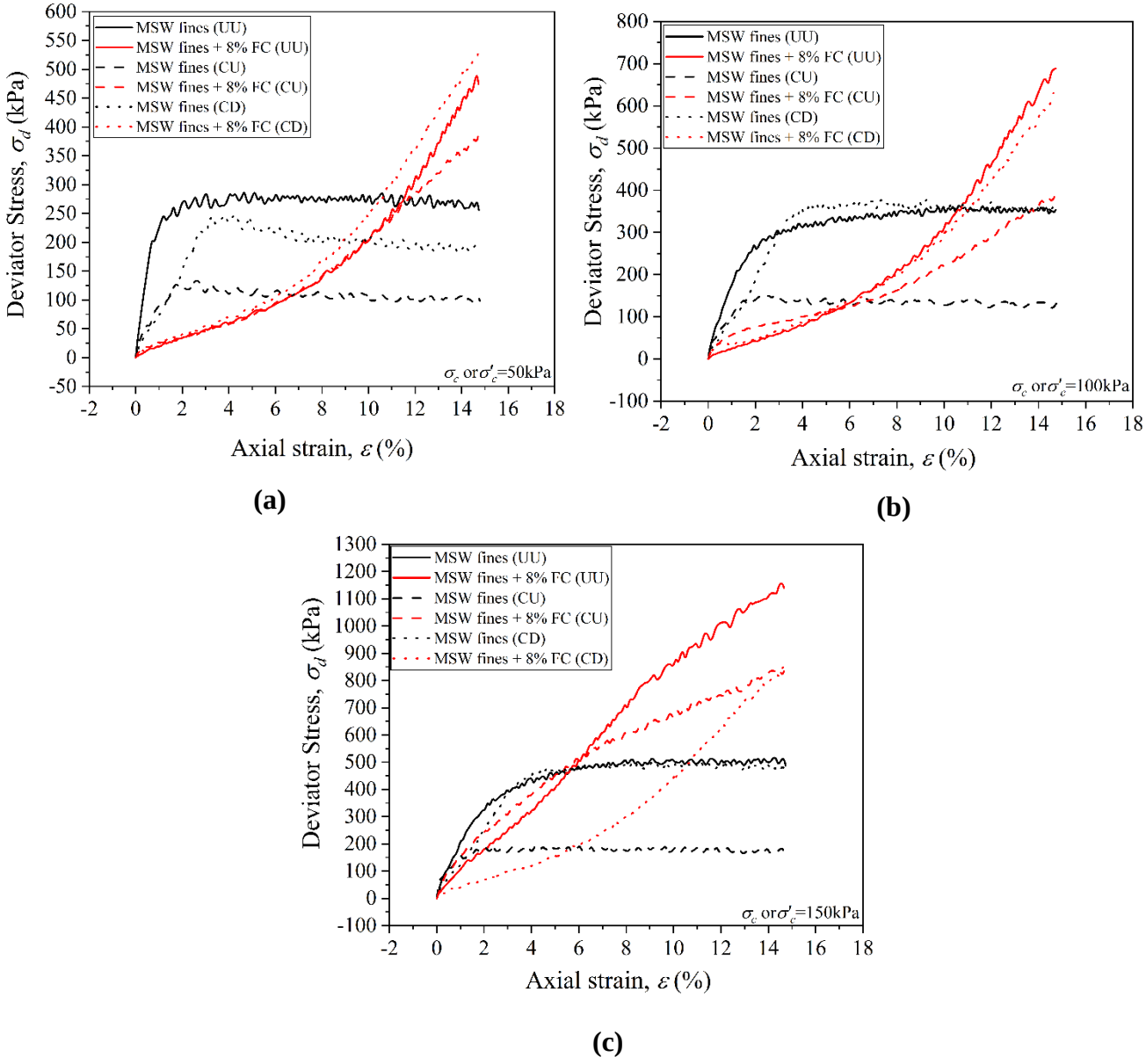

Figure 4.19 Stress-strain behaviour of the unreinforced and reinforced MSW fines with fibers under confining pressure of **(a)** 50 kPa **(b)** 100 kPa **(c)** 150 kPa

4.3 DYNAMIC LABORATORY TEST RESULTS

The laboratory dynamic test study includes the evaluation of dynamic parameters, i.e., dynamic shear modulus (G) and material damping ratio (D) through the strain-

controlled cyclic triaxial test. Additionally, the small-strain shear modulus (G_{max}) through shear wave velocity (V_s) measurement using bender element apparatus was done to propose a normalized modulus reduction (G/G_{max}) curve for the composite material. The cyclic behaviour of the considered materials, i.e., unreinforced MSW fines and reinforced MSW fines with fibers was studied. The sample preparation and methodology of the conducted test were already discussed in the previous chapter.

4.3.1 Strain-Controlled Cyclic Triaxial Test on Unreinforced MSW Fines

This section considered the dynamic study of MSW fine samples through strain-controlled cyclic triaxial test under a consolidated undrained (CU) state. The detailed testing program is provided in chapter III.

4.3.1.1 Cyclic Behaviour of Compacted MSW Fines

The cyclic behaviour of the compacted MSW fine samples in terms of variation of deviator stress, pore water pressure, and effective stress with number of cycles, and variation of deviator stress with axial strain and mean effective stress are discussed below.

4.3.1.1.1 Variation of Deviator Stress, Pore Water Pressure, and Mean Effective Stress with Number of Cycles

The cyclic behaviour of compacted MSW fines in terms of variation of deviator stress, pore water pressure and effective stress with number of cycles for the considered loading frequencies (0.3, 0.7, and 1.0 Hz), effective confining pressures (50, 70, and 100 kPa), relative compactions (90% to 98%) and cyclic shear strains (0.6%, 0.9%, 1.2%, and 1.5%) has been studied and typical plots to represent the effects of the considered parameters on cyclic behaviour has been discussed below.

Typical graphs at effective confining pressure (σ'_c) of 100 kPa, shear strain (γ) of 1.5%, loading frequency (f) of 1Hz, and relative compaction of 90% and 98% can be seen below in Figures 4.20 and 4.21. Figures 4.20(a) and 4.21a show the exponential decay of deviator stress with N (number of cycles) which is an attribute of the sample deformation. The excess PWP (pore water pressure) ratio (r_u) increases gradually with the cyclic loading (Figure 4.20(b) and 4.21(b)) until r_u=1 (i.e., Excess PWP = σ'_c) and at the same time the mean effective stress becomes zero (Figure 4.20(c) and 4.21(c).

A similar response can be seen for sands (Seed and Lee, 1966; Matasović and Vucetic, 1993; Kumar et al., 2017), that is, the cyclic load increases the PWP in saturated samples, which reduces the intergranular forces and, hence, reduces the effective stress and stiffness of the soil or MSW fine fraction.

Figure 4.20 and 4.21 shows the plots for representative samples of MSW fines at two different relative compactions 90 and 98% (i.e., density variation). The number of cycles required to fail or liquefaction of the sample at higher density would be more which is very clear from the figures. By comparing the typical graphs in Figure 4.22 for effective confining pressure (σ'_c) of 50 kPa, shear strain (γ) of 1.5%, loading frequency (f) of 1Hz, and relative compaction of 98% with Figure 4.21 for (σ'_c) of 100 kPa, it can be seen that the rate of development of pore pressure is little slow at low confining of 50 kPa (Figure 4.21(b) and 4.22(b)). The deviator stress at initial cycles may not show any major changes but the number of cycles to bear the stress has increased from 166 to 190 with an increment of σ'_c from 50kPa to 100kPa (Figure 4.21(a) and 4.22(a)). The mean effective stress starts from 50 kPa and 100 kPa according to the considered σ'_c for the sample and decreases to zero as the sample liquefies (Figure 4.21 (c) and 4.22(c)).

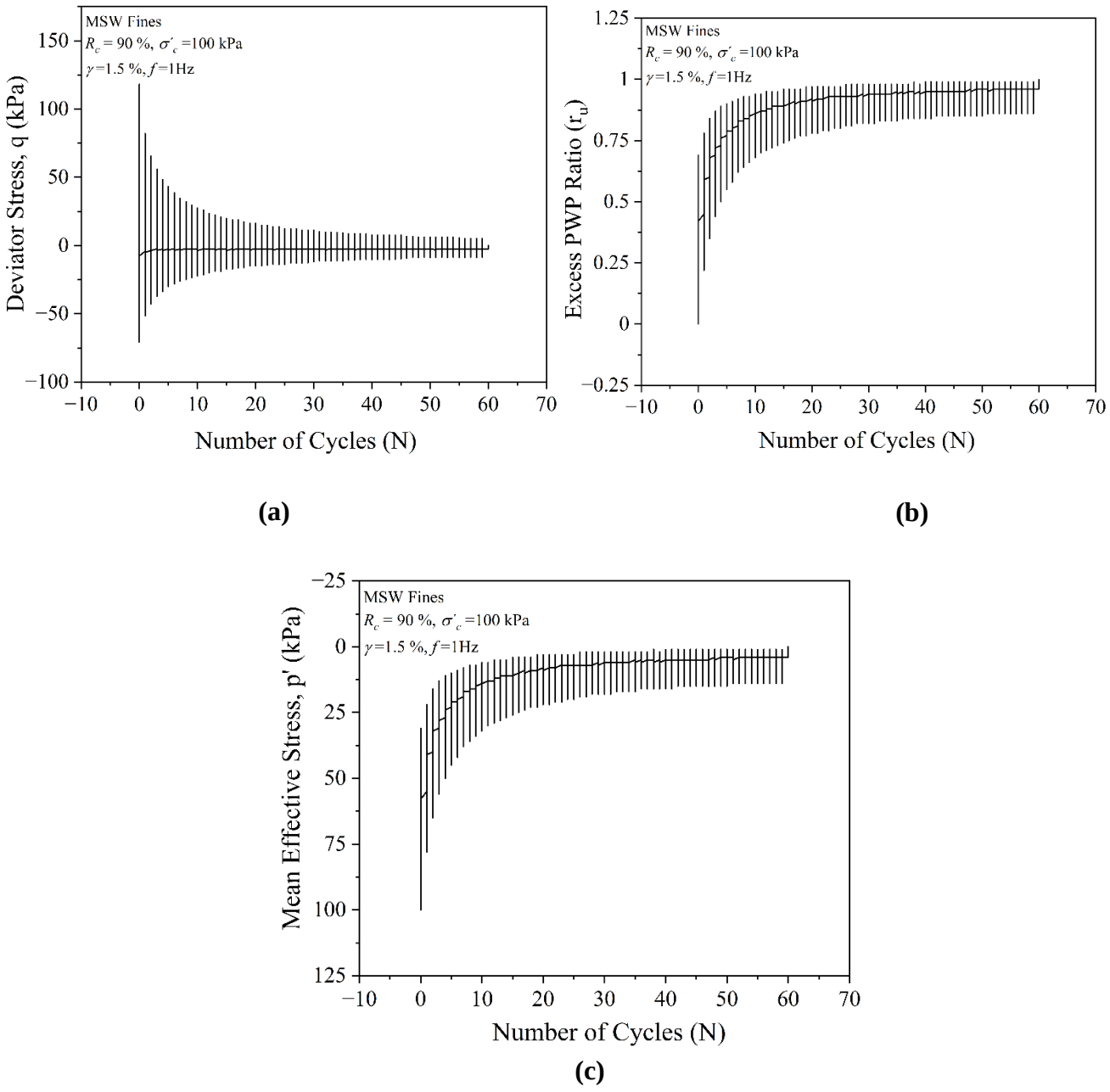

Figure 4.20 Typical test result plots at γ=1.5%, f=1 Hz, σ'_c = 100 kPa and R_c=90%: **(a)** deviator stress (q) versus number of cycles (N); **(b)** excess pore water pressure ratio (r_u) versus number of cycles (N); **(c)** mean effective stress (p′) versus number of cycles (N)

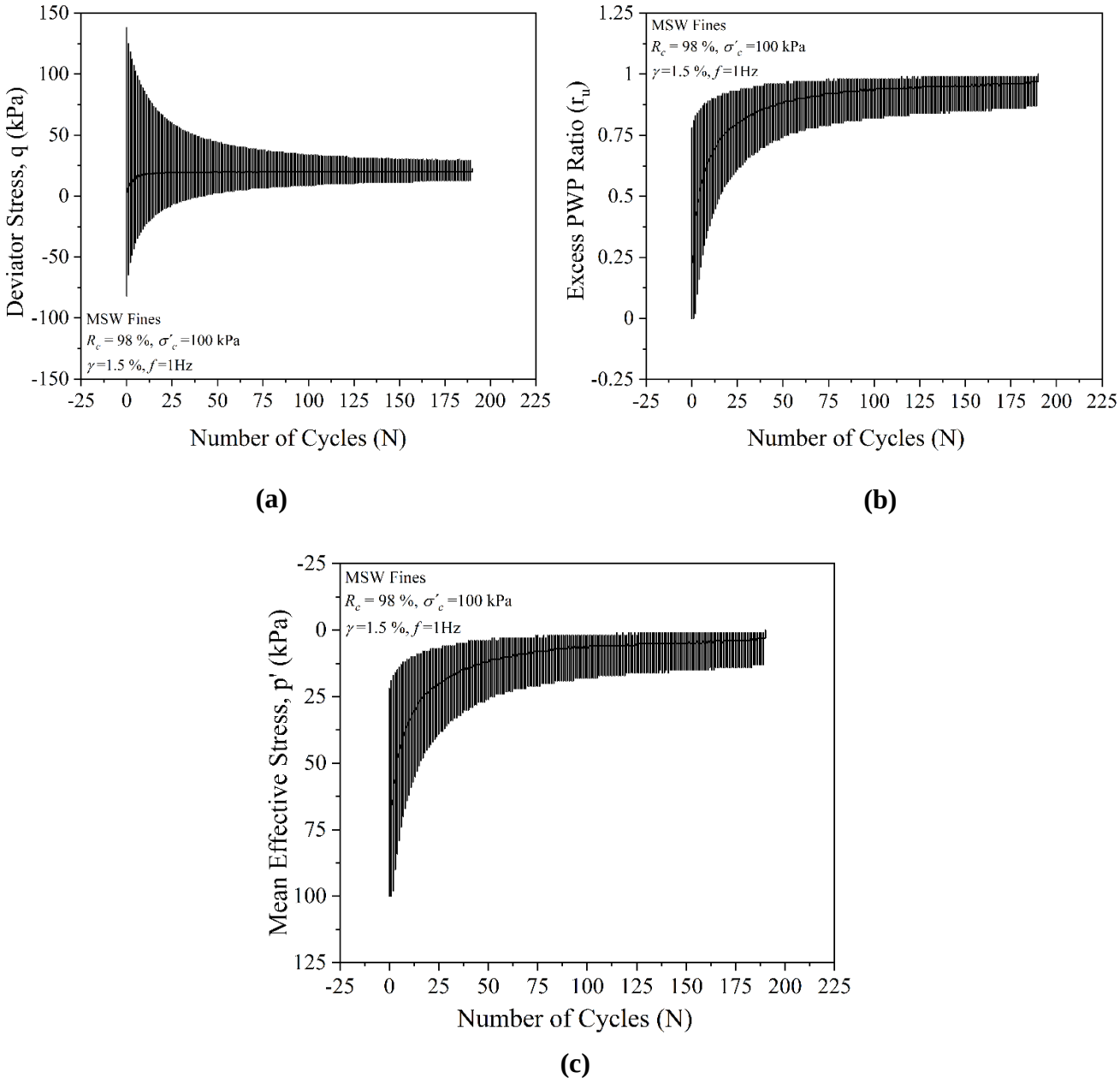

Figure 4.21 Typical test result plots at γ=1.5%, f=1 Hz, σ'_c = 100 kPa and R_c=98%: **(a)** deviator stress (q) versus number of cycles (N); **(b)** excess pore water pressure ratio (r_u) versus number of cycles (N); **(c)** mean effective stress (p′) versus number of cycles (N)

Figure 4.23 illustrate the typical graphs for effective confining pressure (σ'_c) of 100 kPa, shear strain (γ) of 1.5%, loading frequency (f) of 0.3 Hz, and relative compaction of 90% and can be compared to Figure 4.20 at f (1 Hz) for frequency change keeping other parameters constant. The rate of development of pore pressure can be seen little slow for low frequency (0.3 Hz) (Figure 4.23(b)) as compared to high frequency (1Hz) (Figure 4.20b) and causes a delay in liquefaction at f=0.3 Hz for the MSW fines sample.

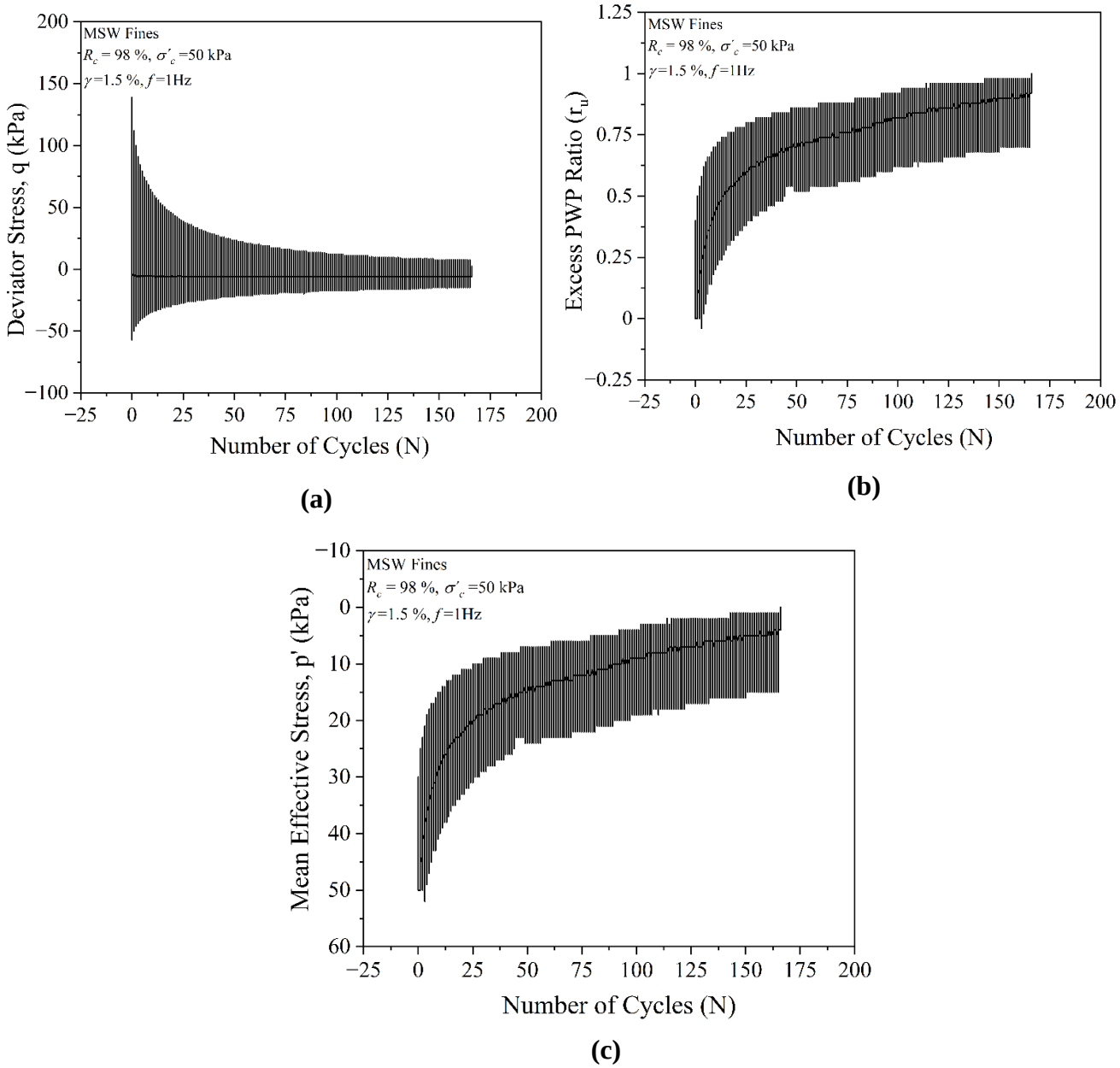

Figure 4.22 Typical test result plots at γ=1.5%, f=1 Hz, σ'_c = 50 kPa and R_c=98%: **(a)** deviator stress (q) versus number of cycles (N); **(b)** excess pore water pressure ratio (r_u) versus number of cycles (N); **(c)** mean effective stress (p′) versus number of cycles (N)

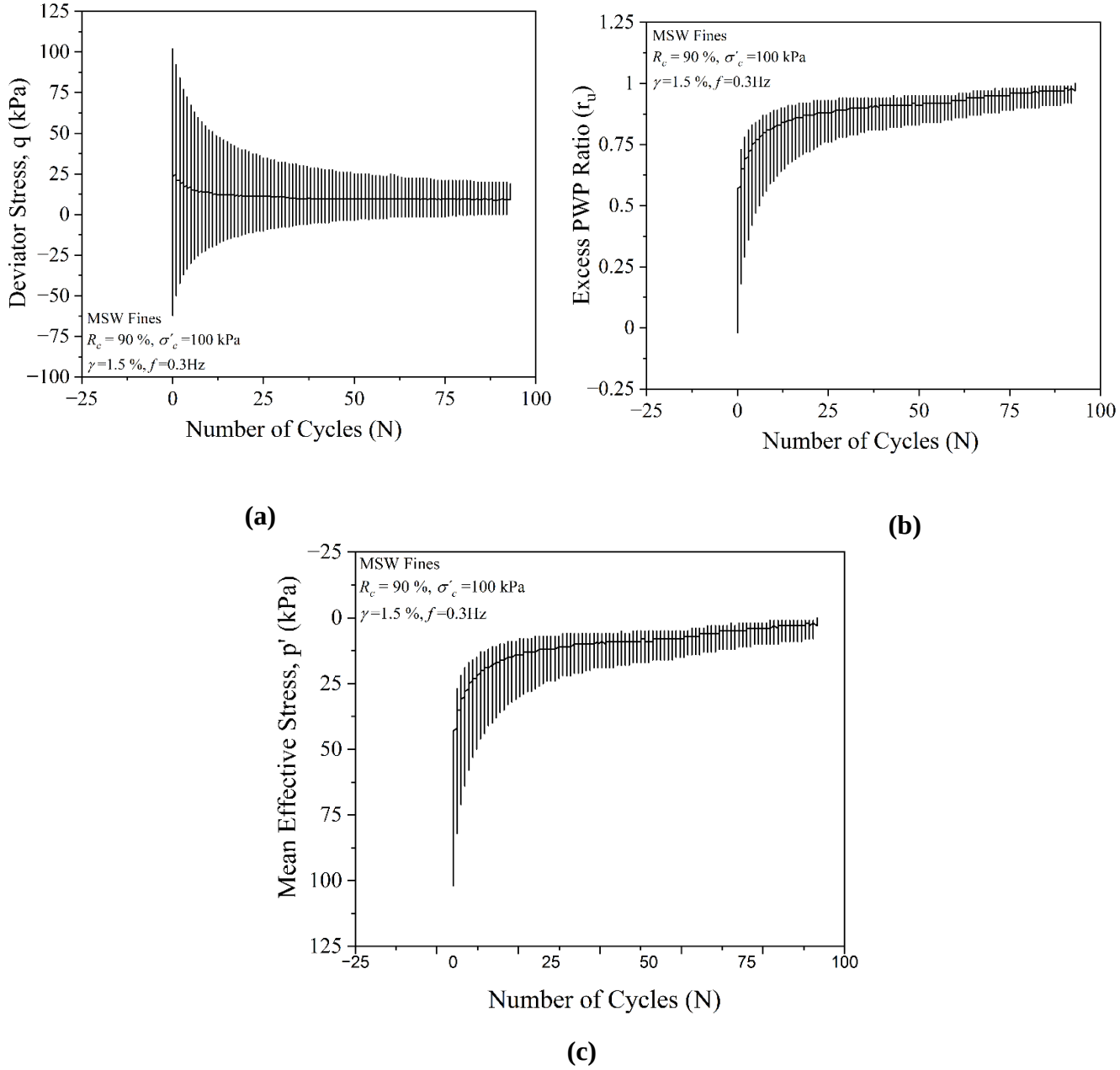

Figure 4.23 Typical test result plots at γ=1.5%, f=0.3 Hz, σ'_c = 100 kPa and R_c=90%: **(a)** deviator stress (q) versus number of cycles (N); **(b)** excess pore water pressure ratio (r_u) versus number of cycles (N); **(c)** mean effective stress (p′) versus number of cycles (N)

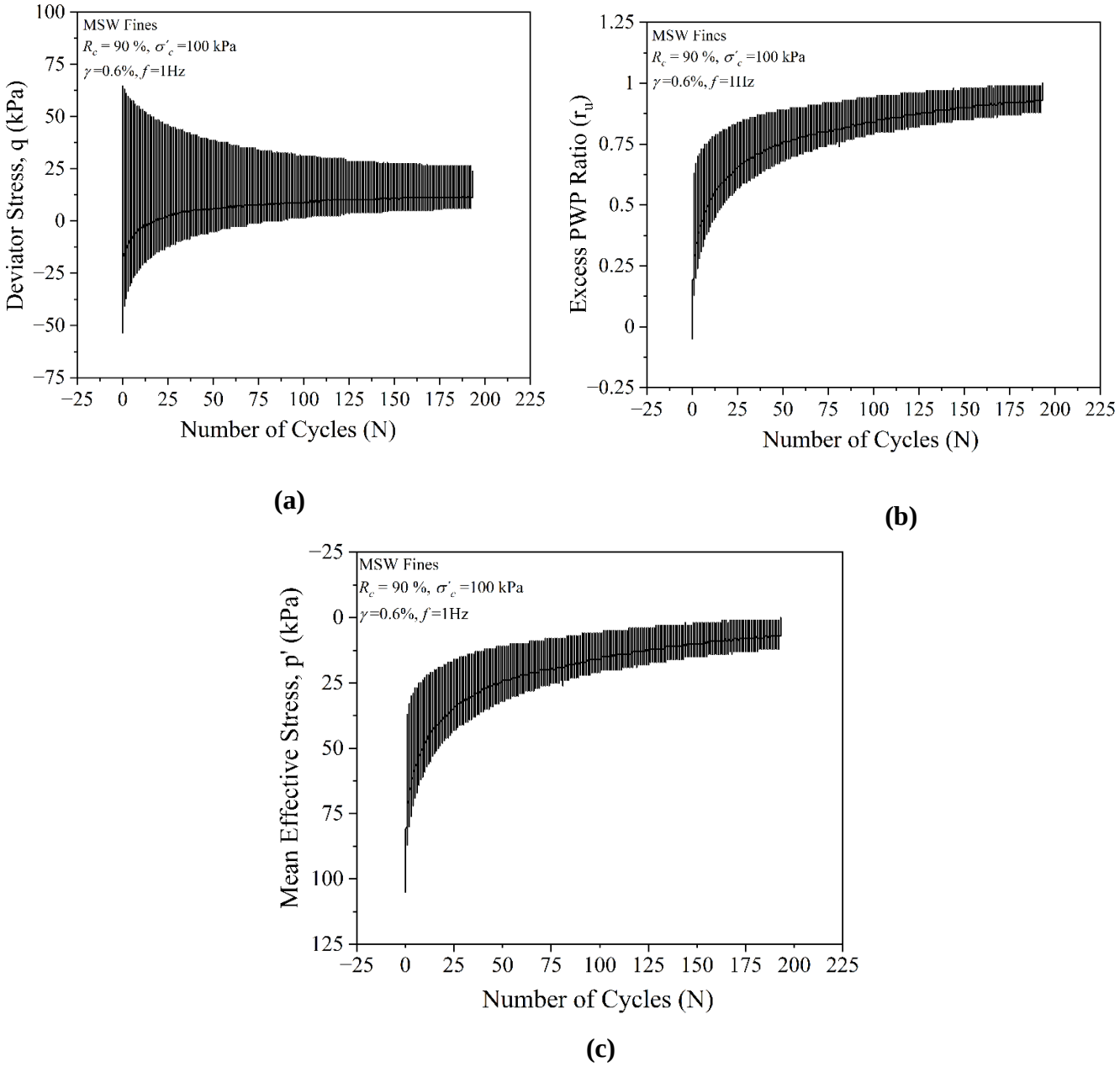

Figure 4.24 Typical test result plots at γ=0.6%, f=1 Hz, σ'_c = 100 kPa and R_c=90%: **(a)** deviator stress (q) versus number of cycles (N); **(b)** excess pore water pressure ratio (r_u) versus number of cycles (N); **(c)** mean effective stress (p′) versus number of cycles (N)

Figure4.24 illustrates the typical plots for effective confining pressure (σ'_c) of 100 kPa, shear strain (γ) of 0.6%, loading frequency (f) of 1 Hz, and relative compaction of 90% and can be compared to Figure4.20 having γ=1.5% keeping other parameters constant. The decrease in shear strain (from 1% to 0.6%) increases the deviator stress (Figure 4.20 (a) and 4.24(a)) which also increases the number of cycles for a sample to liquefy.

4.3.1.1.2 Variation of Deviator Stress with Axial Strain and Mean Effective Stress

The variation of deviator stress with axial strain and mean effective stress for the considered loading frequencies (0.3, 0.7, and 1.0 Hz), effective confining pressures (50, 70, and 100 kPa), relative compactions (90% to 98%) and cyclic shear strains (0.6%, 0.9%, 1.2%, and 1.5%) has been studied and typical plots to represent the effects of the considered parameters on the above-mentioned cyclic behaviour has been discussed below.

The typical plots for MSW fines have been shown for effective confining pressure (σ'_c) of 100 kPa, shear strain (γ) of 1.5%, loading frequency (f) of 1Hz, and relative compaction of 90% and 98% in Figure4.25 and 4.26 respectively. The hysteresis loops of the tested MSW fines become flat with the increasing number of cycles due to the increment of pore water pressure with each cycle. The slope of the hysteresis loops defines the secant or dynamic shear modulus (G), as the slope decreases the G also degrades with cycles (Figure 4.25(a) and 4.26(a)). The effective stress moves towards the left (Figure 4.25(b) and 4.26(b)) indicating a reduction in the deviator stress and means effective stress. Due to the variation in the density of samples of MSW fines at R_c (90%) and R_c (98%), the range of deviator stress can be seen as large for higher R_c, i.e., 98%.

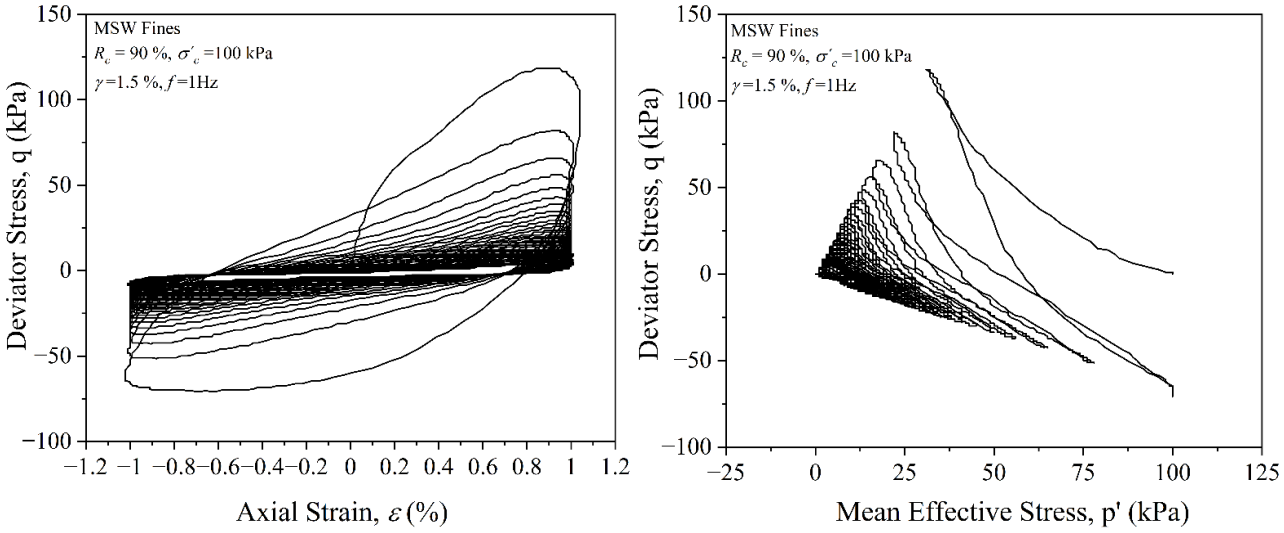

(a) **(b)**

Figure 4.25 Typical test result plots at γ=1.5%, f=1 Hz, σ'_c = 100 kPa and R_c=90%: **(a)** deviator stress (q) versus axial strain (ε); **(b)** deviator stress (q) versus mean effective stress (p′)

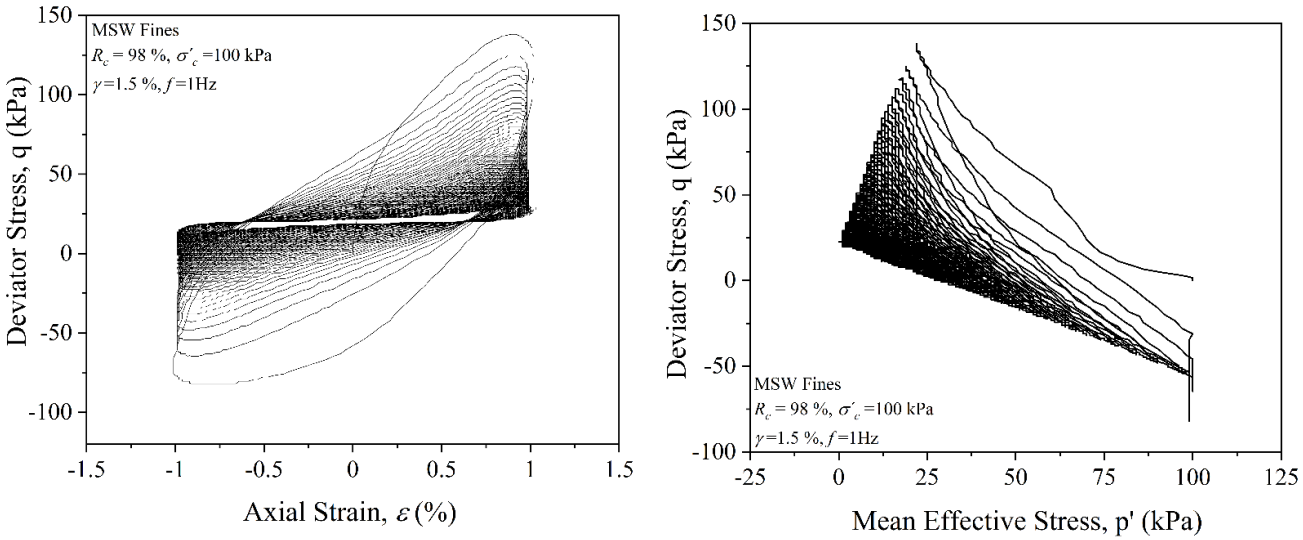

(a) **(b)**

Figure 4.26 Typical test result plots at γ=1.5%, f=1 Hz, σ'_c = 100 kPa and R_c=98%: **(a)** deviator stress (q) versus axial strain (ε); **(b)** deviator stress (q) versus mean effective stress (p′)

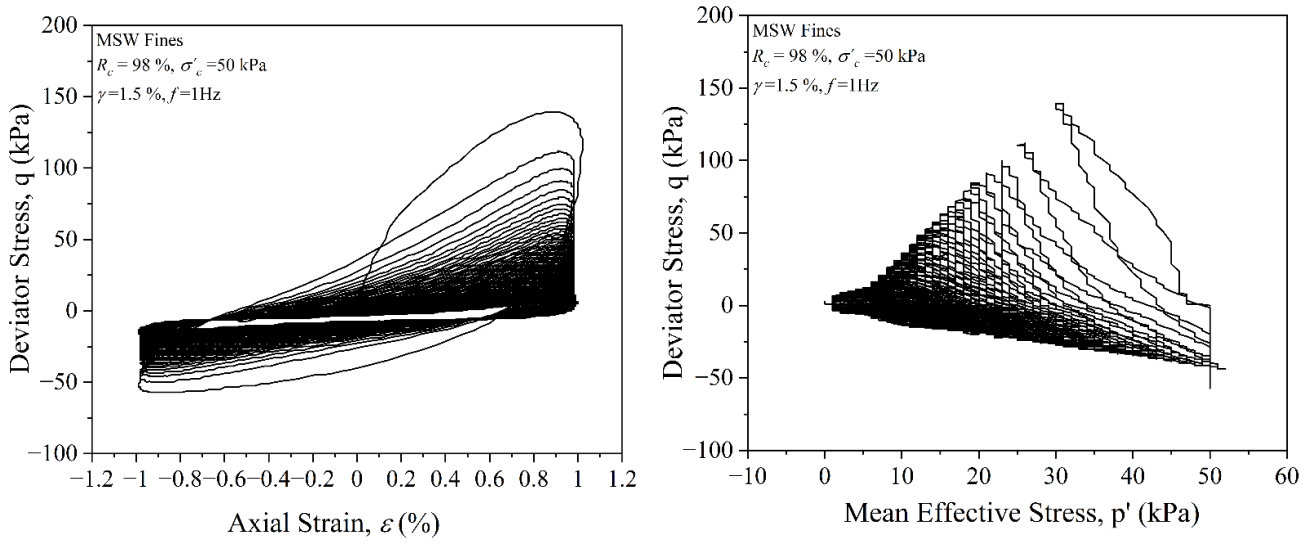

(a) **(b)**

Figure 4.27 Typical test result plots at γ=1.5%, f=1 Hz, σ'_c = 50 kPa and R_c=98%: **(a)** deviator stress (q) versus axial strain (ε); **(b)** deviator stress (q) versus mean effective stress (p′)

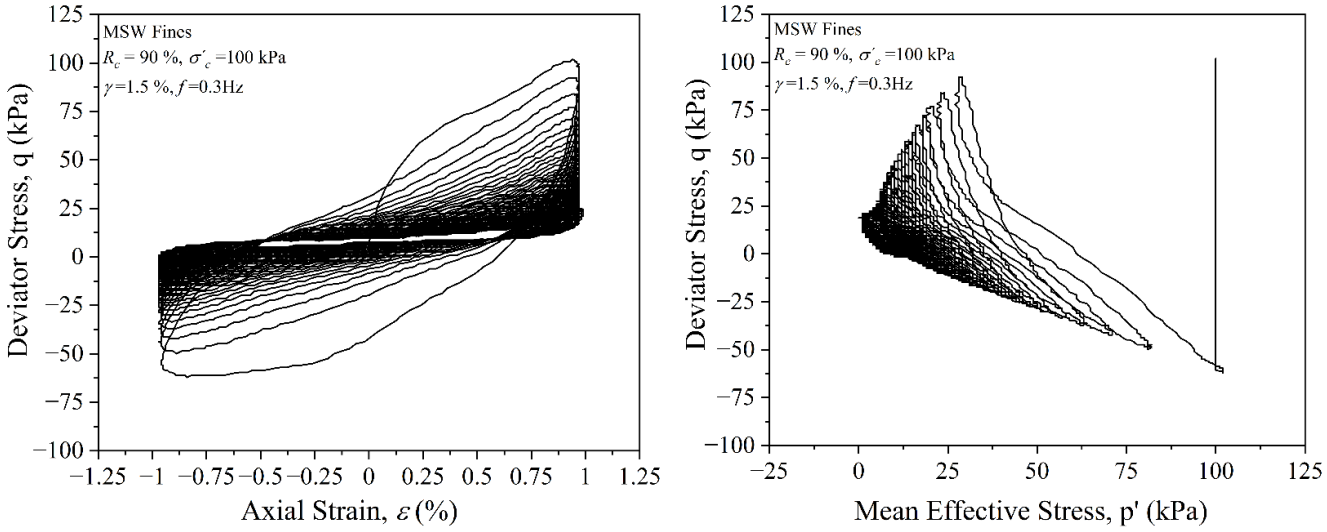

(a) **(b)**

Figure 4.28 Typical test result plots at γ=1.5%, f=0.3 Hz, σ'_c = 100 kPa and R_c=90%: **(a)** deviator stress (q) versus axial strain (ε); **(b)** deviator stress (q) versus mean effective stress (p′)

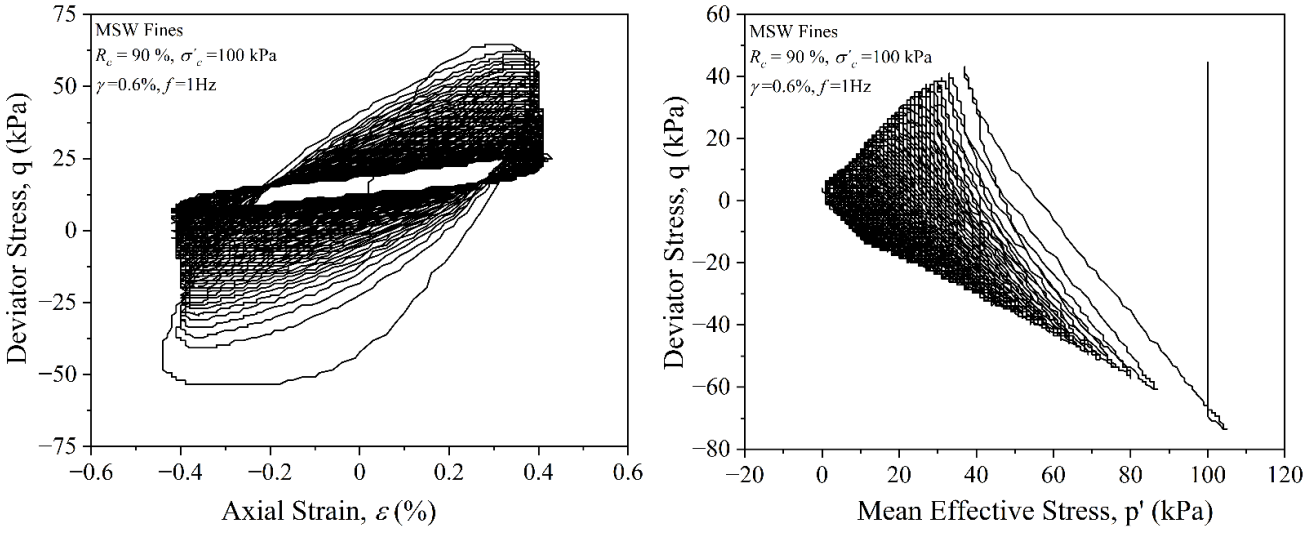

(a) **(b)**

Figure 4.29 Typical test result plots at γ=1.5%, f=0.3 Hz, σ'_c = 100 kPa and R_c=90%: **(a)** deviator stress (q) versus axial strain (ε); **(b)** deviator stress (q) versus mean effective stress (p′)

Figure 4.27 illustrate the typical graphs for effective confining pressure (σ'_c) of 50 kPa, shear strain (γ) of 1.5%, loading frequency (f) of 1 Hz, and relative compaction of 98% and can be compared to Figure 4.26 at σ'_c of 100 kPa for confining pressure changes keeping other parameters constant. Although there are no significant changes can be seen in the deviator stress range with the change in confining pressure, the rate of degradation of the slope of hysteresis loops is more rapid at low σ'_c of 50 kPa (Figure 4.27(a)) as compared to σ'_c of 100 kPa (Figure 4.26(a)). The mean effective stress shifted towards the left as discussed earlier until it becomes zero as the sample also fails and was unable to take a further load and deviator stress also collapse to zero (Figure 4.26(b) and 4.27(b)).

Figure 4.28 illustrate the typical graphs for effective confining pressure (σ'_c) of 100 kPa, shear strain (γ) of 1.5%, loading frequency (f) of 0.3 Hz, and relative compaction of 90% and can be compared to Figure 4.25 at f of 1 Hz for frequency effect changes keeping

other parameters constant. The changes in the deviator stress are not significant with the change in frequency from 1Hz to 0.3Hz.

Figure4.29 illustrate the typical graphs for effective confining pressure (σ'_c) of 100 kPa, shear strain (γ) of 0.6%, loading frequency (f) of 1 Hz, and relative compaction of 90% and can be compared to Figure 4.25 at (γ) of 1.5% to check the shear strain effect keeping other parameters constant. At a low shear strain of 0.6% (Figure 4.25(a)) the hysteresis loop is more inclined as compared to the considered sample tested at γ(1.5%) (Figure 4.29(a)). The inclination of the loop also indicates the stiffness of the material, i.e., the greater the slope greater the stiffness.

4.3.1.2 Liquefaction Potential of Compacted MSW Fines

When the developed maximum excess pore water pressure equals the initially applied confining pressure, the initial liquefaction occurs. The developed excess pore water pressure reaches 100% in this condition. The failure criterion for all samples is defined as the number of loading cycles required to develop 100% excess pore water pressure. The effect of effective confining pressure, relative compaction, shear strain, and loading frequency has been analyzed. The typical plots to show the effect of the considered parameters have been discussed below.

The effect of relative compaction on the liquefaction potential of the compacted MSW fines is shown in Figure 4.30 for all R_c (90 to 98%) at three shear stains (γ) 0.6, 0.9 and 1.5% keeping frequency (f) and effective confining pressure (σ'_c) constant, i.e., at 1 Hz and 100 kPa respectively. The trends of initial cycles of liquefaction (N_L) can be seen increasing with the relative compaction variation from 90% to 98%. In the same plot, it can be observed that the shear strain is inversely proportional to the initial cycles of liquefaction (N_L) and liquefaction resistance.

Comparing the lowest (90%) and the highest (98%) relative compaction the no. of initial liquefaction cycles increases from 193 to 367 (at γ=0.6%), i.e., an increase of 174 cycles; 152 to 245 (at γ=0.9%), i.e., increase of 93 cycles; and 60 to 190 (at γ=1.5%), i.e., increase of 130 cycles.

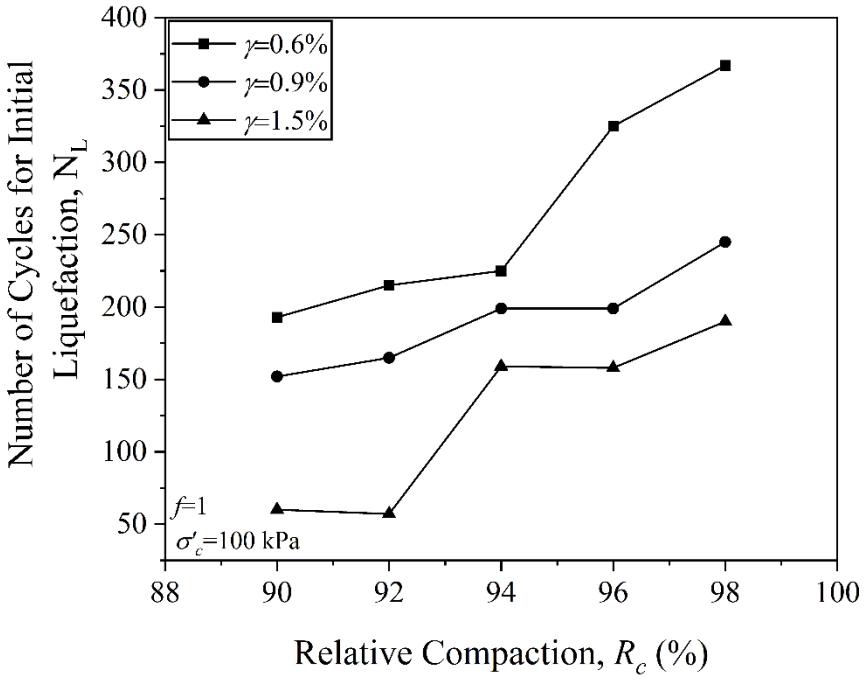

Figure 4.30 Effect of relative compaction (R_c) on liquefaction potential of compacted MSW fines

The effect of confining pressure (σ'_c) on the liquefaction potential of compacted MSW fines is shown in Figure 4.31 at three shear stains (γ) 0.6, 0.9, and 1.5% keeping frequency (f) and relative compaction (R_c) constant at 1 Hz, and 98% respectively. The cycle for initial liquefaction increases as the confining pressure increase from 50 to 100 kPa, and this is true as the load-carrying capacity of the sample increases when the lateral confinement increases. The number of initial liquefaction cycles increases from 179 to 367 when σ'_c increases from 50 kPa to 100 kPa at γ(0.6%), 192 to 245 at γ(0.9%), and 166 to 190 at γ(1.5%). The difference in the number of initial liquefaction cycles at the considered lowest (50 kPa) and highest (100 kPa) σ'_c can be seen more at low shear strain (0.6%).

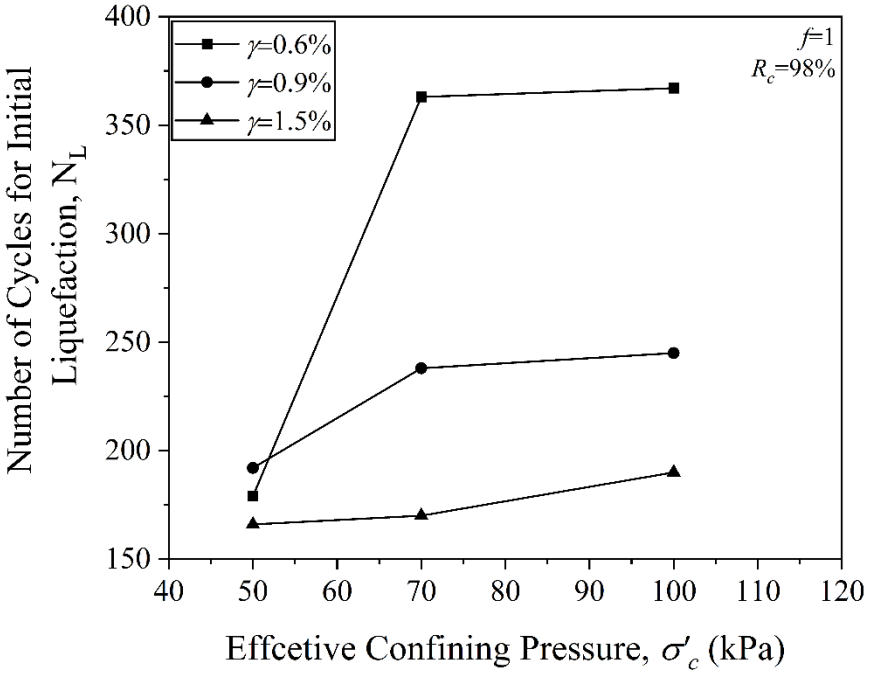

Figure 4.31 Effect of effective confining pressure (σ'_c) on liquefaction potential of compacted MSW fines

The effect of the frequency on the initial liquefaction cycles cannot be predicted considering loading frequencies (*f*) of 0.3,0.5, and 1Hz for the present study. The trends were too random to produce any concluding remarks on the effect of loading frequency on the liquefaction potential of compacted MSW fines.

4.3.1.3 Dynamic Properties of Compacted MSW Fines

It includes the study of dynamic properties (dynamic shear modulus (G) and damping ratio (D)) of MSW fines and the effect of different parameters (relative compaction, strain, frequency, and effective confining pressure) on these dynamic properties.

4.3.1.3.1 Effect of Loading Frequency on Dynamic Properties of Compacted MSW Fines

The considered MSW fine fraction samples were tested under three frequencies (0.3, 0.5, and 1 Hz). The effect of the loading frequency was studied by keeping the other

parameters constant (relative compaction and effective confining stress). The results are illustrated in Figure 4.32. It can be seen in Figure 4.32(a and b) that G and D decrease with the increase in N for all the frequencies at R_c = 96%, σ'_c = 100 kPa, and γ= 1.5%. The difference in the initial cycles is low, but it eventually increases with the number of cycles. Figure 4.32(c) clearly illustrates that there is a little increment in the dynamic shear modulus (G) with frequency at lower compaction values or almost no change in higher compaction values. However, not many conclusions can be made for the damping ratio in Figure 4.32(d) but in general, the trends are increasing. The studies in the past also show an almost negligible effect of frequency on the dynamic parameters of the soil and MSW as discussed below.

Keramati et al. (2018) illustrated that the shear modulus and damping ratio increase and decrease (very small), respectively, with the increment in loading frequency from 0.1 to 0.5 Hz. Towhata (2008) mentioned no significant influence of frequency on the dynamic parameters and justified this by comparing MSW material to clayey or paste material. Kumar et al. (2013) have done an extensive review of the parameters influencing dynamic soil (mostly non-cohesive) properties and concluded that the frequency of cyclic load does not significantly influence the shear modulus, but the damping ratio was significantly influenced.

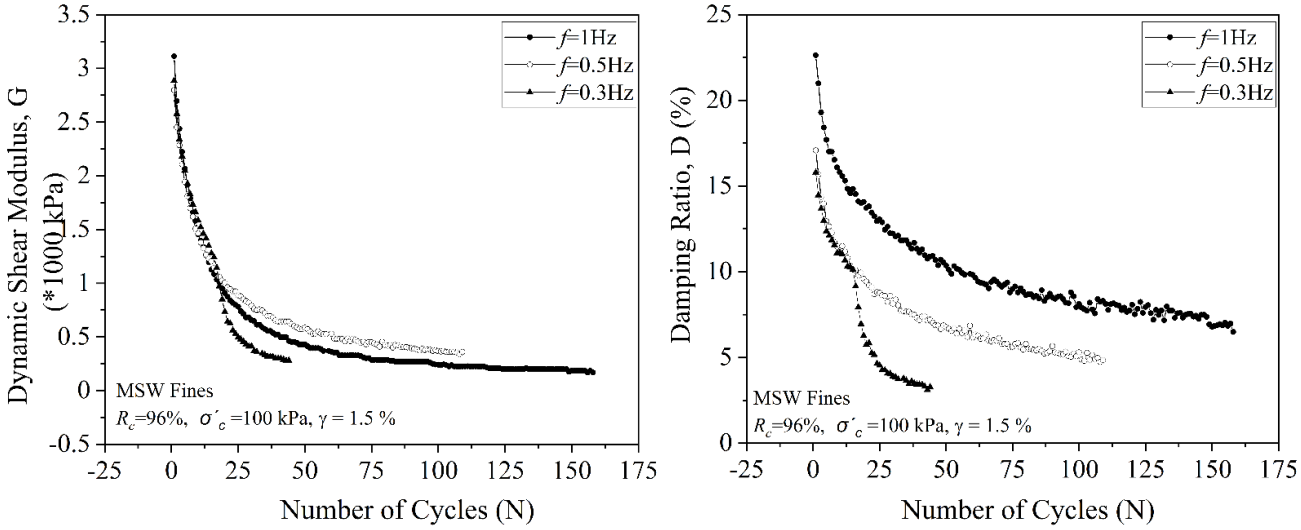

(a) **(b)**

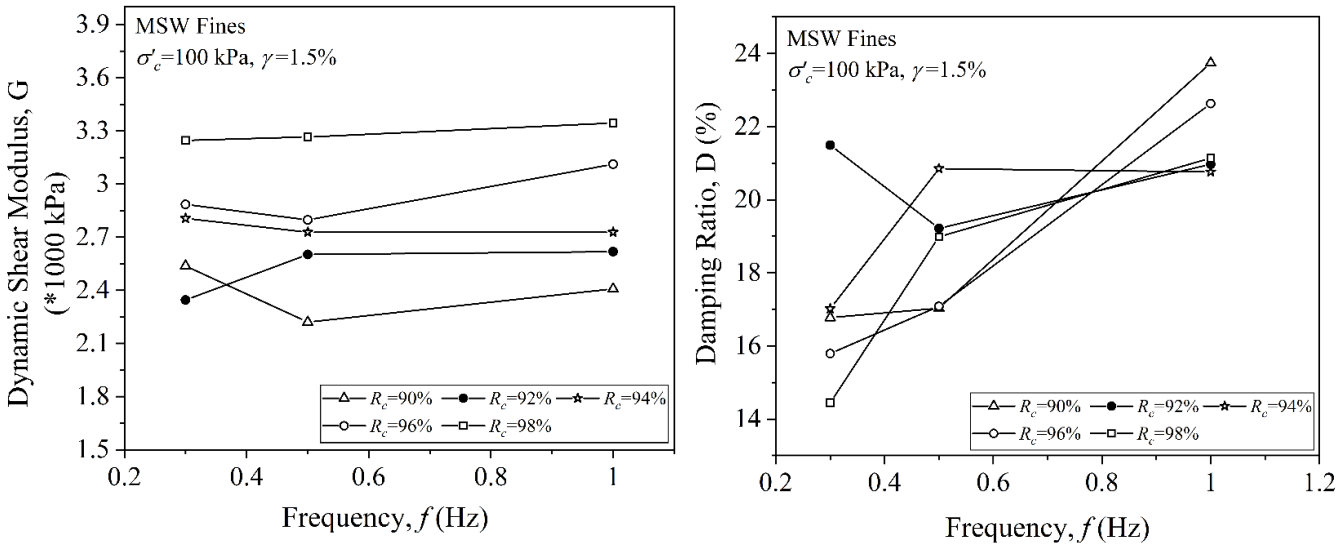

(c) **(d)**

Figure 4.32 Variation of **(a)** dynamic shear modulus (G); and **(b)** damping ratio (D) with number of cycles (N) for different frequency (*f*), variation of **(c)** dynamic shear modulus (G); and **(d)** damping ratio (D) with frequency (*f*) for different R_c corresponding to σ'_c = 100 kPa and γ=1.5%

4.3.1.3.2 Effect of Confining Pressure on Dynamic Properties of Compacted MSW Fines

The samples of considered MSW fine fractions were tested under three series of confining pressures, i.e., 50, 70, and 100 kPa. Considering the application of MSW fine fractions in the backfill/embankment fill material (approximately 5m to 10 m height), the effective confining pressure of 50 kPa, 70 kPa, and 100 kPa has been considered here. So, the in-situ confining pressure condition can be simulated in the laboratory environment. Most of the research related to the dynamic characterization of MSW has also considered confining pressure range from 25 to 100 kPa or 150 to 200 kPa (Zekkos et al. 2008; Keramati et al. 2018). It is clear from Figure 4.33(a) that there is a considerable increment in the dynamic shear modulus (G) of the MSW fine fractions with the increase in confining stress. Figure 4.33(a and b) shows the typical plots of G and D with number of cycles (N) for 96% R_c. Figure 4.33(c and d) shows the plots of G and D with effective confining stress at different R_c. Figure 4.33(c) also confirms the increment in G with the increase in

confining stress for all the R_c. However, it does not have any significant effect on the damping ratio (D), and no conclusion can be made from Figure 4.33(d). Due to the increment in confining pressure, there will be a contraction of air voids by which MSW fine particles draw closer, which results in better interlocking between the particles. This results in an increase in the shear modulus of the MSW fine fractions. The increment in the value of G with confining pressure was also stated in other studies on MSW (Zekkos et al. 2008; Keramati et al. 2018; Towhata and Uno 2008; Naveen et al. 2014a; Ramaiah et al. 2016b) whereas for damping ratio no such major changes were observed in the past studies. The variations in the shear modulus and damping ratio in different studies are mainly due to the composition of the waste, which influences every parameter, and, hence, different wastes cannot be treated as the same, but they can be compared.

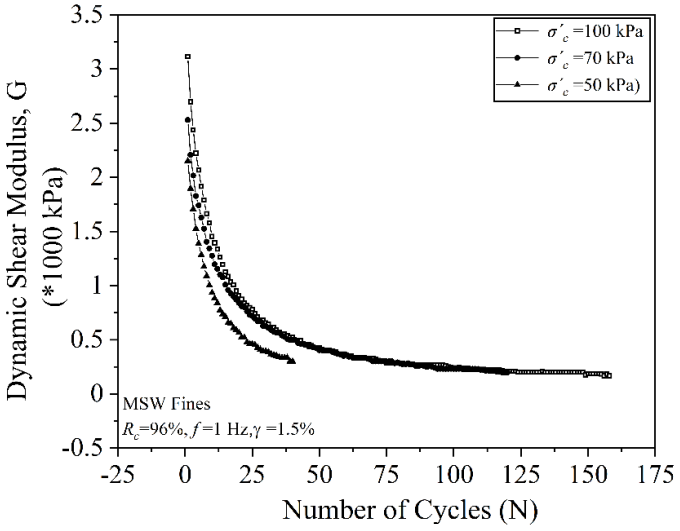

(a)

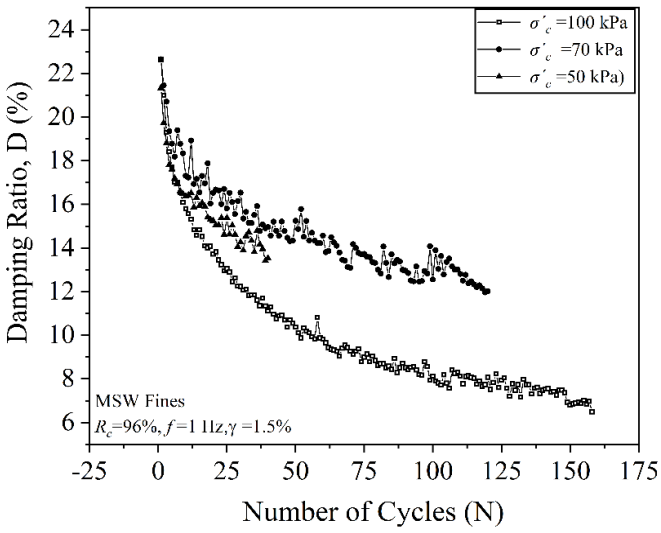

(b)

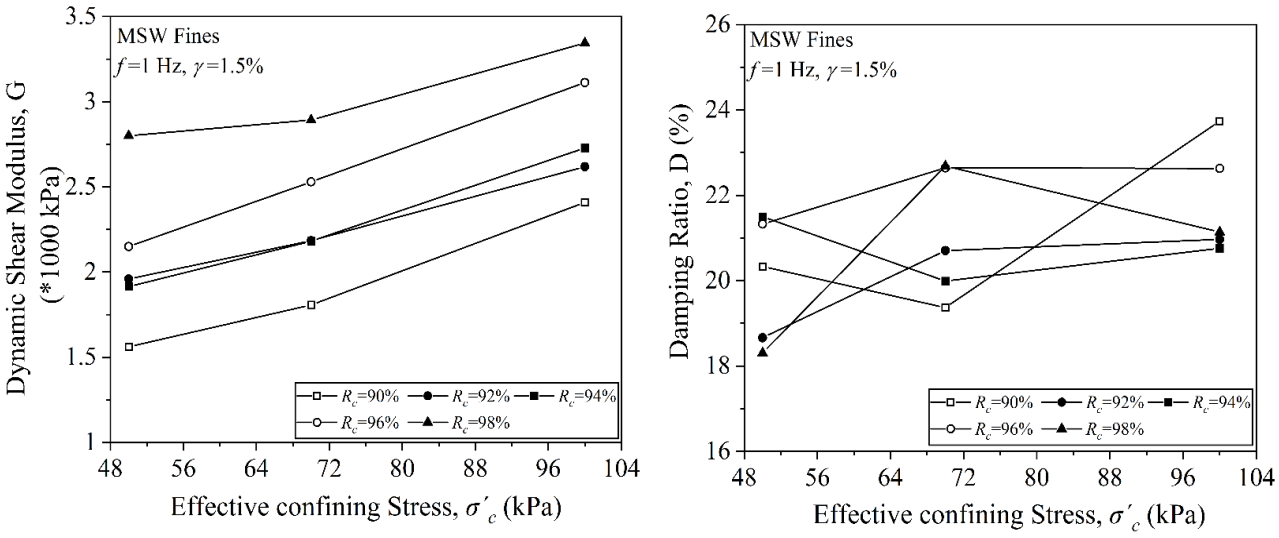

Figure 4.33 Variation of **(a)** dynamic shear modulus (G); and **(b)** damping ratio (D) with number of cycles (N) for different σ'_c, variation of **(c)** dynamic shear modulus (G); and **(d)** damping ratio (D) with σ'_c for different R_c corresponding to f=1 Hz and γ=1.5%

4.3.1.3.3 Effect of Relative Compaction on Dynamic Properties of Compacted MSW Fines

The relative compaction (R_c) and the particle density influence the unit weight of the MSW fine fractions. The cyclic triaxial test (CTT) setup has been discussed in the previous section and the samples were prepared at five different relative compactions. The field studies indicate that unit weight increases with the depth, and the shear wave velocity profile also shows an increment in V_s with depth, which concludes that the unit weight or relative compaction is an important influencing parameter for dynamic properties of MSW (Zekkos et al. 2010c). A typical case corresponding to f=1 Hz, σ'_c = 100 kPa, and γ=1.5% is shown in Figures 4.34(a and b), both the dynamic shear modulus and damping ratio decrease with the increase in N for all the considered relative compactions (R_c). As with the increase in unit weight, the compaction effort also increases, due to which stiffness of the MSW fine fractions increases, which can be observed in Figure 4.34(c) as the R_c increases the G value (for the 1st cycle) increases. The increment in G value between two

R_c values is almost less than 10%. However, the overall increment in G value is around 38.9%, with an increase in R_c from 90% to 98%. On the other hand, there could not be seen any significant trends for the damping ratio (Figure 4.34(d)). This may be because of the heterogeneity, physicochemical, and morphological characteristics of the MSW fine fractions. Past studies on MSW and fibrous waste show the unclear effect of unit weight on the damping ratio (D) or a less important influencing factor in the study of damping ratio (Zekkos et al. 2008; Alidoust et al. 2018).

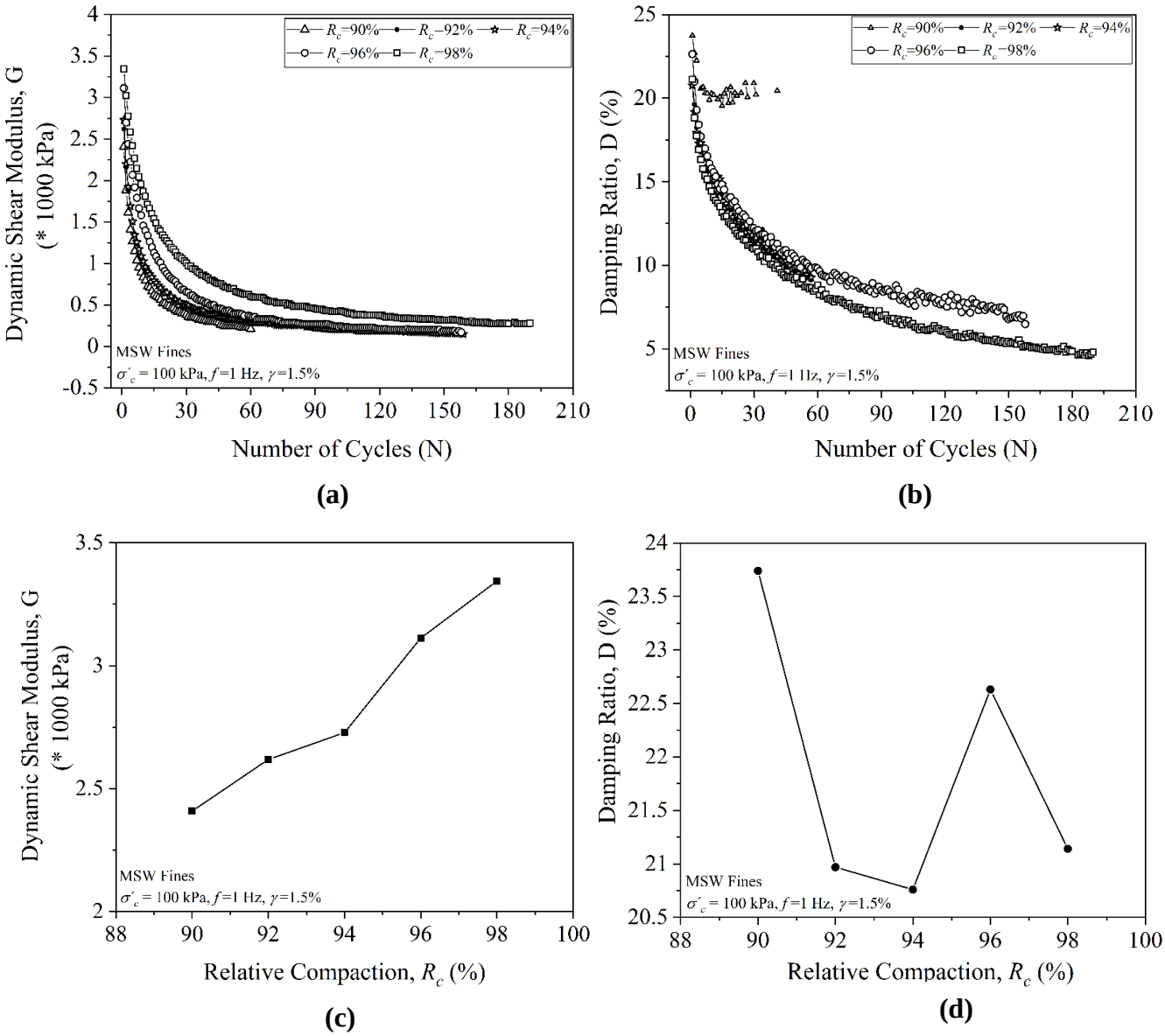

Figure 4.34 Variation of **(a)** dynamic shear modulus (G); and **(b)** damping ratio (D) with number of cycles (N) for different R_c, variation of **(c)** dynamic shear modulus (G); and **(d)** damping ratio (D) with R_c corresponding to f =1 Hz, σ'_c = 100 kPa, and γ=1.5%

4.3.1.3.4 Effect of Strain Amplitude on Dynamic Properties of Compacted MSW Fines

Figure 4.35 shows the variation of G and D with strain (high shear strain range). It can be observed from Figure 4.35(a and c) that shear modulus decreases with the increment in shear strain and that is also confirmed by other studies. It is not easy to predict the behaviour of the damping ratio of MSW fine fractions with shear strain from the results provided in Figure 4.35(b and d); even the data points are insufficient to make any conclusive remarks. However, in general, the trends of damping ratio are declining, which is the reverse of many past studies. The frequency influence of *G* and *D* is shown in Figure 4.35(e and f). It can be observed that with the change in frequency, there is a very small change in *G* values and the change in *D* values are also not significant. Zekkos et al. (2005, 2010c) from their many studies on MSW mentioned that loading frequency has no significant role in G/G_{max} versus γ and D versus γ curves. Towhata et al. (2004) observed that the damping ratio increases and shear modulus decrease with the increase in strain range (axial strain: 0.1 to 0.3%) for artificially made organic waste. Keramati et al. (2018) observed similar kind of results in an axial strain range of 0.05 to 2.5%, where 70% of the waste was of organic and paste-like material. Many other researchers also reported the same from inversion, field, or laboratory testing for the shear strain of a maximum of up to 2% (Idriss et al. 1995; Gunturi 1996; Morochnik et al. 1998; Augello et al. 1998; Zekkos et al. 2008; Keramati et al. 2016; Ramaiah et al. 2016a). The results presented for the damping ratio may not coincide with the past studies but, it can be tried to be justified because of its composition. In the present study, only a selected part of the waste was used from which all the coarse material was removed, and the sample was almost silty sand. The other major reason could be that the tests were conducted at higher strains, whereas most of the studies were conducted at low strains (up to 1%). The studies conducted on soils show that the response of soils at high strain is somewhat different from that at low stains, primarily due

to the nonlinear stress–strain behaviour and damping characteristics at higher strains (Ishihara 1996). Kumar et al. (2017) also found very contradictory results for non-cohesive soils, where the damping ratio shows an increment with strain up to a certain limit of γ =0.5% or in some cases 1% and then decreases at high strain values. Similar evidence was found in another few studies also (Matasović and Vucetic 1993; Kiku and Yoshida 2000).

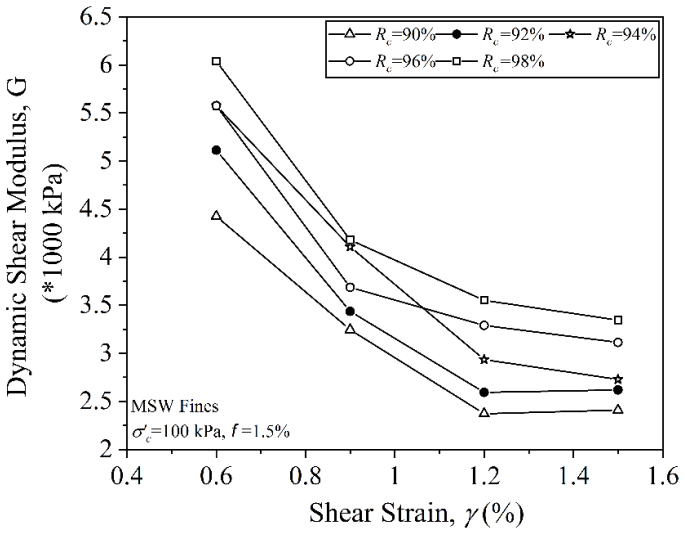

(a)

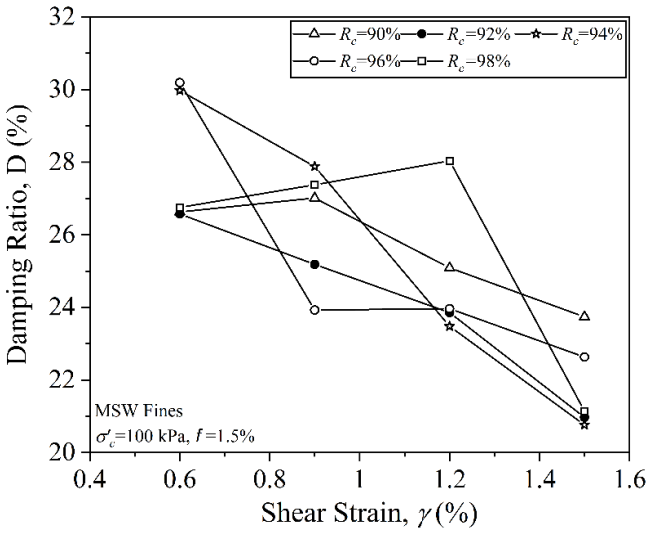

(b)

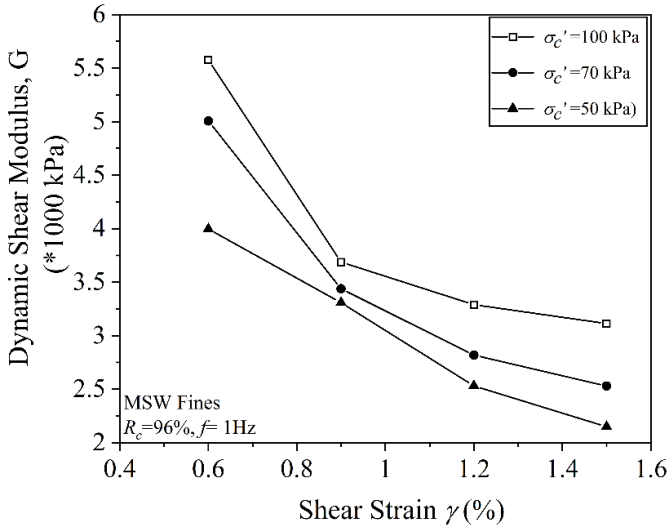

(c)

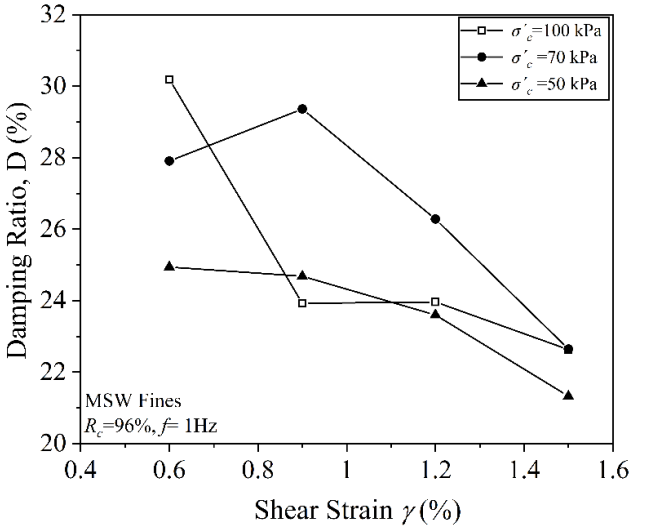

(d)

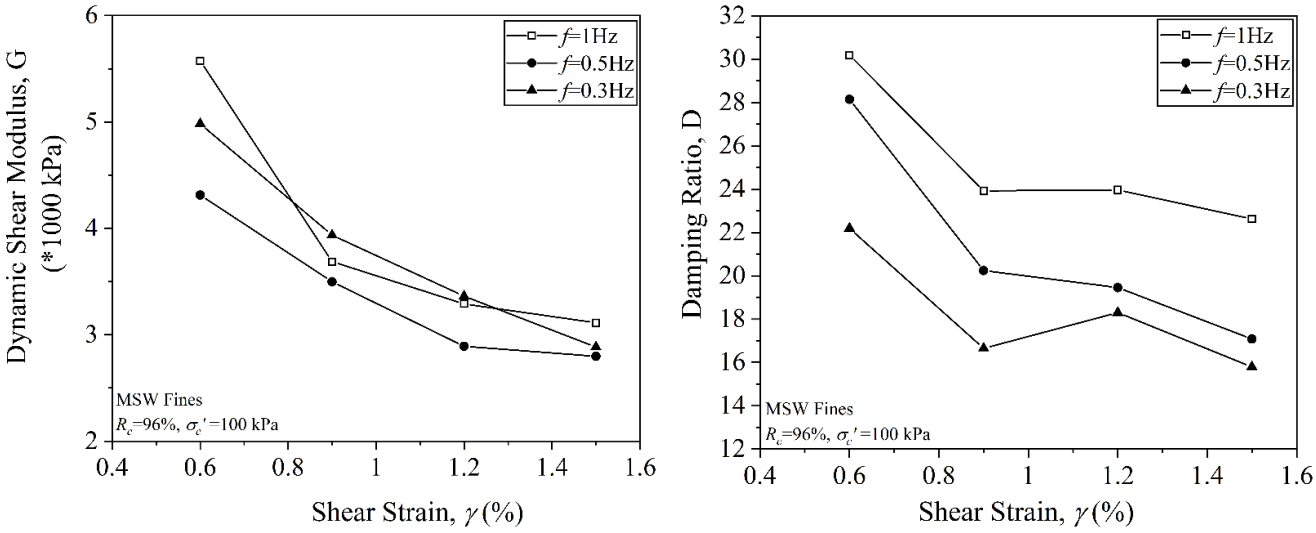

(e) **(f)**

Figure 4.35 Variation of **(a)** dynamic shear modulus (G); and **(b)** damping ratio (D) with the shear strain (γ) for different R_c corresponding to σ'_c = 100 and f=1 Hz, variation of **(c)** dynamic shear modulus (G); and **(d)** damping ratio (D) with the shear strain (γ) for different σ'_c corresponding to f =1 Hz and R_c =96%, variation of **(e)** dynamic shear modulus (G); and **(f)** damping ratio (D) with the shear strain (γ) for different frequency (f) corresponding to R_c =96%

Most of the past dynamic studies conducted on soils are on non-cohesive sand or sand mixed with fines (silt), which can be compared with the present study results of MSW fine fractions. A brief comparison of the effect of different parameters on the dynamic properties of the MSW fines and sand is shown in Table 4.11. In the case of MSW fines, the composition of the waste is the most significant parameter, whereas, for sand, the variation of silt content has no significant effect on dynamic parameters. In the case of non-plastic cohesionless soils such as sand, the confining pressure and relative density are the important parameters that influence the shear modulus of the soil. Loading frequency has a less significant influence in the case of MSW fines, but it significantly affects the damping ratio of sand.

Table 4.11 Effect of different parameters on the dynamic properties of MSW fine fractions and sand.

Materials	Parameters				Small-strain shear modulus, G_{max}	Shear modulus, (G)	Material Damping	References
	Composition/ Percentage fines	Confining stress	Unit weight/ Relative density	Loading frequency				
MSW	X				Most important	-	Most important	Zekkos et al., 2008
		X			Important	-	Likely important	
			X		Important	-	Not important	
				X	Less important	-	Not important	
Sand	X				-	Not significantly affected	Decrease with increment in percentage fine	Hanumantharao and Ramana, 2008
		X			-	Significantly affected (increase with increment in confining pressure)	Significantly affected (decrease with increment in confining pressure)	Sitharam et al., 2004; Tatsuoka et al., 1978; Iwasaki et al., 1978; Kokusho, 1980; Lin et al., 1996; Feng et al., 2000
			X		-	Moderate effect	No significant effect	Maheshwari et al., 2012a
				X	-	Not significantly affected	Significantly affected (increase with increment in loading frequency)	GovindaRaju, 2005; Kumar et al., 2013

4.3.1.4 Degradation Index of Compacted MSW Fines

The degradation index (δ) is defined as the dynamic shear modulus of the N^{th} cycle (G_N) to the dynamic shear modulus of the first cycle (G_1) (Equation 4.3) (Idriss et al. 1978). The degradation phenomenon also represents the decrease in the shear modulus of the sample with the increases in loading cycles (Dobry and Vucetic 1987).

$$\delta = \frac{G_N}{G_1} \tag{4.3}$$

The degradation rate of the dynamic shear modulus of the considered MSW fines is represented through the typical plots to show the effect of different parameters on the material loss in strength concerning number of cycles. The dynamic strength degradation curves are studied for the MSW fines to check the effect of various considered parameters (relative density, effective confining pressure, and shear strain) on it. The effect of frequency has not been considered as it has the least affecting parameter.

The degradation index curve for different relative compaction at two different shear strains (γ=0.6,1.5%) at a fixed frequency of 1Hz and effective confining pressure of 100 kPa is shown in Figure 4.36. It can be noticed that the degradation rate of the considered MSW fines is comparatively low at high relative compaction, i.e., for 98% it is highest for both the strains, i.e., γ=0.6% (Figure 4.36(a)) and γ=1.5% (Figure 4.36(b)). The rate of degradation at high strain is more as compared to the lower one which can be confirmed through the steep slope of the curves in Figure 4.36(b) and 4.37(b).

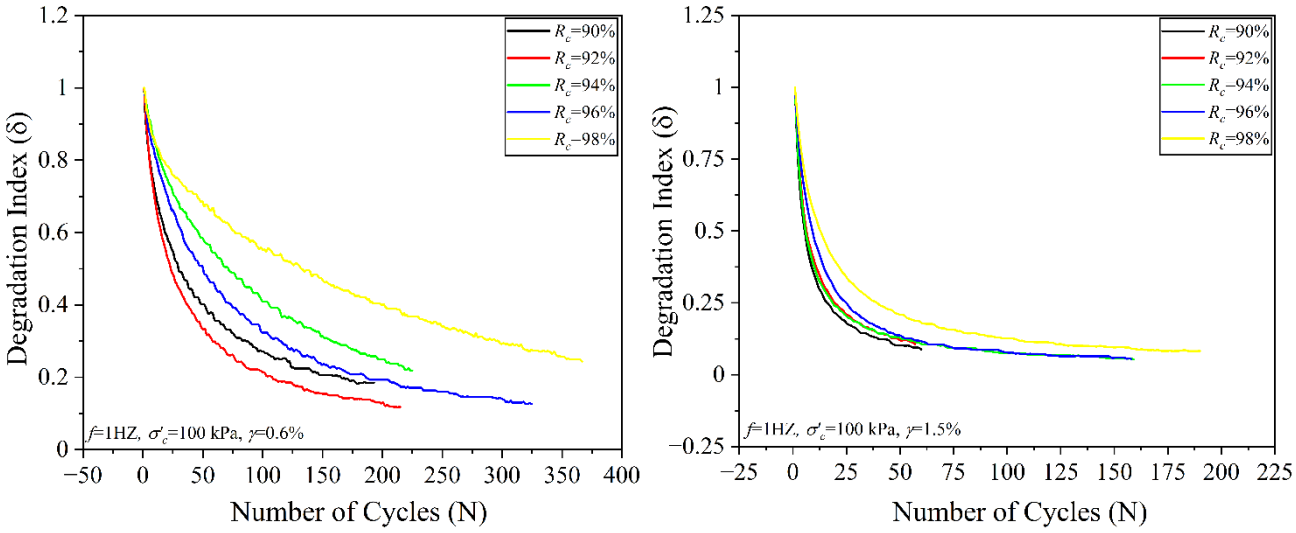

(a) **(b)**

Figure 4.36 Degradation index plot with respect to number of cycles for different relative compaction (R_c) at **(a)** f=1Hz, σ'_c=100 kPa, γ=0.6% **(b)** f=1Hz, σ'_c=100 kPa, γ=1.5%

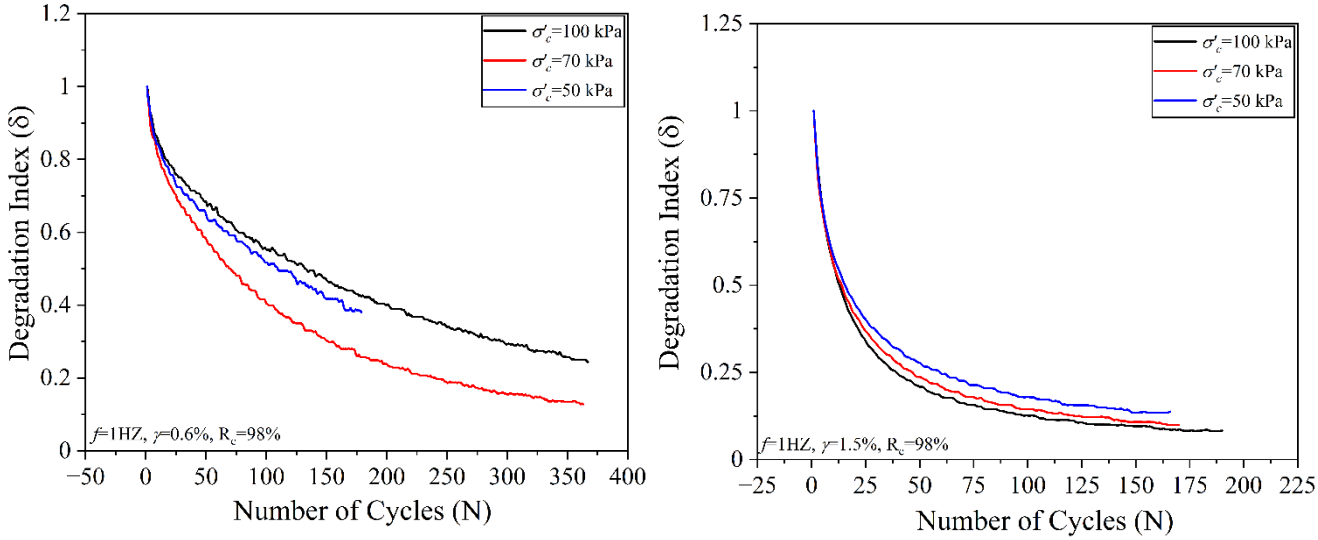

(a) **(b)**

Figure 4.37 Degradation index plot with respect to number of cycles for different effective confining pressure (σ'_c) at **(a)** f=1Hz, γ=0.6%, R_c=98% **(b)** f=1Hz, γ=1.5%, R_c=98%

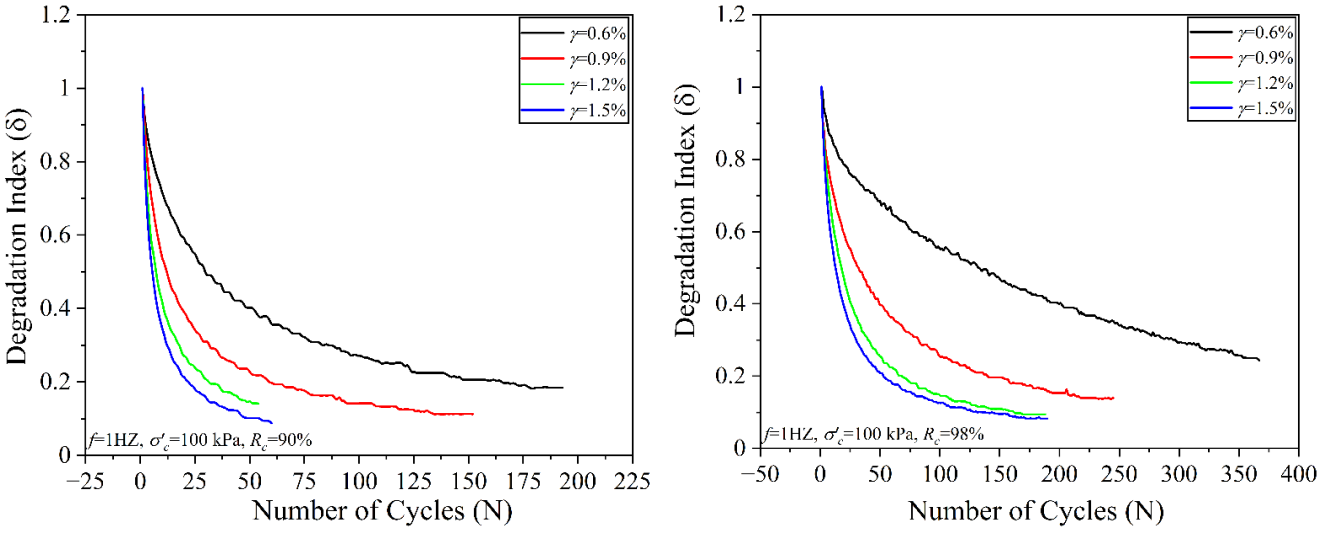

Figure 4.38 Degradation index plot with respect to number of cycles for different shear strain (γ) at **(a)** f=1Hz, σ'_c =100 kPa, R_c=90% **(b)** f=1Hz, σ'_c =100 kPa, R_c=98%

The degradation index curve for different effective confining pressure at two different shear strains (γ=0.6,1.5%) at a fixed relative density of 98% and effective confining pressure of 100 kPa is shown in Figure 4.37. The degradation index rate pattern is different for both the considered stains, i.e., γ=0.6 % (Figure 4.37(a)) and 1.5% (Figure 4.37b). At low shear strain (0.6%), the rate of degradation is low for high confining pressure of 100 kPa whereas the trend reverses at high shear strain (1.5%).

The degradation index curve for different shear strains at two different relative compactions (R_c=90 and 98%) at a fixed frequency of 1Hz and effective confining pressure of 100 kPa is shown in Figure 4.38(a) and 4.38(b). The high degradation rate can be seen at higher shear strain which reduces as the strain value decreases.

4.3.2 Dynamic Characterization of Fiber-Reinforced MSW Fines

This section includes the study of cyclic or dynamic strength parameters (G and D) and pore water pressure ratio variations due to the percentage increment in fiber content in MSW fines, i.e., 0.5,1,2,4,8, and 10%.

4.3.2.1 Effect of FC on Cyclic Strength Parameter "G" of Fiber-Reinforced MSW Fines

The influence of the fibers can be observed through deviator stress variations of MSW fines unreinforced and reinforced with fibers at different FC (Figure 4.39). The area of the hysteresis loop (for the 1st cycle) decreases as the FC increases, which can be seen for both cyclic UU and CU cases. The deviator stress and the slope of the hysteresis loop also declined as the FC increased in MSW fines, which shows the degradation of strength with an increment of FC.

The same can be verified from Figure 4.40(a) in the case of the cyclic UU test where the G value was decreased with the increase in fiber content. However, no major variation was observed with the increase in loading cycles. In the case of cyclic CU tests (for γ= 0.6%, shown in Figure 4.40(b)) for an unreinforced MSW fines sample, the rate of decrease in G was faster as compared to reinforced MSW fine samples with fibers. Although the dynamic shear strength is high for reinforced MSW fines at low strain after 100^{th} loading cycles, the same was not validated for higher strain (γ) rates of 0.9 and 1.2% (Figure 4.40(c) and 4.40(d)). The G values for the first cycle (Figure 4.40(e)) show continuous degradation of G with the fiber enclosure as well as with an increase in axial strain. The enclosure of fiber shows almost no improvements in higher strains. The study on reinforced waste with plastic fibers shows the efficiency of the fiber reinforcement is dependent on the values of the confining pressure as an increase in confining pressure increases the bonding between

fibers and waste (Alidoust et al. 2018). Clayey sand reinforced with Polypropylene fibers (FC: 0.25 to 2%; fiber length of 6 mm) also shows degradation in G values for γ below 1% and even above that fiber inclusion shows no remarkable improvements (Bozyigit et al. 2017).

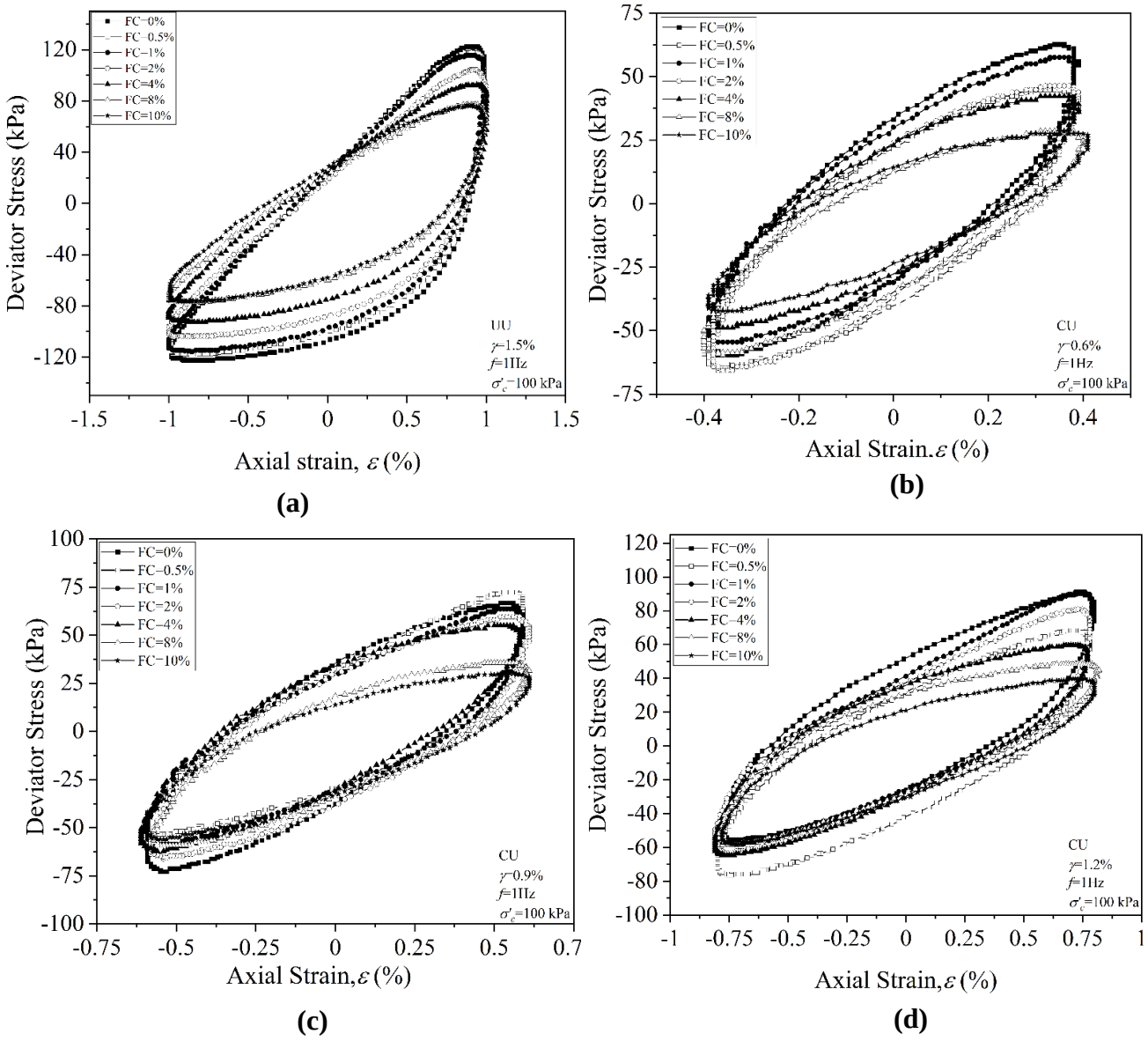

Figure 4.39 First cycle hysteresis loop for different FC (**a)** at γ=1.5% (UU condition) **(b)** γ=0.6%, (**c)** γ=0.9%, and **(d)** γ=1.2% for CU condition

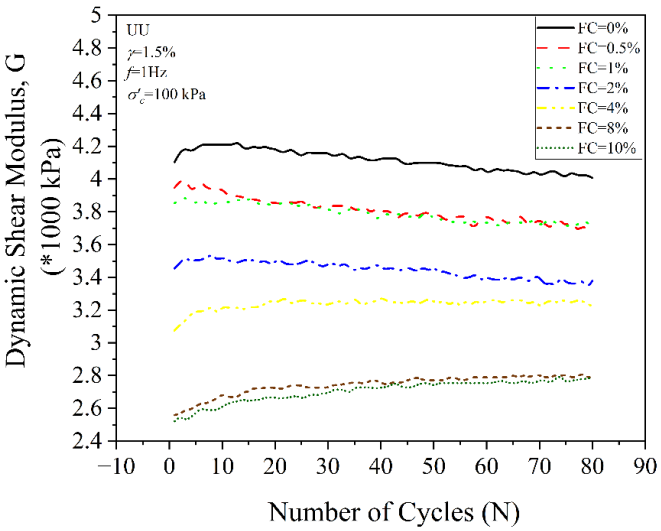
UU
γ=1.5%
f=1Hz
σ'c=100 kPa
FC=0%
FC=0.5%
FC=1%
FC=2%
FC=4%
FC=8%
FC=10%
Dynamic Shear Modulus, G (*1000 kPa)
Number of Cycles (N)

(a)

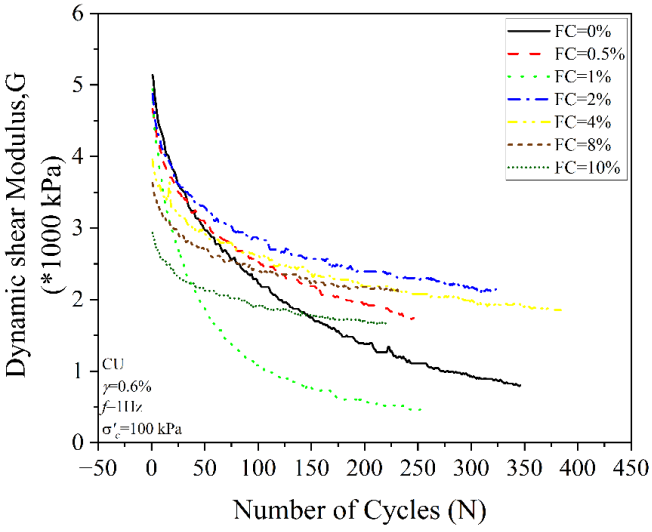
CU
γ=0.6%
f=1Hz
σ'c=100 kPa
FC=0%
FC=0.5%
FC=1%
FC=2%
FC=4%
FC=8%
FC=10%
Dynamic shear Modulus,G (*1000 kPa)
Number of Cycles (N)

(b)

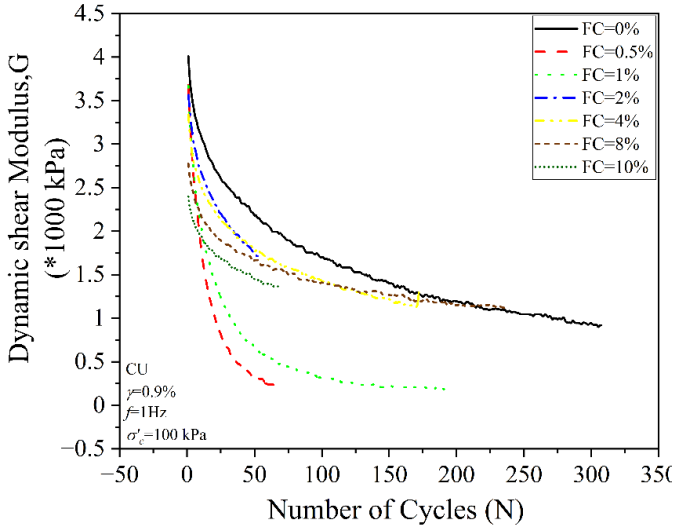
CU
γ=0.9%
f=1Hz
σ'c=100 kPa
FC=0%
FC=0.5%
FC=1%
FC=2%
FC=4%
FC=8%
FC=10%
Dynamic shear Modulus,G (*1000 kPa)
Number of Cycles (N)

(c)

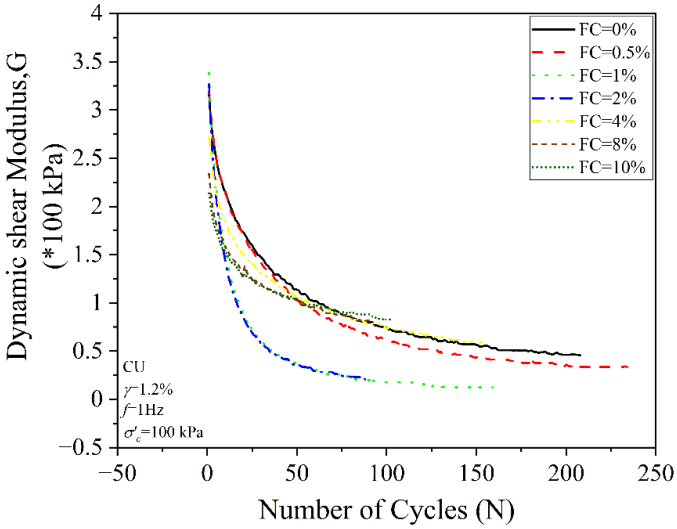
CU
γ=1.2%
f=1Hz
σ'c=100 kPa
FC=0%
FC=0.5%
FC=1%
FC=2%
FC=4%
FC=8%
FC=10%
Dynamic shear Modulus,G (*100 kPa)
Number of Cycles (N)

(d)

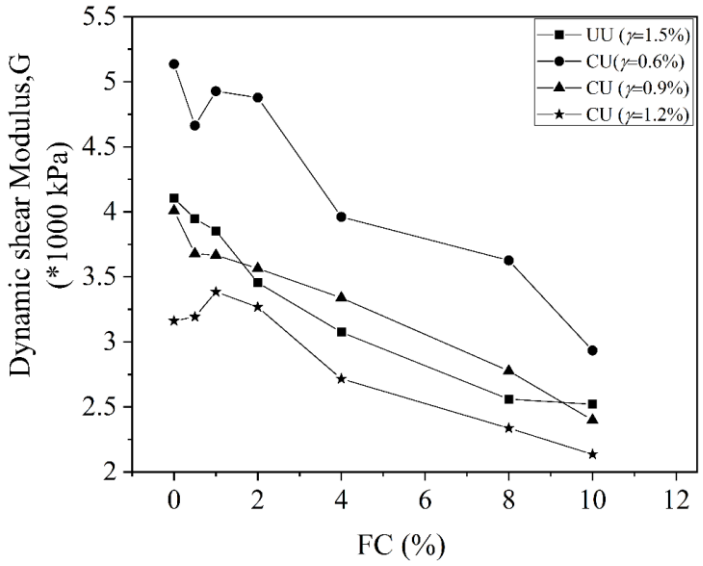

(e)

Figure 4.40 Variation of dynamic shear modulus (G) with no. of loading cycles (N) for (**a)** at γ=1.5% (UU condition) **(b)** γ=0.6%, (**c)** γ=0.9%, and **(d)** γ=1.2% for CU condition. **(e)** G (for first cycle) variation with FC at different γ

4.3.2.2 Degradation Index of Fiber-Reinforced MSW Fines

The degradation index of MSW fines has been studied with different fiber content under two sets of the cyclic triaxial test (UU and CU). The 1st set under the unconsolidated undrained cyclic triaxial test (Figure 4.41(a)) shows a very unique pattern of degradation index with a total of 80 cycles. The degradation index graph shows improvement in G values at higher FC (4, 8, and 10%), for 8 and 10% the δ values increase from 1 to 1.1, i.e., 10% improvement in G with N. The second set of tests includes consolidated undrained cyclic triaxial tests (for γ: 0.6, 0.9, and 1.2%) where the degradation index is aligned with the above results of G variation with N. The steep downfall curve in Figures 4.41(b), 4.41(c), and 4.41(d) shows rapid degradation in strength. At higher shear strains of 0.9 and 1.2%, the rate of degradation of strength is high up to 50 cycles (Figure 4.41(c) and 4.41(d)). The degradation index values are high for the FC of 8 and 10%, which indicates a relatively low reduction in strength as compared to low fiber content.

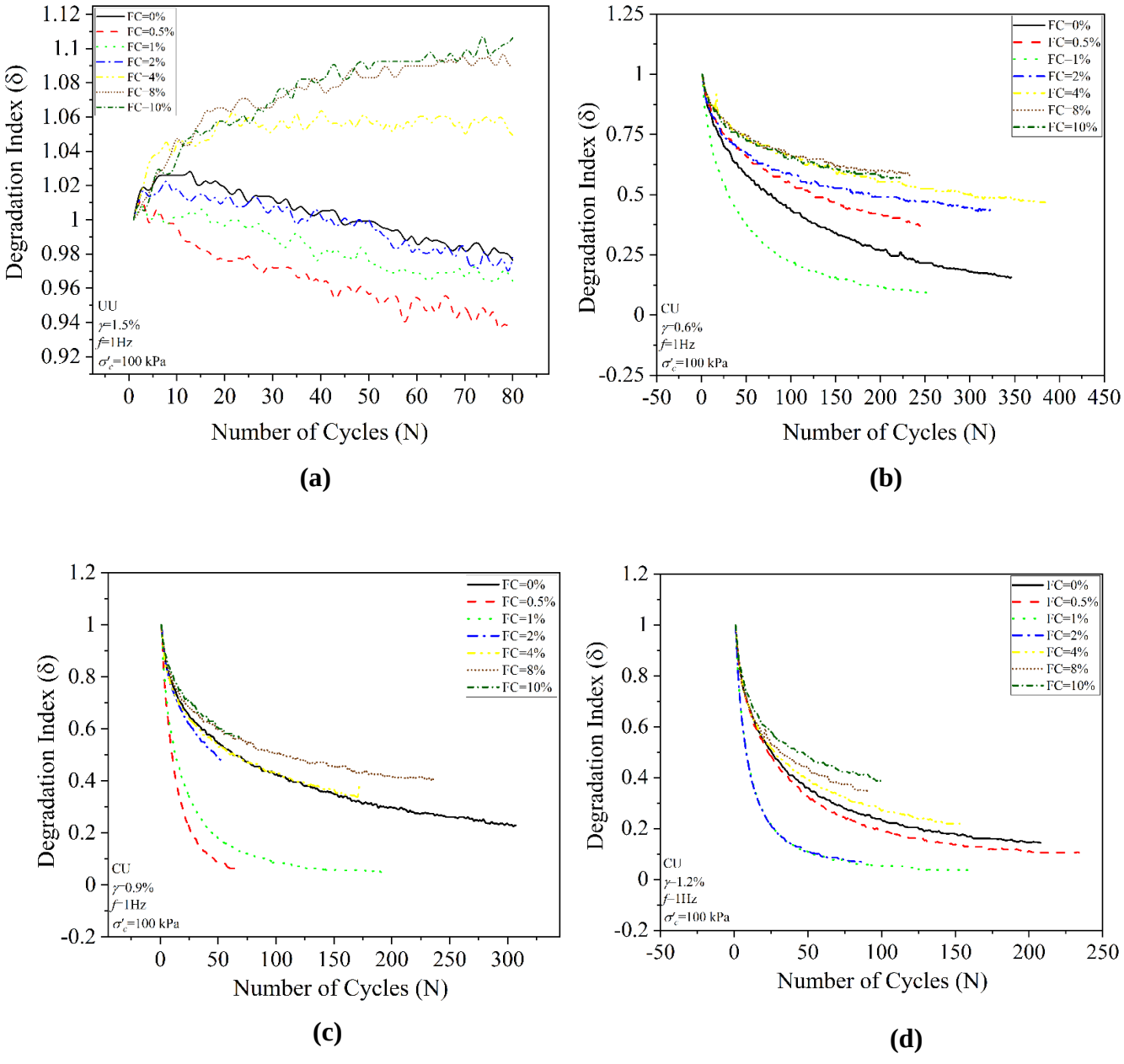

Figure 4.41 Degradation index variation with no. of loading cycles (N) for **(a)** at γ=1.5% (UU condition) **(b)** γ=0.6%, **(c)** γ=0.9%, and **(d)** γ=1.2% for CU condition

4.3.2.3 Effect of FC on Cyclic Strength Parameter "D" of Fiber-Reinforced MSW Fines

The damping ratio variations with loading cycles show degradation in D for both reinforced and unreinforced MSW fines for both UU and CU cases (Figure 4.42). At higher FC, i.e., 8 and 10% the damping ratio is higher as compared to the other FC. Comparing the damping values for the first loading cycle (Figure 4.42(e)), the general trends show an increase in D with fiber inclusion and a decrease with strain in the case of CU tests and for the UU case, the damping is low because of higher strain value. The down trends of D with shear strain are similar to the unreinforced MSW fines. The inclusion of fibers at high concentrations behaves as a cushion when mixed with MSW fines helping in dissipating the energy. The reinforcement of 8% increases the D value by about 61% (γ=0.6%), 36% (γ=0.9 and 1.2%) for CU cases, and 41% (γ=1.5%) in the case of UU as compared to the unreinforced one. Whereas for the 10% reinforcement an increment of about 20% (γ=0.6%), 40% (γ=0.9), 46% (γ=1.2%) was noticed for CU cases and 46% (γ=1.5%) in the case of UU.

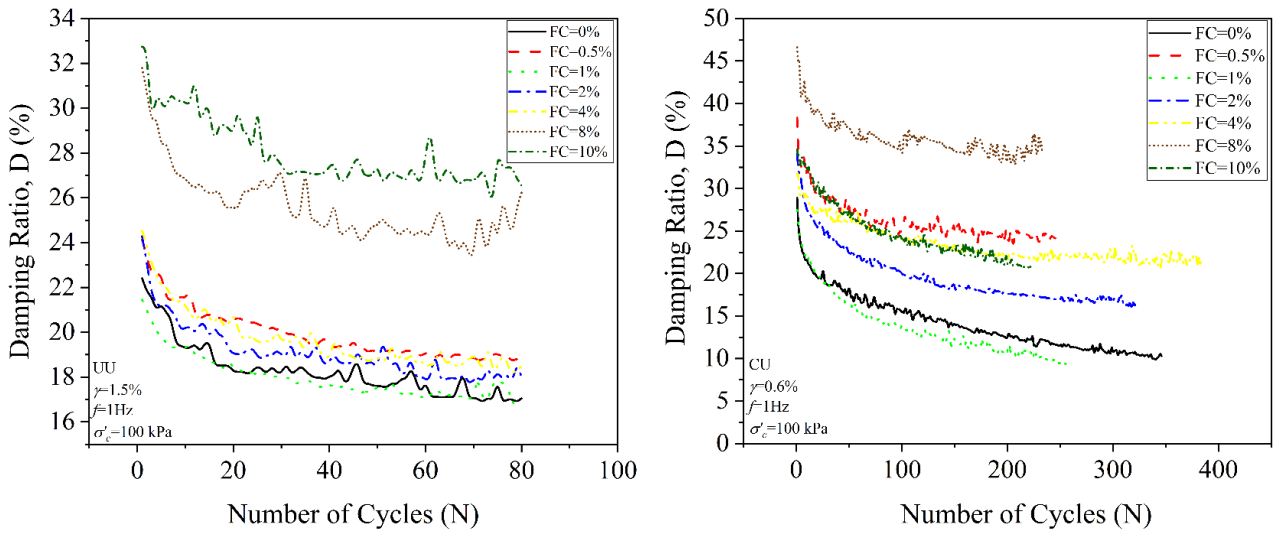

(a) **(b)**

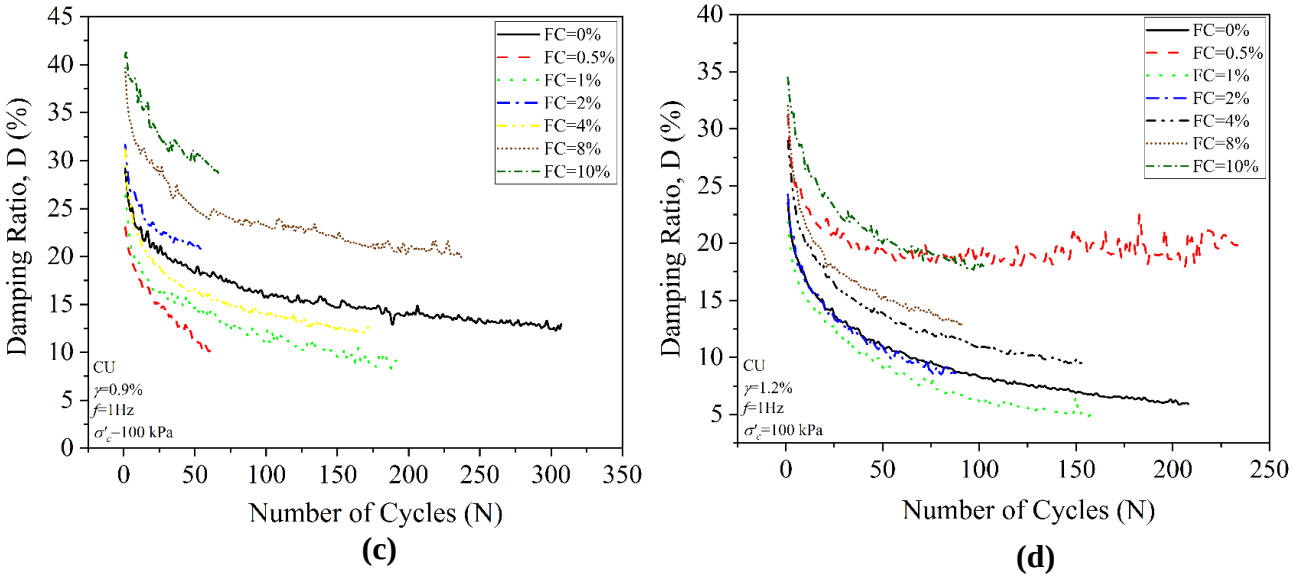

(c) **(d)**

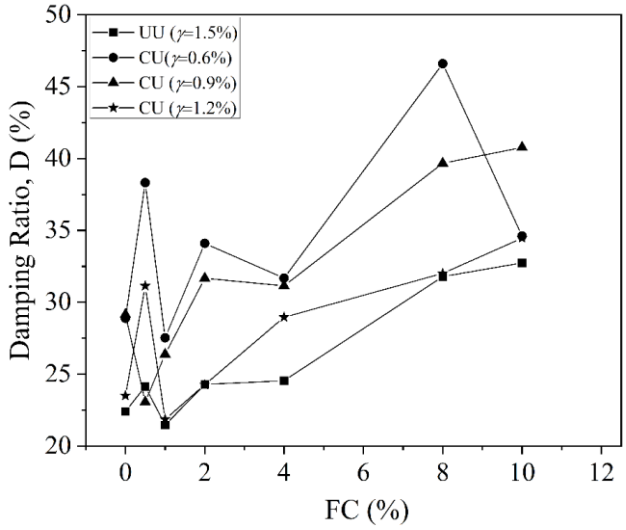

(e)

Figure 4.42 Variation of damping ratio (D) with no. of loading cycles (N) for (**a**) at γ=1.5% (UU condition) **(b)** γ=0.6%, (**c**) γ=0.9%, and **(d)** γ=1.2% for CU condition. **(e)** G (for first cycle) variation with FC for different γ

4.3.2.4 Effect of FC on r_u (excess pore water pressure ratio) of Fiber-Reinforced MSW Fines

The variation of excess pore water pressure ratio (r_u) for MSW fines mixed with different FC are compared in Figure 4.43. The r_u increases with the increase in loading cycles, i.e., N_L for each case but the rate of built-up of r_u varies with FC as well as with strain rate. The patterns are different as compared to that of the sand reinforced with fibers, where the slope of the pore water pressure decreases with an increment in fiber inclusion

(Zhang et al., 2021a). In the present fiber-reinforced MSW fines study, as the content of fiber increases the rate of accumulation of pore water pressure also increases that can be observed by comparing the slopes of the reinforced and unreinforced MSW fines at different shear strains (0.6, 0.9, and 1.2%) shown in Figure 4.43(a), 4.43(b) and 4.43(c)). At a low strain of 0.6%, for FC more than 4% (Figure 4.43(a)), the r_u value suddenly increases to 0.85, i.e., high pore water pressure development was noticed with the inclusion of fibers in MSW fines. However, there is not much difference in liquefaction cycles, i.e., around 300 to 350 cycles with FC at the low strain of 0.6%. The loading cycles for liquefaction drastically reduced at higher strains of 0.9 and 1.2% (Figure 4.43(b) and 4.43(c)) with FC (0.5%, 2%, and higher content of 10%). At higher strains comparing different FC, 8% fiber inclusions show the highest liquefaction resistance, but no improvements were observed as compared to the unreinforced MSW fines.

The optimum quantity of FC was found to be 8% in the case of monotonic static loading case. If we compare the unreinforced sample with reinforced (FC=8%) MSW fines for r_u variations for different strains, there is not much effect of strain on the number of liquefaction cycles in the case of unreinforced one (Figure 4.43(d)) but with the inclusion of fibers (8%) the liquefaction cycle was reduced at a higher strain of 0.9 and 1.2% (Figure4.43(e)). At a low strain of 0.6% (Figure 4.43(d) and 4.43(e)), there is no effect of reinforcement on the number of cycles to liquefy but r_u develops immediately with the inclusion of reinforcement makes it more susceptible to liquefaction, it can also be verified from Figure 4.43(a). At a higher strain rate, the development of r_u is almost the same for the reinforced and unreinforced cases.

In most of the past studies, fiber existence causes a major change in the liquefaction behaviour by reducing the susceptibility of soil to liquefy and increasing the number of

cycles triggering liquefaction (Uzdavines, 1989; Maher and Woods, 1990; Maheshwari et al., 2012b; Eskisar et al., (2015, 2016)).

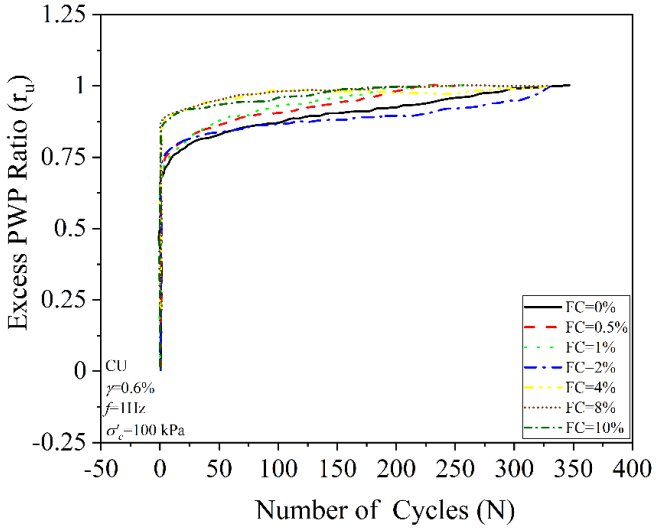

(a)

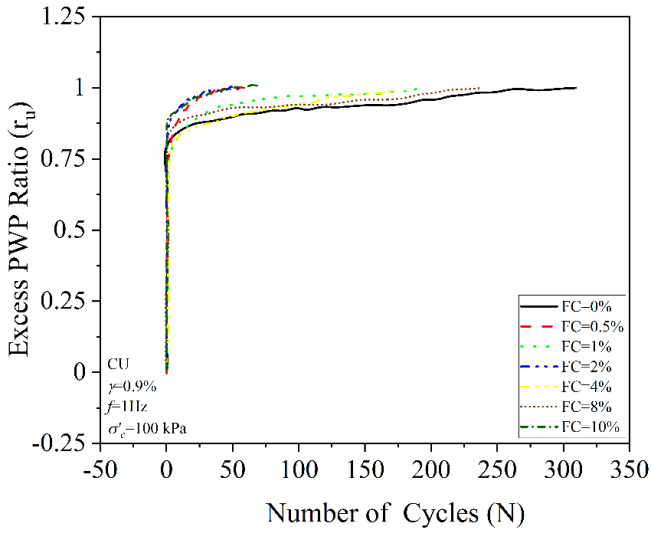

(b)

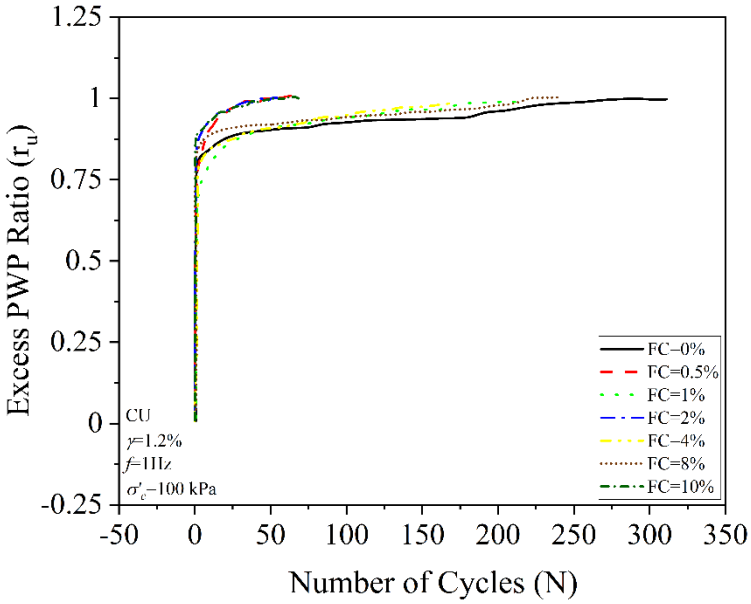

(c)

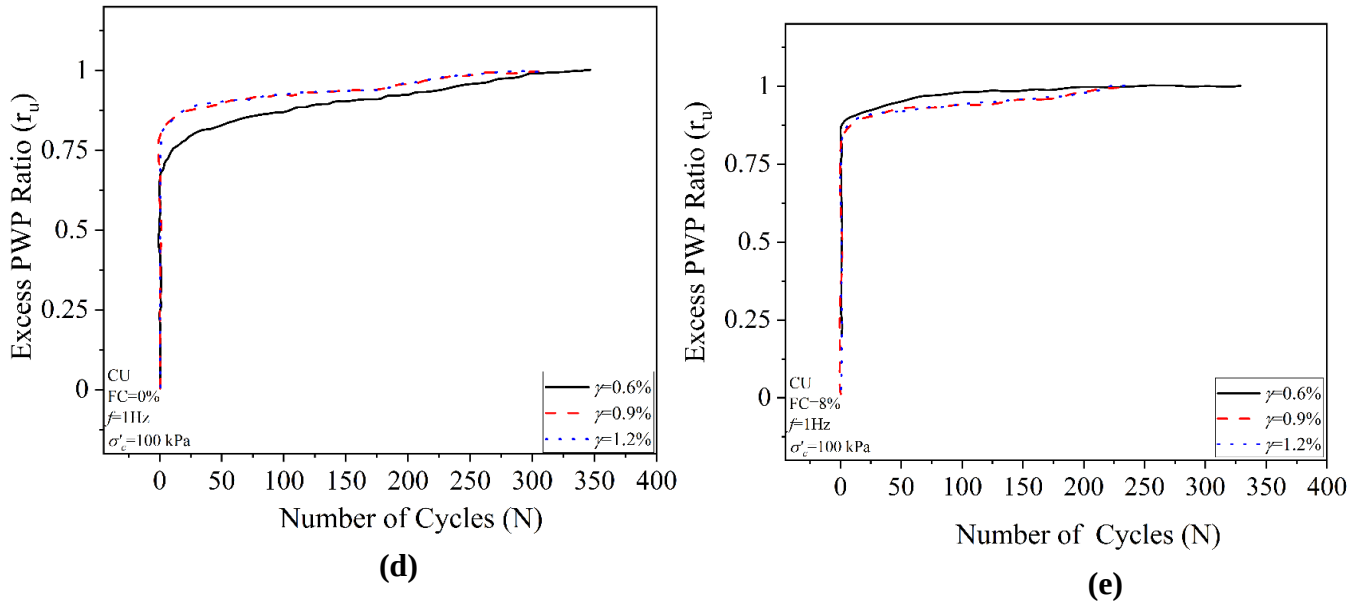

Figure 4.43 Excess PWP ratio (r_u) variations with FC at **(a)** γ=0.6%, **(b)** γ=0.9%, and **(c)** γ=1.2%. Variation of r_u with N at **(d)** 0% FC **(e)** 8% FC for different γ

4.3.3 Shear Wave Velocity Determination Through Bender Element Analysis for Unreinforced and Reinforced MSW Fines with Fibers

4.3.3.1 Consideration of Parameters for Bender Element Test

A total of five parameters were considered for the bender element study, i.e., R_c, σ_c, f, FC, and saturation which has already been discussed in the testing methodology. The study considered the time domain's first peak-to-peak analysis approach for the estimation of travel time as the peaks of the output signal was predominant and can be identified easily. However, more research is required to comment on which method works better for the geomaterials. The first start-to-start method was suggested as reliable by Georgetti et al. (2013) and was used by some other researchers for waste and additive mix soils (Ram and Mohanty, 2021; Heidarizadeh et al., 2021). But it is sometimes difficult to identify the actual start point of the output signal. The input and output signals (sinusoidal) at different

conditions with travel time can be seen in Figure 4.44. It can be noticed that when the sample of MSW fines is unsaturated and unconfined (Figure 4.44(a)), the output peaks (in blue) are predominant for all the frequencies up to 2kHz but as the sample is confined under σ_c =100 kPa for UU (unconsolidated undrained) conditions (Figure 4.44(b)), the first arrival output peak almost suppressed or vanished. This evaluates the first arrival output peaks at higher frequencies and confinement. When the MSW (fines) sample is saturated and the test was conducted under CU (consolidated undrained) conditions at σ'_c =100 kPa (Figure 4.44(c)), the predominant peaks can be seen again. A typical input-output signal graph at different FC at a constant density (MDD) and *f*=1kHz is shown in Figure 4.44(d).

4.3.3.2 Effect of Considered Parameters on Shear Wave Velocity (V_s)

4.3.3.2.1 Effect of Excitation Frequency (f) on V_s

The effect of the considered frequency range can be seen on the shear wave velocity (V_s) considering different FC and R_c (Figure 4.45(a) and 4.45(b)). The V_s variation at every unconfined and confined (σ_c: 50, 100, and 150 kPa) condition for UU tests at different fiber content shows that V_s almost linearly varies with the excitation frequency of the wave (Figure 4.45(a)). The concentration of fibers shows very minute effects on the V_s for every frequency. For the case of V_s variations with *f* for different R_c (Figure 4.45(b)), the trends show slight improvement with the excitation frequency. For unconfined or low confined (50 kPa) cases, the samples of lower R_c values show no improvement with the increase in the excitation frequency. The improvements can be seen for higher σ_c, i.e., above 50 kPa for all R_c values. The effect of R_c cannot be clarified from Figure 4.45(b) and is discussed in the next section. Past researchers suggested the excitation frequencies for different types of soils for the sample aspect ratio of 2, i.e., silty sand (10 kHz) (Donovan et al., 2015); high plasticity clay (6 kHz) (Black et al., 2009); poorly graded sand (7 and 5 kHz) (Fonseca

et al., 2009; Sanchez-Salinero, 1986); and well-graded sand (10 kHz) (Palczynska et al., 2014). The present MSW fines look like soils and are categorized as per the soil classification as silty sand but the behavior of the material is quite different from that of the exact silty sand soil. This may be because of the heterogeneity of the material characteristics in the fines of the MSW.

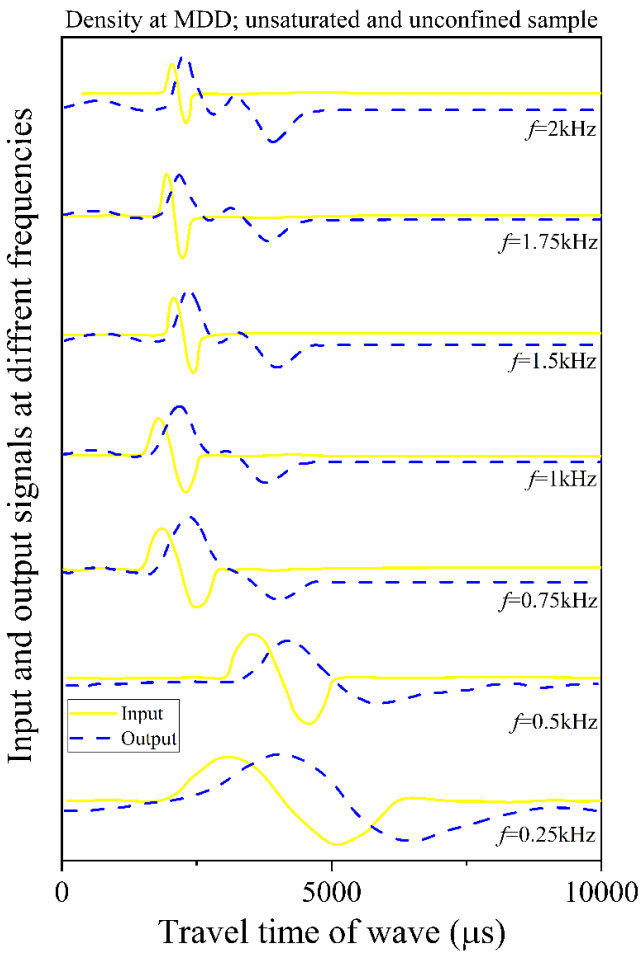

(a)

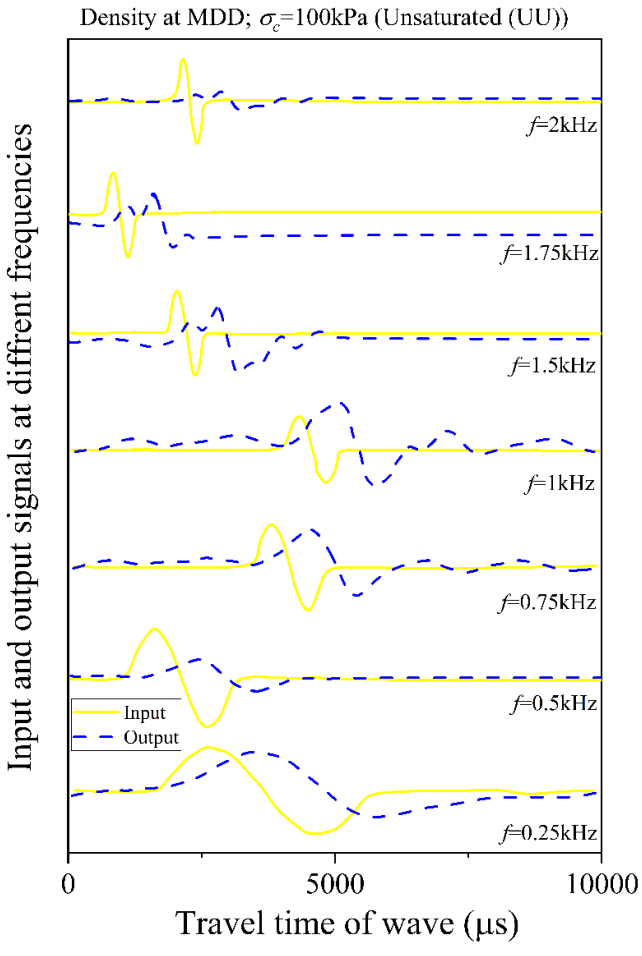

(b)

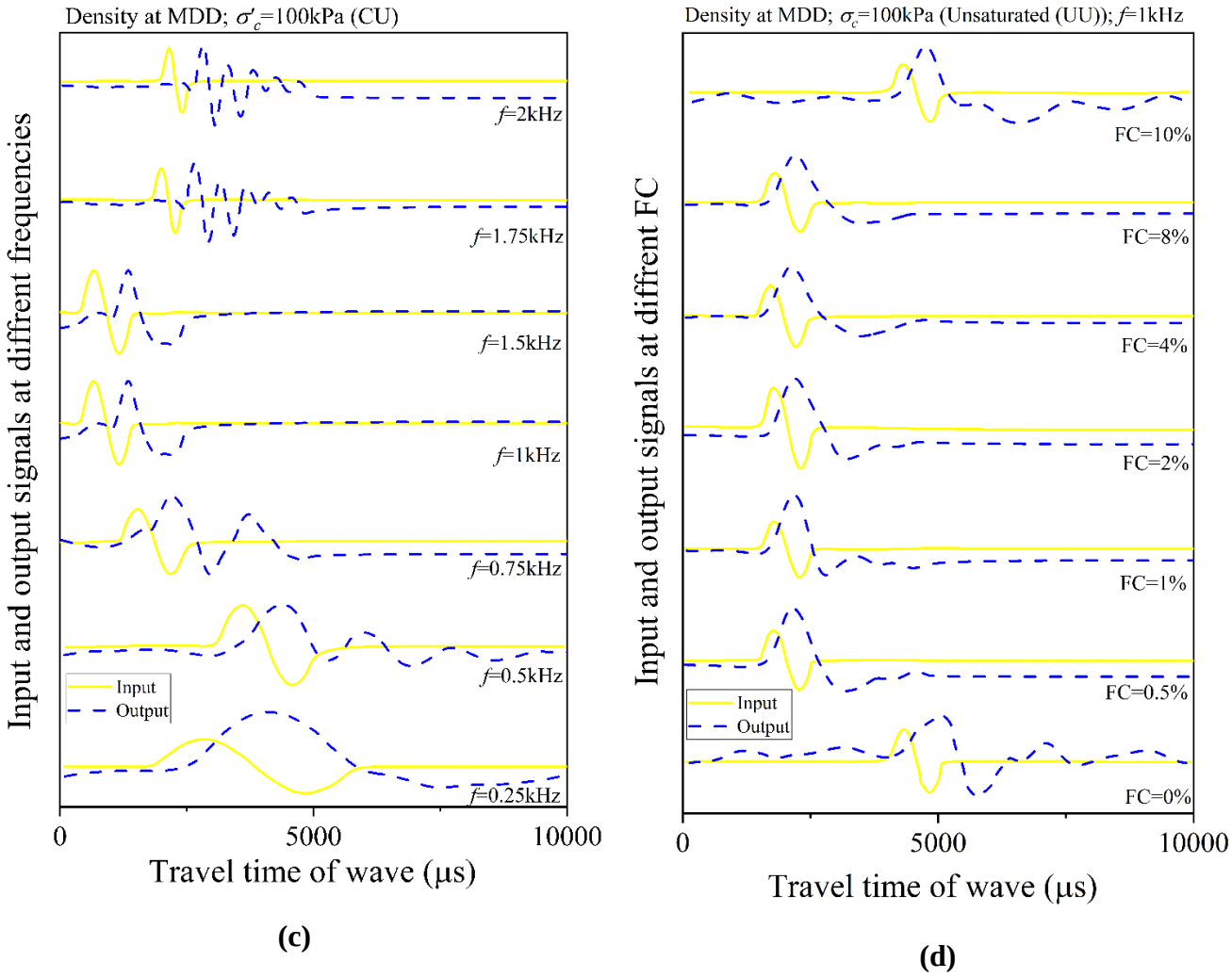

Figure 4.44 Input-output wave response for **(a)** unconfined unsaturated MSW fine sample at MDD **(b)** unsaturated (UU) sample of MSW fine at σ_c (100 kPa) **(c)** saturated (UU) sample of MSW fine at σ'_c (100 kPa) at different excitation frequencies. **(d)** Input-output wave response at different FC for unsaturated MSW fine sample at σ_c (100 kPa) and f (1kHz)

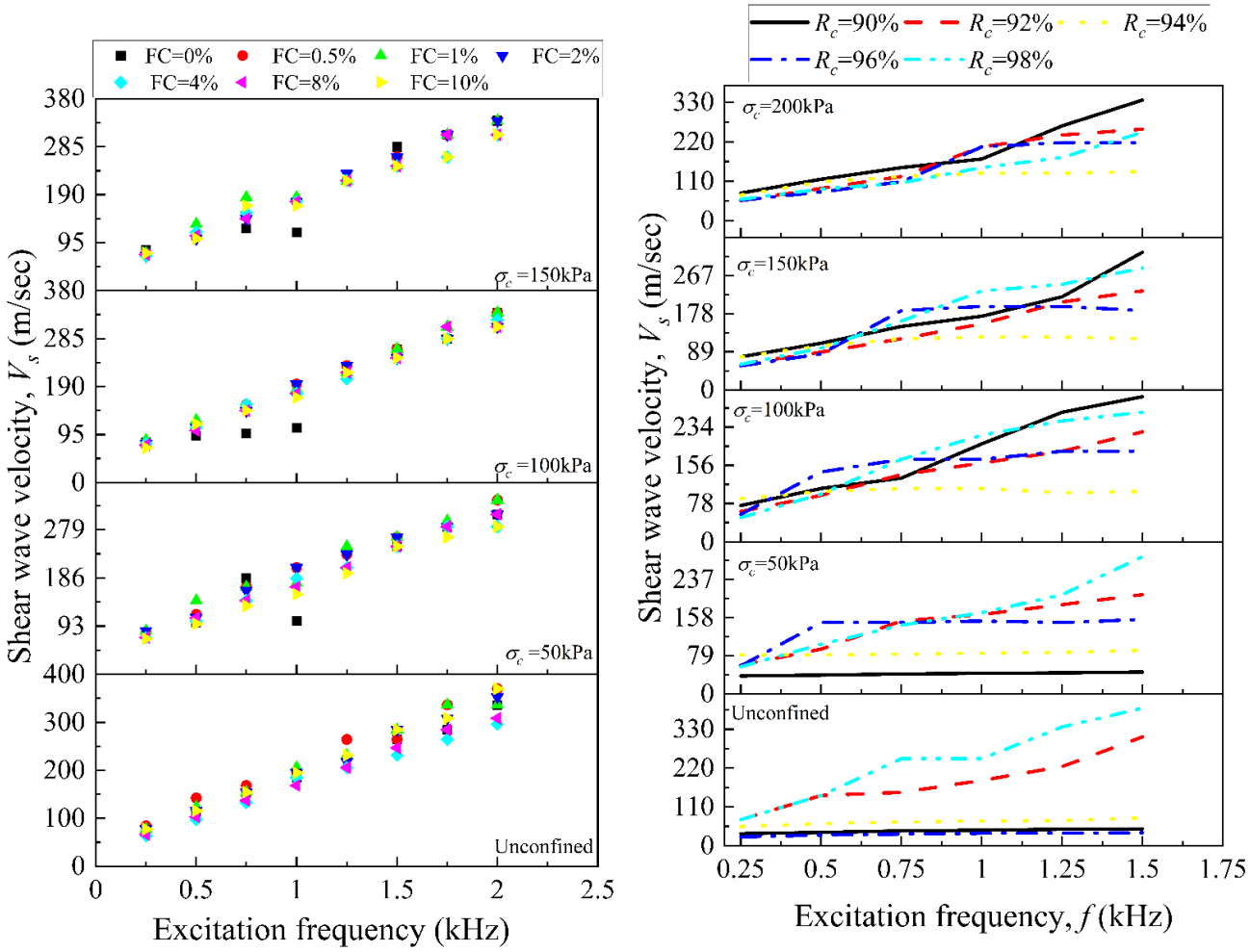

(a) **(b)**

Figure 4.45 Shear wave velocity (V_s) variations with excitation frequency (f) for **(a)** different fiber content (FC) **(b)** different relative compaction (R_c)

4.3.3.2.2 Effect of Relative Compaction (R_c) on V_s

The density or the weight variation between R_c was not very distinguishable, so the trends of the V_s with R_c were not very clear to present any conclusions. The improvement in V_s is remarkable, i.e., more than 100% improvement was noticed for the lowest and the highest R_c, i.e., 90 and 98% (Table 4.12), at the unconfined state or low confinement (50kPa). But with the increase in σ_c, either there is a slight positive variation for frequencies (0.75 and 1kHz) or even reduced V_s was noticed at R_c (98%) for different frequencies (0.25, 0.5, and 1.5 kHz).

Table 4.12 R_c effect on V_s at different confining pressures and excitation frequencies.

σ_c (kPa)	Unconfined		50 kPa		100 kPa		150 kPa	
R_c(%) / f (kHz)	90	98	90	98	90	98	90	98
0.25	34.26	74.00	37.00	56.06	74.00	49.33	77.08	59.68
0.5	37.75	142.31	38.94	102.78	108.82	97.37	108.82	97.37
0.75	42.045	246.67	41.11	142.31	129.82	168.18	148.00	160.87
1	44.047	246.67	42.53	168.18	200.00	217.65	172.09	231.25
1.25	46.84	336.36	43.53	205.56	264.29	246.67	217.65	246.67
1.5	48.05	389.47	45.12	284.62	296.00	264.28	321.74	284.62

*All the V_s values are in m/sec
V_s = Shear wave velocity; R_c= Relative compaction; σ_c= Confining pressure; f= Frequency
Testing conditions: Unconsolidated undrained (UU) without saturation

4.3.3.2.3 Effect of Confining Pressure (σ_c) on V_s

The confining pressure has almost no effect on V_s of the MSW fines whether unreinforced or reinforced with fibers (Figure 4.46). For the case of unreinforced some fluctuations can be seen for the frequency range of 0.5 to 1 kHz, but with fiber reinforcement, these fluctuations get almost smooth. It can be seen in Table 12 that at two different R_c, higher confinements (i.e., 100 and 150 kPa) have improved the V_s compared to the unconfined one. However, there is not much variation in the improvement when going from 100 to 150 kPa and at lower R_c of 90% this improvement is more. In Figure 4.46 all the samples were prepared at a fixed density (1.51g/cc) which is the maximum dry density of the MSW fines, so it is very difficult for the rearrangements of the particles or density change due to the applied confining pressures. However, in the case of R_c (90%) where the density is lower than MDD, these arrangements could be possible due to lower compaction.

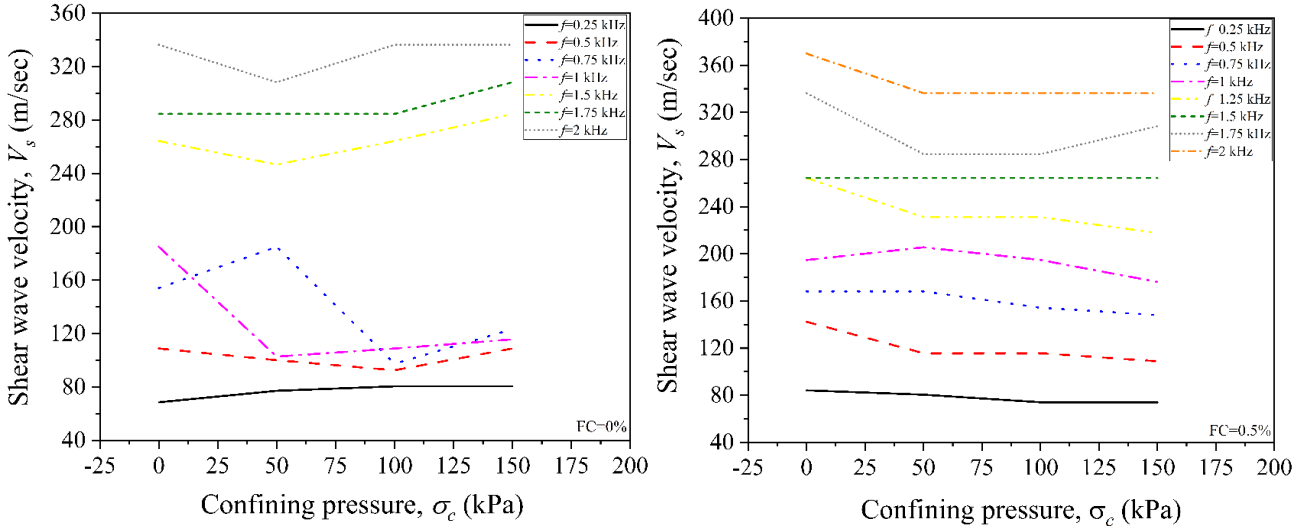

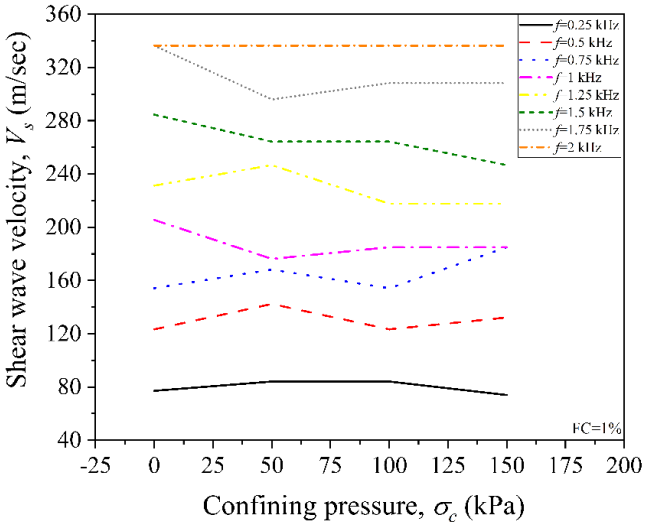
Shear wave velocity, V_s (m/sec)
Confining pressure, σ_c (kPa)
f=0.25 kHz
f=0.5 kHz
f=0.75 kHz
f 1 kHz
f 1.25 kHz
f=1.5 kHz
f=1.75 kHz
f=2 kHz
FC=1%

(c)

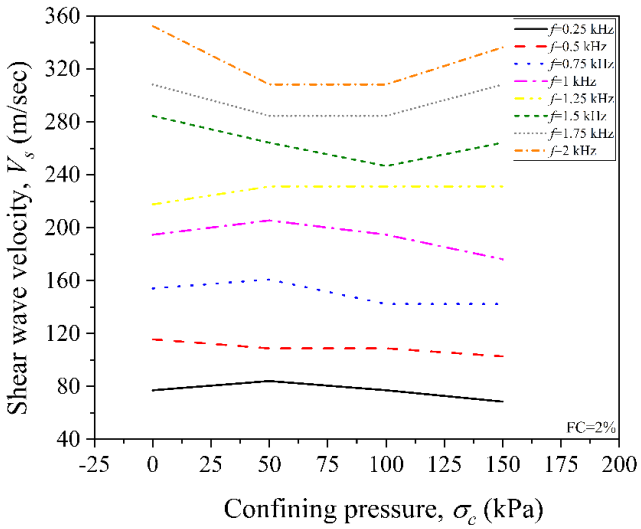
Shear wave velocity, V_s (m/sec)
Confining pressure, σ_c (kPa)
f=0.25 kHz
f=0.5 kHz
f=0.75 kHz
f=1 kHz
f=1.25 kHz
f=1.5 kHz
f=1.75 kHz
f=2 kHz
FC=2%

(d)

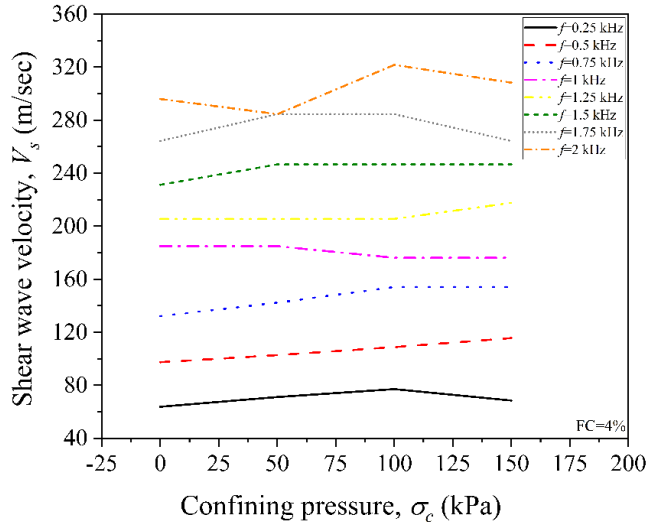
Shear wave velocity, V_s (m/sec)
Confining pressure, σ_c (kPa)
f=0.25 kHz
f=0.5 kHz
f=0.75 kHz
f=1 kHz
f=1.25 kHz
f 1.5 kHz
f=1.75 kHz
f=2 kHz
FC=4%

(e)

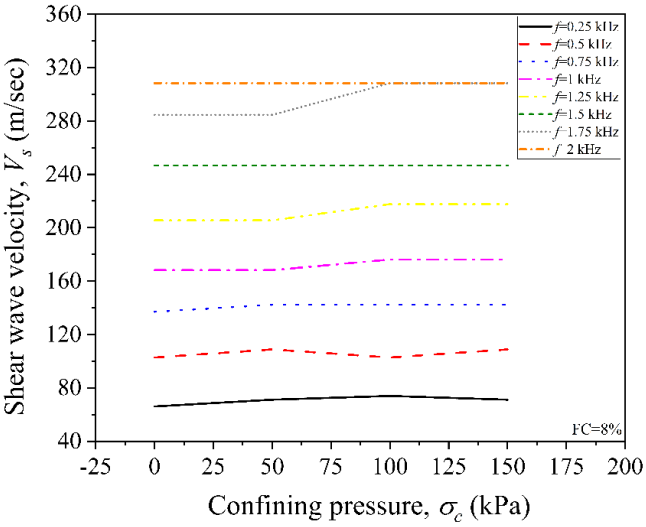
Shear wave velocity, V_s (m/sec)
Confining pressure, σ_c (kPa)
f=0.25 kHz
f=0.5 kHz
f=0.75 kHz
f=1 kHz
f=1.25 kHz
f=1.5 kHz
f 1.75 kHz
f 2 kHz
FC=8%

(f)

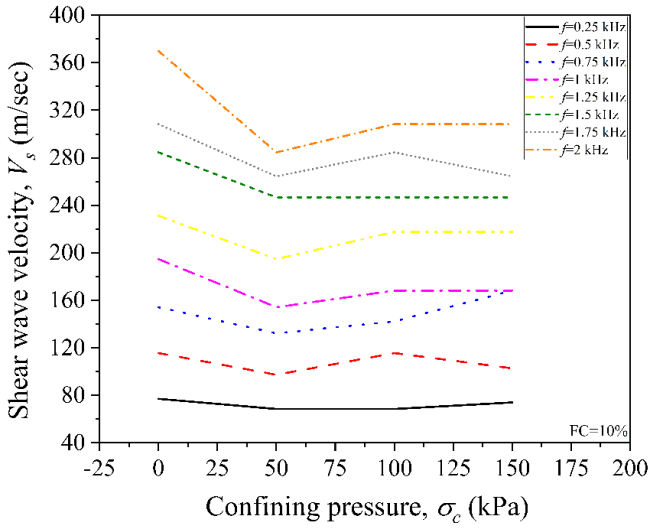

(g)

Figure 4.46 Shear wave velocity (V_s) variation with confining pressure (σ_c) for different excitation frequencies (f) at fiber content (FC) of **(a)** 0% **(b)** 0.5% **(c)** 1% **(d)** 2% **(e)** 4% **(f)** 8% **(g)** 10%

4.3.3.2.4 Effect of Fiber Content (FC) on V_s

To check the effect of FC on the V_s, two frequencies were considered, i.e., 0.5 kHz (low) and 2 kHz (high) from the frequency range considered in this study. The analysis was made for four conditions, (1) the samples were unsaturated and unconfined, (2) the samples were tested under unconsolidated undrained (UU) conditions at σ_c of 50, 100 and150 kPa, (3) the samples were tested under consolidated undrained (CU) conditions at σ'_c of 100 kPa, and (4) unconfined sample after the third condition mentioned above. By comparing Figure 4.47(a) for a frequency of 0.5 kHz and Figure 4.47(b) for 2 kHz, the trends are almost the same, i.e., the maximum value of V_s can be seen for FC of 1% except for the condition (3) at 2kHz frequency. Figure 4.47(a) also clears better results for unconfined or low confinement and after 4% fiber inclusions the trends change. There is no significant difference in V_s values was noticed with confinement for condition (2). However, in Figure 4.47(b) the trends can be seen, i.e., higher V_s values at higher confinement with varying FC but the changes are not very significant. The unconfined sample (condition 1) of MSW with

fiber reinforcement of 1% or 10% shows better performance at both the considered frequencies. To check the reinforcement effect on the maximum or small-strain shear modulus (G_{max}), the normalized values were considered, i.e., the ratio of G_R (reinforced shear modulus) to G_{UR} (unreinforced shear modulus). Typical plots were made for condition (2) in Figure 4.47(c) and it can be seen for every case almost the peaks are at 1% FC (except f :1 kHz & σ_c: 50kPa considered as an anomaly). The better results can be seen for f of 1 kHz, but the effect of increased confining is still unpredictable.

4.3.3.2.5 Effect of Saturation on V_s

The saturation of the sample fills the voids with water which makes shear (S) waves take more time to travel through the medium because S waves could not pass through the liquid medium. This can also be seen in Figures 4.47(a) and 4.47(b) for condition (3), as the sample gets saturated the V_s values drop compared to the other conditions considered. The plot of V_s with the excitation frequency for UU and CU conditions shows unstable results (Figure 4.48(a)). At low and high frequencies, the V_s is comparatively higher for UU conditions when the sample is in dry condition, but the difference is not very large. Comparing the two conditions at different R_c (Figure 4.48(b)), a large variation can be seen especially at low densities and minimum at MDD. The sample prepared at MDD (maximum dry density), and OMC (optimum moisture content) are assumed to be almost saturated and likely to be less affected by the saturation and consolidation process.

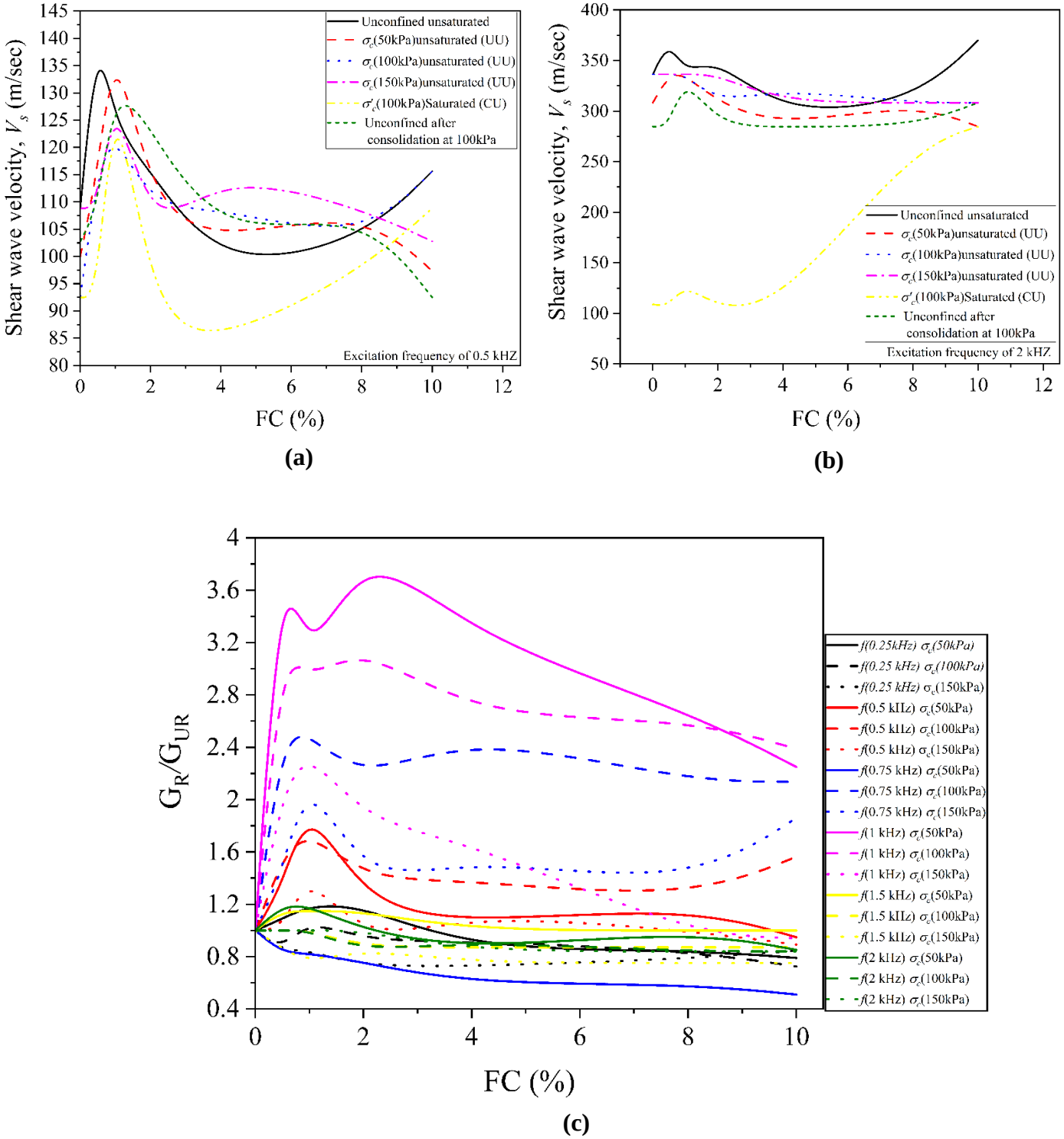

Figure 4.47 Shear wave velocity (V_s) variation with fiber content (FC) at excitation frequency (f) of **(a)** 0.5 kHz (**b)** 2 kHz. **(c)** Variation of G_R/G_{UR} ratio with FC for different excitation frequencies and confining pressure

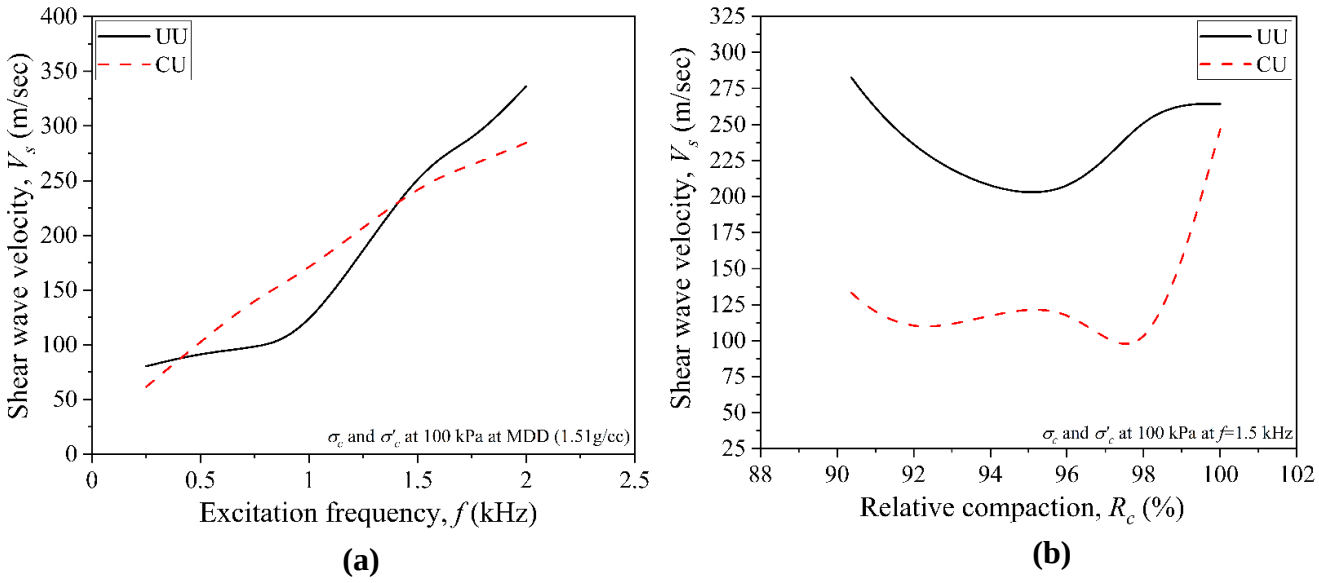

Figure 4.48 Shear wave velocity (V_s) variation with **(a)** excitation frequency (f) **(b)** relative compaction (R_c) at f (1.5kHz), for the MSW fine sample at MDD at UU and CU conditions

4.3.3.3 Comparison of Present Study Results with Past Literature

The laboratory studies on the MSW are very limited, especially on the BE equipment. The major reason is the large particle size of the waste and the equipment size constrain the reliability of the data. The present study only considered the fine fraction, i.e., particle size less than 4.75 mm soil-like material of MSW. So, it can be compared with the other soil data. Naveen (2018) found the V_s and G_{max} for MSW samples less than 4 mm from the Mavallipura landfill site as 85, 95, 120 m/s and 5.05, 7.22, and 12.96 MPa respectively for the density of 7, 8, and 9 kN/m^3. The data in the present study shows a great variation in V_s values as compared to the R_c as shown in Table 12. The major reasons for this much disparity in the results of MSW considered from the two sites are the (1) densities considered for the present study the MDD is about 15.1kN/m^3 (higher than considered in the above study); (2) the difference in the mechanical properties of the wastes; (3) heterogeneity at the micro level; (4) test conducted for analysis, as for the present study BE

test was carried out whereas ultrasonic test was carried out for the Mavallipura landfill site waste.

Few past studies have been compared to the present fiber-induced MSW in Figure 4.49. It can be observed that the inclusion of fibers (synthetic fibers) in sands generally reduces the G_{max} or the stiffness of the composite material. In the case of MSW, Alidoust et al. (2018) mentioned that the inclusion of fiber contents reduces the arrival time of the received wave, because of the increased stiffness of the samples, while, at the same time, the bender receives low-voltage waves. The observations are the same in the case of the present study (at an excitation frequency of 1kHz) as the FC percentage increases the stiffness of the composite material improves up to a certain concentration in the unsaturated case and reduces for higher FC. The trends are reversed for the saturated and consolidated sample at 100 kPa. The only justification could be the material properties of the fiber, which are itself very heterogeneous as they were part of the 1%waste only. In past studies the induced fibers generally used were synthetic or some type of disintegrated plastics, but the fibers used for this study were more disintegrated textile fabric and less plastic as per the visual interpretations.

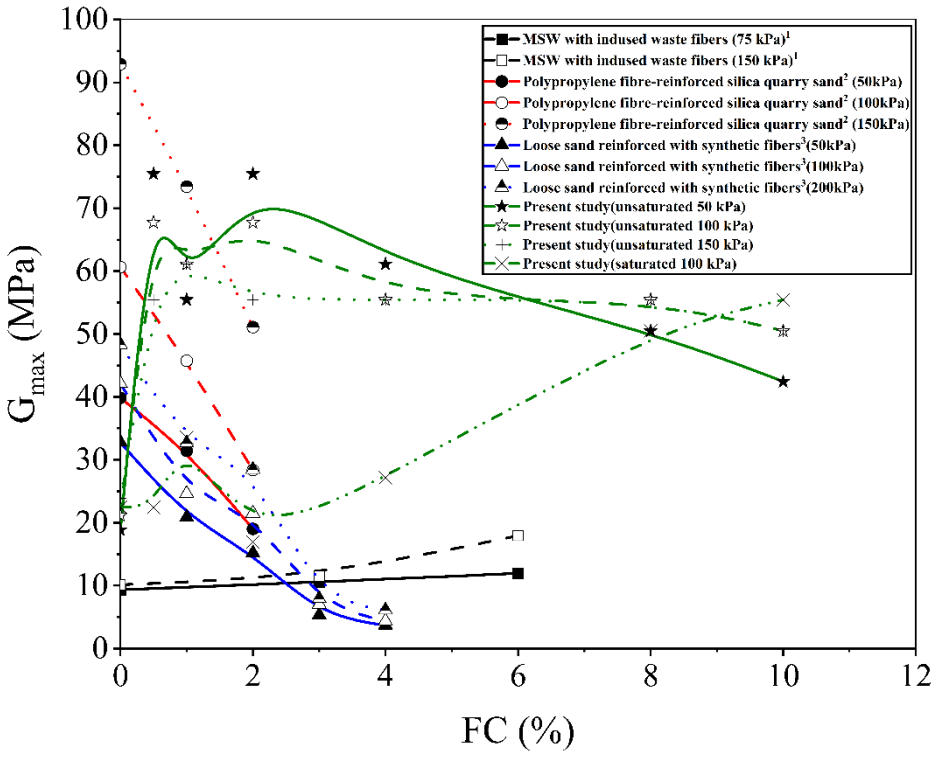

Figure 4.49 Comparative past studies of small strain shear modulus (G_{max}) with fiber content (FC). (1-(Alidoust et al., 2018); 2-(Li and Senetakis, 2017); 3-(Claria and Vettorelo, 2016))

4.4 SUMMARY

The extensive experimental studies of MSW fines and reinforced MSW fines show approximately 60% of the waste material was nonplastic silty sands with medium compressibility, medium permeability, and good shear strength. Furthermore, the low specific gravity of MSW fines (2.32), made it appropriate for lightweight fill material. Further, the addition of waste fibers in optimum quantity (i.e., 8% by weight) in the same MSW fines shows remarkable improvements in the strength characteristics of MSW fines at higher strains. When reinforced with an optimum fiber content of 8%, the behaviour of the unreinforced MSW fines under any condition (UU, CU, and CD) shifted from ductile to elastic. More detailed chemical investigations may be required as the concentration of a few heavy metals, organic content, or the colour of leachates, for example, could cause a

serious problem if ignored. As a result, proper treatment of MSW fines may be required before they can be implemented in specific areas.

According to the findings from the cyclic triaxial tests, the G (dynamic shear modulus) of the considered MSW fine fractions is highly sensitive to increasing confining pressure and relative compaction, which is also true for non-cohesive soils. However, as the strain increases, both G and D decrease while the other parameters remain constant. The D versus strain trends were found to be significantly different from many previous studies, but this can be justified based on the strain range, heterogeneity, physicochemical, and morphological characteristics of the considered MSW fine fractions. The loading frequency has no effect on G values, which is consistent with previous research on MSW and non-cohesive soils. The fiber-reinforced MSW fines show no improvement in dynamic shear strength (G) of MSW fines with FC, although the degradation of strength is comparatively low at a higher percentage of FC (8 and 10%). The damping ratio (D) has significantly improved with a higher percentage of FC (8 and 10%). The reinforcement of MSW fines with waste fibers show the faster accumulation of pore water pressure under cyclic loading condition, this limits its use in high seismic zones. The small-strain shear modulus (G_{max}) was computed through the bender element apparatus in the laboratory and the effect of different considered parameters was observed on V_s and G_{max}. The small-strain shear parameters (V_s and G_{max}) were linearly varied with the wave frequency (f). A slight improvement was seen with relative compaction, but no improvements were seen with confining pressure (at higher densities). Whereas the saturation decreases the shear parameter values. The optimum fiber content from the study was obtained at 1% for any σ_c and f for which V_s or normalized G_{max} values were highest.